UNIVERSIDADE DE SÃO PAULO
ESCOLA DE ENGENHARIA DE SÃO CARLOS
DEPARTAMENTO DE HIDRÁULICA E SANEAMENTO

JEAN MAIKON SANTOS OLIVEIRA

MULTIPLE STAGE ANAEROBIC TREATMENT FOR REDUCTIVE DECOLORIZATION OF AZO DYE IN THE PRESENCE OF SULFATE

VERSÃO CORRIGIDA

São Carlos – SP
2022

JEAN MAIKON SANTOS OLIVEIRA

MULTIPLE STAGE ANAEROBIC TREATMENT FOR REDUCTIVE DECOLORIZATION OF AZO DYE IN THE PRESENCE OF SULFATE

Dissertation presented to the São Carlos School of Engineering, University of São Paulo, as a requisite for obtaining the title of Doctor in Science: Hydraulic Engineering and Sanitation.

Supervisor: Prof. Tit. Eugênio Foresti
Co-supervisor: Prof. Dr. Álvaro José dos Santos Neto

São Carlos – SP
2022

Ficha catalográfica elaborada pela Biblioteca Prof. Dr. Sérgio Rodrigues Fontes da EESC/USP com os dados inseridos pelo(a) autor(a).

O48m

Oliveira, Jean Maikon Santos
Multiple stage anaerobic treatment for reductive decolorization of azo dye in the presence of sulfate / Jean Maikon Santos Oliveira; orientador Eugênio Foresti; coorientador Álvaro José dos Santos-Neto. São Carlos, 2022.

Tese (Doutorado) - Programa de Pós-Graduação em Engenharia Hidráulica e Saneamento e Área de Concentração em Hidráulica e Saneamento -- Escola de Engenharia de São Carlos da Universidade de São Paulo, 2022.

1. Anaerobic digestion. 2. Bioremediation. 3. Xenobiotics. 4. Proteomics. 5. Mass spectrometry. 6. Textile wastewater. 7. Amplicon sequencing. I. Título.

Eduardo Graziosi Silva - CRB - 8/8907

FOLHA DE JULGAMENTO

Candidato: Engenheiro **JEAN MAIKON SANTOS OLIVEIRA.**

Título da tese: "Tratamento anaeróbio em múltiplas etapas para a descoloração de corante azo na presença de sulfato".

Data da defesa: 12/08/2022.

Comissão Julgadora	**Resultado**
Prof. Titular **Eugenio Foresti** **(Orientador)** (Escola de Engenharia de São Carlos/EESC-USP)	APROVADO
Profa. Dra. **Sandra Imaculada Maintinguer** (Universidade Estadual Paulista "Júlio de Mesquita Filho"/UNESP-Rio Claro)	APROVADO
Profa. Dra. **Márcia Helena Rissato Zamariolli Damianovic** (Escola de Engenharia de São Carlos/EESC-USP)	APROVADO
Profa. Dra. **Silvana de Queiroz Silva** (Universidade Federal de Ouro Preto/UFOP)	APROVADO
Profa. Dra. **Sávia Gavazza dos Santos Pessoa** (Universidade Federal de Pernambuco/UFPE)	APROVADO

Coordenador do Programa de Pós-Graduação em Engenharia Hidráulica e Saneamento:
Prof. Dr. **Luiz Antonio Daniel**

Presidente da Comissão de Pós-Graduação:
Prof. Titular **Murilo Araujo Romero**

Aos meus pais,
Salete e Reinaldo.
À minha vó,
Carmen.
Dedico.

ACKNOWLEDGMENTS

Getting closer to the final stages of my doctorate degree, I caught myself wondering how much of my work is brought up in this dissertation. Each page is probably a result of countless hours spent in learning new tools, processing data using different approaches, discussing with colleagues to get new ideas or trying to make sense of the data I just acquired… and I didn't mention the failed experiments! This dissertation brings more than a couple years of experiments. I am truly grateful for the opportunity that Prof. Eugênio Foresti provided me of being a member of his group and working at the Biological Processes Laboratory (LPB, USP). His trust in my work made everything easier, and I was so lucky to have such an encouraging and supportive supervisor.

Anaerobic treatment of azo dyes is a topic brought to our study group by Professors Márcia and Sávia, who gave me unconditional support. Prof. Márcia felt like an unofficial co-supervisor. But as co-supervision is never too much, Prof. Álvaro (the official one) helped me in finding my way through the world of the analytical chemistry. Trying to develop a method for determination of azo compounds in complex matrices was a very challenging step of my Ph.D., and was very relieving to count on him and Dr. Carolina Sabatini with this task!

Dr. Carolina Sabatini not only helped me with the mass spectrometry analysis, but in several other tasks at both the Analysis and Chromatography laboratories. I am grateful to the whole LPB technician crew (Dr. Ângela Adorno, Dr. Eloisa Pozzi and Dr. Isabel Sakamoto) for their help in many techniques, such as chromatography, microbiology and molecular biology.

My friends in LPB were the greatest support I could ever have. There is a bit of each of them in this work. From the conceptualization of the project, reactor designing & operation, data processing… up to having a nice talk over coffee or going out for a beer (or two). I could not go far in my dissertation without them. Foresti's research group was small and still I had the right ones around me. And I could always count on friends from other groups, including Prof. Marcia's, Prof. Bernadete's, and Prof. Marcelos's.

But my lab acquaintances do not stop there. Prof. Jeppe Lund Nielsen kindly had me as a guest researcher at Aalborg University for one year. I had the opportunity to learn so much

about biomolecular analyses, things I could never imagine before. I made some great friends in his lab, and their help was fundamental during the last stage of my research.

Finally, my family is my unconditional support and I have no words to describe how much they have always helped me. My parents (Salete and Reinaldo) have always trusted in me and made everything they could to ease even the most difficult parts of my journey. I also have friends outside the professional range that were so important that they felt like family to me (you know who you are). I cannot count on my fingers how many times Daniel made my life easier by doing things such as driving me somewhere far away for a visa or hosting me whenever I needed. I really found true friends throughout this journey, both in Brazil and in Denmark.

I shall not linger more, and I hope not being unfair by not mentioning every name. Writing this section, with my dissertation nearly done, evokes plenty of emotions. It is a period of transition and I still do not know how much of my past years will fit in my suitcase. I just hope that I will enjoy my next journey as much as I enjoyed this one!

“What we know is a drop,
what we don't know is an
ocean.”
~Isaac Newton

RESUMO

OLIVEIRA, J.M.S. **Tratamento anaeróbio em múltiplas etapas para a descoloração de corante azo na presença de sulfato**. 2022. Tese (Doutorado em Engenharia Hidráulica e Saneamento – Escola de Engenharia de São Carlos, Universidade de São Paulo, São Carlos, 2022.

A descoloração redutiva é amplamente utilizada para a remoção de cor de águas residuárias que contém corantes têxteis azo. Embora eficiente, esse processo possui algumas limitações relacionadas à interferência de íons sulfato, que podem competir por equivalentes redutores. Neste estudo, propôs-se a utilização do tratamento anaeróbio em dois estágios para resolver os problemas relacionados a essa competição. Os resultados demonstraram que os elétrons foram preferencialmente utilizados para a redução do azo no reator anaeróbio de 1ª etapa (R1), onde a sulfetogênese e metanogênese foram inibidos pelas condições operacionais aplicadas, i.e. elevada carga orgânica volumétrica e baixo pH. Observou-se que a descoloração redutiva é um processo cometabólico e associado a rotas metabólicas produtoras de hidrogênio na fase acidogênica. O reator de 2ª etapa (R2) atingiu eficiências completas de remoção de matéria orgânica e de sulfato, além de atuar no polimento do efluente para melhoria da remoção de cor. Constatou-se que as bactérias acidogênicas em R1 são sensíveis e selecionadas na presença do corante, enquanto as comunidades microbianas em R2 são expostas a menores níveis do corante e por isso se mostram mais robustas. Para melhor elucidar o mecanismo de redução do azo, uma cepa de *Lactococcus lactis*, enriquecida durante a operação, foi isolada e estudada utilizando-se análise de proteômica. O mecanismo envolveu biossorção por glicoconjugados, particularmente exopolissacarídeos e ramnolipídeos, uma vez que proteínas relacionadas ao metabolismo de lipopolissacarídeos foram estatisticamente mais abundantes em células expostas ao corante azo. Os elétrons foram transferidos pela matriz do biofilme por *hopping*, num mecanismo que envolveu uma oxidorredutase da família de desidrogenase/redutases de cadeia curta e o mediador redox riboflavina. Os resultados sugerem que enzimas promíscuas estão envolvidas na degradação cometabólica de corantes azo por culturas microbianas sintróficas. Ainda, a configuração proposta se mostrou efetiva na remoção de cor, matéria orgânica e sulfato de efluentes contendo azo-corantes, e sua aplicação industrial mostra-se viável devido à performance estável e capacidade de receber cargas maiores de corante azo comparado aos processos de estágio único.

Palavras-chave: Digestão anaeróbia. Sistema de duas fases. Biorremediação. Sequenciamento de amplicons. Proteômica. Espectrometria de massas.

ABSTRACT

OLIVEIRA, J. M. S. **Multiple stage anaerobic treatment for reductive decolorization of azo dye in the presence of sulfate**. Tese (Doutorado em Engenharia Hidráulica e Saneamento – Escola de Engenharia de São Carlos, Universidade de São Paulo, São Carlos, 2022.

Reductive decolorization is widely used for removal of color from azo dye textile wastewater. Although efficient, this process has some drawbacks regarding the interference caused by sulfate ions, which may cause a competition mechanism for reducing equivalents. We propose the use of multiple stage anaerobic treatment to eliminate issues related to this competition. Results showed that electrons were driven to preferentially reduce the azo dye in the 1st-stage reactor (R1), where methanogenesis and sulfidogenesis were inhibited by the operating conditions applied, i.e. low pH and high organic loading rate. Reductive decolorization was found to be co-metabolic and mainly associated with hydrogen-producing pathways. The 2nd-stage reactor (R2) achieved nearly complete organic matter and sulfate removals, and also kept the overall decolorization efficiencies around 90% even when R1 presented decreased performance. Acidogens from R1 were observed to be sensitive and undergo selection upon exposure to azo dyes, whereas microbial communities in R2 are exposed to lower levels of dye and therefore appear less sensitive. To further elucidate the azo reduction mechanism, a *Lactococcus lactis* strain that was enriched throughout the operation was isolated from R1 and investigated using proteomics analysis. The mechanism involved biosorption by glycoconjugates, particularly exopolysaccharides and rhamnolipids, as proteins from the LPS O-antigen metabolism were statistically more abundant in cells challenged with the target compound. Electrons were transferred through the biofilm matrix by hopping, in a mechanism that involved a SDR family oxidoreductase and riboflavin carriers. The results show that enzymes with broad substrate specificity are involved in the co-metabolic degradation of azo dyes by syntrophic microbial communities. The proposed configuration was proven effective in the removal of color, organic matter, and sulfate from azo dye textile wastewaters and showed feasibility for industrial application due to its stable performance and higher azo dye load capacity when compared to single-stage systems.

Keywords: Anaerobic digestion. Two-phase system. Bioremediation. Amplicon sequencing. Proteomics. Mass spectrometry.

LIST OF FIGURES

LIST OF TABLES

LIST OF ACRONYMS AND ABBREVIATIONS

Ace	acetone
AD	anaerobic digestion
AnSTBR	anaerobic structured-bed reactor
ANVISA	Agência Nacional de Vigilância Sanitária
APBR	anaerobic packed-bed reactor
AzoL	*L. lactis* LLSP-01 azoreductase
BDL	below detection limits
BFR	biogas flow rate
n-BuOH	n-butanol
CH	carbohydrates
CE_{CH}	conversion efficiency of total carbohydrates
CID	collision-induced dissociation
COD	chemical oxygen demand
DB22	Direct Black 22
dsrB	dissimilatory sulfite reductase β-subunit
EGSB	expanded granular sludge bed reactor
ESI	electrospray ionization
ESI^-	electrospray ionization in negative mode
EtOH	ethanol
FC	fold-change
fhs	formyltetrahydrofolate synthetase
HAc	acetic acid
HBu	n-butyric acid

HCa	n-caproic acid
HIsoBu	isobutyric acid
HIsoVa	isovaleric acid
HPr	propionic acid
HVa	n-valeric acid
HPLC	high performance liquid chromatography
HRT	hydraulic retention time
LAB	lactic acid bacterium/bacteria
LC	liquid chromatography
LC-ESI-MS/MS	liquid chromatography – electrospray ionization tandem mass spectrometry
LPB	Biological Processes Laboratory
mcrA	methyl coenzyme-M reductase
MeOH	methanol
MMF	methane molar flow
MS	mass spectrometry
MS/MS	tandem mass spectrometry
OLR	organic loading rate
PCR	polymerase chain reaction
PU	polyurethane
RmlB	dTDP-glucose 4,6-dehydratase
RmlC	dTDP-4-dehydro-β-L-rhamnose
RT-PCR	reverse transcriptase-polymerase chain reaction
R1	1st-stage reactor
R2	2nd-stage reactor
SDR	short-chain dehydrogenases/reductase

SAOB	syntrophic acetate oxidizing bacteria
SPE	solid-phase extraction
SRB	sulfate reducing bacteria
UASB	upflow anaerobic sludge blanket reactor
VFA	volatile fatty acids
VHPR	volumetric hydrogen production rate
VMPR	volumetric methane production rate
VSS	volatile suspended solids

TABLE OF CONTENTS

Chapter 1
Introduction

A normal sized textile industry consumes an average of 1600 m^3 of water per day (Bhatia et al., 2017). Textile wet processing operations comprise steps such as desizing, scouring, bleaching, mercerizing and dyeing, each of which produces wastewater with distinct characteristics (Santos et al., 2007). The final outcome is an effluent rich in organic matter, salts, acids, bases, alkalis, and recalcitrant compounds such as surfactants and synthetic dyes (Khandare and Govindwar, 2015; Santos et al., 2007). Synthetic dyes are used to give color to the fabrics, but they present poor rates of fixation. As a result, about 20% of the dyes used are assumed to be discarded in the effluent (Azbar et al., 2004). This dissertation will address the bioremediation of dyes belonging to the class *azo*, which represents approximately 60% of the dyes used in the textile sector (Catanho et al., 2006).

It is not only bad that textile wastewaters are often rich in organic matter. Carbohydrates such as starch used in steps that precede the dyeing baths can be used as source of reducing equivalents to cleave azo bonds (which are double N=N bonds). This transfer of electrons occurs under low redox potential conditions and is therefore named *reductive decolorization*. This reaction results in color removal due to the conversion of the dye molecules into colorless aromatic amines. Aromatic amines are toxic products from the partial degradation of azo dyes and are not expected to be degraded under anaerobic conditions, as biodegradation of these compounds depend on the incorporation of oxygen atoms into the aromatic rings by oxygenase enzymes.

Until this point, there is nothing novel in this dissertation. The mechanism of reductive decolorization was proposed decades ago, and research in developed countries moved on to focus on newer contaminants of emerging concern. However, many gaps remained unsolved as textile industries migrated to developing countries. The problem was solved for the so-called first-world countries, but countries such as Brazil, India, China and many others still face challenges regarding proper handling of textile wastes.

The development of appropriate methods for the monitoring of azo dyes in wastewaters are among the gaps in this field. Methods based on color are unspecific and therefore unable to distinguish dyes from other colorful substances. The **Chapter 3** of this dissertation is an attempt

of using high selective techniques (e.g. liquid chromatography – tandem mass spectrometry analysis) to determine the model azo dye Direct Black 22 (DB22) in biological reactor effluents. Although challenges such as matrix interference were expected, we ended up facing higher challenges such as the instability of DB22 in aqueous solution.

Other unresolved challenge is the competition observed between azo reduction and other electron-demanding processes. There are several reports indicating that effluents discharged by textile industries located in the Agreste Pernambucano – Brazil are rich in sulfate, which can outcompete azo dyes depending on the dye's redox potential. Multiple stage anaerobic treatment was proposed as a strategy for solving this issue and is covered in the **Chapter 4**. The mechanism of DB22 biodegradation and microbial communities involved are addressed in the **Chapter 5**.

The new advances in the OMICS technologies have brought the opportunity of studying enzymes involved in the biodegradation of azo dyes. A bacterium culture with high relative abundance in the two-stage anaerobic digestion system and capable of decolorizing DB22 was isolated, and proteins differentially expressed in the presence of the azo dye were investigated. These findings are described in the **Chapter 6** of this thesis.

HYPOTHESES OF THIS DISSERTATION

i. The azo dye DB22 can be monitored in the effluent from biological reactors using solid-phase extraction and liquid chromatography – tandem mass spectrometry analysis;

ii. Multiple stage anaerobic treatment is an effective way of minimizing the impacts of sulfidogenesis and methanogenesis on the decolorization and biotransformation of azo dyes;

iii. The anaerobic digestion of azo dyes by syntrophic microbial communities is a co-metabolic process that involves distinct microbial communities and metabolic pathways;

iv. Enzymes with broad substrate specificity are involved in reductive decolorization of azo dyes.

Chapter 2
Literature review

1. Production of wastewater in the textile and clothing industry

The textile and clothing sector drives the local economy and creates jobs. However, large amounts of wastewater are produced during textile wet processing operations (Bhatia et al., 2017). The National Environmental Act (*Política Nacional do Meio Ambiente* - PNMA) has as guiding principles, among others, the protection of ecosystems and the control of potentially or effectively polluting activities (Brasil, 1981). Therefore, effluents from the textile industry must be appropriately managed and treated prior to disposal into water bodies.

Table 2. 1 contains a description of the main physical-chemical characteristics of the textile effluents based on recent studies conducted in Brazil and over the world. Usually, these wastewaters have pH values ranging from neutral to basic, high chemical oxygen demand (COD) values and varying degrees of salinity and total dissolved solids (TDS). Chloride, sodium and sulfate ions are usually present as a result of salts addition (e.g., NaCl or Na_2SO_4) to improve dye adhesion to the fibers (EPA, 1997). According to the United States Environmental Protection Agency (1995), salts are added to propitiate the exhaustion of binding sites in anionic dyes, e.g. direct and reactive dyes. The weight of salts added during dyeing baths is estimated to be around 80% of the weight of the fabrics. Moreover, textile industries located in the Agreste Pernambucano are reported to consume large amounts of sodium metabisulfite ($Na_2S_2O_5$) used as a bleach to brighten fabrics and remove stains, generating an effluent containing high concentrations of sulfate (Amaral et al., 2017, 2014).

2. Brazil's legislation and dyes of anthropic origin

The CONAMA (Conselho Nacional de Meio Ambiente) Resolution n. 430/2011 for wastewater discharge does not stipulate a maximum permissible dye concentration in discharged wastewater, but the discharge of dye-containing effluents shall not change the quality of the receiving water body. The CONAMA Resolution n. 357/2005 stablishes limits of true color that depends on the quality of the water bodies. Dyes of anthropic origin should be virtually absent in Class 1 water bodies; and the presence of these compounds are tolerated in Classes

2 and 3 rivers, provided that the dyes can be removed in processes involving coagulation, sedimentation and filtration.

Table 2. 1. Physical-chemical characteristics of textile wastewaters produced during wet processing operations of some textile industries in Brazil and over the world.

Reference	Predominant azo dye	pH	COD (mg L^{-1})	Salinity (%.)	TDS (mg L^{-1})	Cl^- (mg L^{-1})	Na^+ (mg L^{-1})	SO_4^{2-}(mg L^{-1})
Amaral et al. (2014)	Direct Black 22		~1000	4.4				269-464
Amaral et al. (2017)	Mixture of up to 28 dyes	7.5 ± 0.7	692 ± 459	3.2				334 ± 40
Amorim et al. (2013)	Direct Black 22		730 (394-1062)			10430		
Ferraz et al. (2011)	Direct Black 22	6.9 (6.1-8.3)	728	2.6	3600	949 (880-10430)	1500 (800-15300)	21 (17-24)
Kurade et al. (2017)	Not specified	9.3	3500		240			
		10.1	5610		360			
Mirbolooki et al. (2017)	Not specified	7.5	140.8		1470			
Santos et al. (2005)	Reactive dyes	10.2-11.6	747-32600					990-12100
Şen e Demirer (2003)	Remazol, Everzol and Levafix	9.1	1029			609.8		2.36
		9.9	1157			594.8		1.94
		8.9	1063			557.33		4.23
		8.9	1018			569.8		6.43
Phugare et al. (2011)	Not specified	8.1	9860		8756	1254	89	1123
Telke et al. (2010)	Reactive, disperse and direct dyes	8.2	1000		8770			
Wang et al. (2008)	Not specified	6.9 (5.9-7.9)	1200 (430-2500)			133 (102-750)		107 (86-210)
Yang et al. (2009)	Reactive and disperse dyes	6.0-7.0	750-1175					
Zaroual et al. (2006)	Not specified	10.6	485			27069	5965	2161

3. Azo dyes and biodegradation products

Dyes are classified into major classes according to their chemical structures (Christie, 2015; Forgacs et al., 2004). Within the scope of wastewater treatment, classifying dyes is important because the design of biological treatment processes is based on the metabolism of the microorganisms involved, which includes the microorganisms' ability to produce enzymes capable of cleaving the targeted compound. Namely, dye's biodegradation depends on the

presence of bonds that can be attacked by functional groups in the active site of enzymes; or on the presence of organic functional groups in the dye molecule that can bind to these active sites so that the reaction occurs (Lima et al., 2001).

Dyes which contain the azo chromophore, i.e. that presents one or more -N=N- groups, are classified as azo dyes and are particularly relevant because they are extensively used worldwide (Kunz et al., 2002). This class of dyes is environmentally relevant due to its difficult treatability in conventional wastewater treatment plants and high toxicity (Forgacs et al., 2004; Pinheiro et al., 2004; Shaul et al., 1991).

The environmental relevance of azo dyes extends to its treatment process, as incomplete degradation leads to the formation of carcinogenic aromatic amines which are recalcitrant to anaerobic digestion (Pandey et al., 2007). In this context, some authors have focused on the study of biological processes in which the produced metabolites are less toxic or are further mineralized (Sen et al., 2016; Tan et al., 2013).

4. Direct Black 22 and reduction products

Direct Black 22 (DB22) was chosen because it has been extensively used in the Brazilian textile industry (Amorim et al., 2013). DB22 biodegradation in effluents from denim fabric manufacturing industries located in Caruaru – PE (Brazil) was studied by several authors, which observed color removal efficiencies of up to 67% by anaerobic granular sludge (Amaral et al., 2017, 2014; Júnior, 2010). Moreover, these studies reported the formation of aromatic products recalcitrant to the anaerobic digestion (AD), which were not properly identified. Qualitative assessment of aromatic amines resulting from the DB22 biotransformation was assessed by UV spectrophotometry (Pinheiro et al., 2004). Gavazza et al. (2015) speculated that DB22 biodegradation may lead to the formation of compounds such as aniline, naphthalene-1-sulfonic acid and sulfanilic acid.

5. Analysis of sulfonated azo dyes by liquid chromatography – electrospray ionization tandem mass spectrometry

Most studies on biodegradation of azo dyes use color to monitor the removal of these compounds. Nevertheless, spectrophotometric methods are susceptible to interference caused by metabolites produced in biological reactors. These interferences are even more significative in processes carried by mixed microbial consortia, which is the case of anaerobic digestion. Figure 2. 1 shows that the number of studies in the *Google Scholar* platform mentioning the

term *azo* in association with words such as *spectrophotometry*, *ADMI*, *color removal*, *maximum /wavelength* or *absorbance* is much higher than that in which the term *azo* is associated with direct quantification techniques, i.e. *chromatography*, *HPLC*, *LC*, *LC-MS*, *MS/MS*. When the search is restricted to studies on the biodegradation of azo compounds, the number of studies decreases further to 85 results.

Figure 2. 1. Number of studies in the *Google Scholar* platform related to azo compounds and quantification (direct or indirect) of these compounds. **A)** mentions to the term *azo* associated with *spectrophotometry* or *chromatography* quantification techniques. **B)** mentions to the term *azo* and *biodegradation* associated with *spectrophotometry* or *chromatography* quantification techniques.

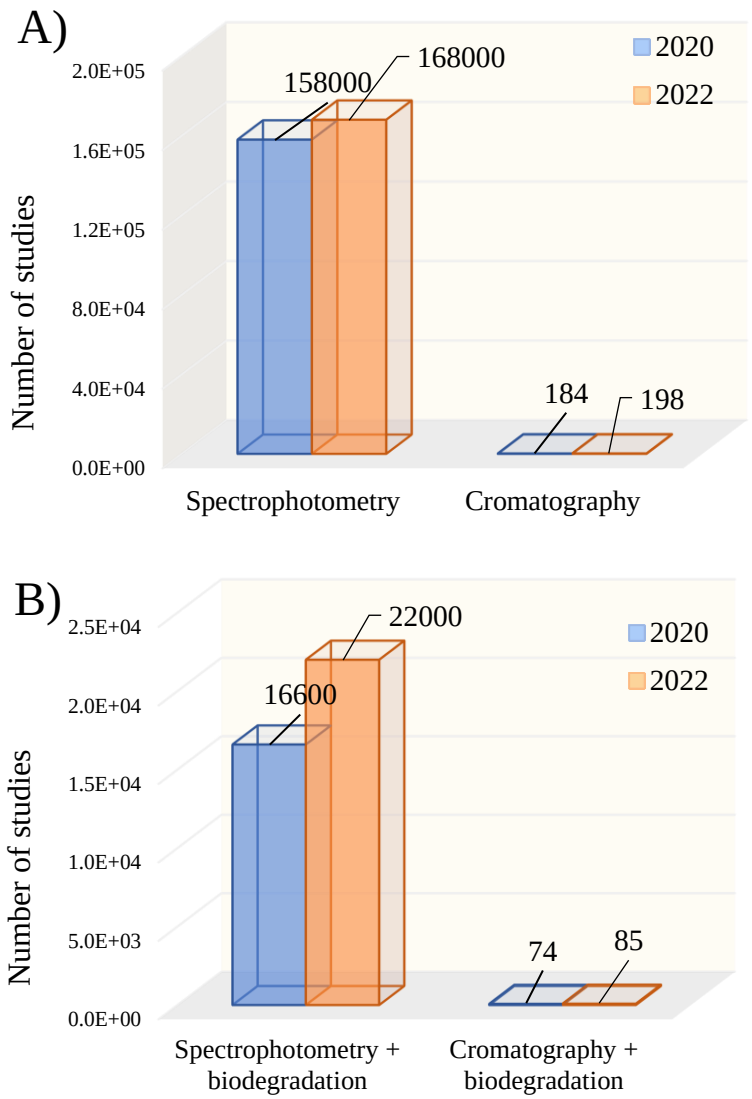

The main disadvantage associated with quantification of azo compounds using chromatographic techniques lies in the difficulty of developing methods for the multitude of azo dyes that can be found in dye-related wastes, and which possess distinct physical and chemical

Table 2. 2. Detection and quantification of azo dyes in complex matrices, extraction methods and validation parameters.

Reference	Azo dye	Matrix	Extraction method	Quantification /Detection	Quality of the analytical method
Fuh and Chia (2002)	Tartrazine, Amaranth, New Coccine, Sunset Yellow FCF, Allura Red AC, Ponceau R, Ponceau 3R, Orange I, Orange II and Metanil Yellow	Soda, fruit jam and salted fruit stuff	Liquid-Liquid	LC-UV (LC-MS used only for confirmation)	Linearity: 0.05-10.0 mg L^{-1} (R^2 = 0.999) DL: 0.01 mg L^{-1}
Edlund et al. (1989)	Acid Yellow 23, Red 14 and Yellow 49	Domestic sewage	SPE (octadecylsilane)	LC-UV-MS/MS	Linearity: 0.5-5 mg.L^{-1} (analytical curve parameters not presented) DL: 0.05 - 0.15 mg.L^{-1} RSD: 5.4 - 12%
Rehorek and Plum (2007)	Reactive Black 5, Reactive Orange 16, Reactive Orange 107	Biological reactor effluent	--	LC-MS/MS and LC-DAD	Linearity: 0.1-300 µmol L^{-1} (R^2 > 0.99) DL: 0.001-0.59 µmol L^{-1}
Ding et al. (2009)	Direct Black 38, Direct Blue 6, Direct Red 28, Acid Red 26 and Disperse Yellow 3	Cotton, acrylic and polyester fabrics	Liquid-Liquid	LC-MS/MS	Linearity: γ > 0.995 (linearity interval not shown) DL: 0.005-0.25 mg.kg^{-1}
Franca et al. (2019)	Acid Red 14 and metabolites	Biological reactor effluent	SPE (Oasis HLB generics)	LC-MS/MS	Qualitative method
Li et al. (2013)	Sudan (I–IV), Para Red and Chrysoidin	Chili products	Liquid-Liquid	LC-MS/MS	Linearity: 0.002-0.1 mg L^{-1} (R>0.991) Matrix effect: -17.1 to 6.6% DL: 0.3-0.6 µg kg^{-1} QL: 0.75-3 µg kg^{-1}
Copaciu et al. (2013)	Nylosan Red N-2RBL	Domestic sewage	SPE (Strata WAX/NH_2)	LC-MS/MS	Linearity: 0.001-0.1 mg L^{-1} (R=0.9985) Recovery: 89.7 - 98.3% DL: 0.285 ng mL^{-1} QL: 0.864 ng mL^{-1}

Abbreviations. Methods: SPE = solid phase extraction; LC-UV = liquid chromatography with ultraviolet detection; LC-DAD = liquid chromatography with diode array detection; LC-MS: liquid chromatography coupled to mass spectrometry analysis; LC-MS/MS: liquid chromatography coupled to tandem mass spectrometry analysis. **Others:** DL = detection limit; QL = quantification limit; RSD = relative standard deviation.

characteristics (Voyksner et al., 1993). Extraction of these compounds from complex matrices to minimize matrix effect is another bottleneck. However, methods based on solid-phase extraction (SPE) may offer good results in terms of elimination of interferents from these matrices (Table 2. 2). Regarding detection, mass spectrometers interfaced with electrospray ionization (ESI-MS) have been successfully implemented for identification of sulfonated azo dyes in particular cases, and ionization in negative mode (ESI^-) is often preferred due to the presence of sulfonic acid groups in these compounds (Ding et al., 2009; Holčapek et al., 2001, 1999; Reemtsma, 2003).

6. Biological treatment of effluents from the textile industry

Physical-chemical treatment of textile wastewater has been the choice of many industries. However, processes involving chemical coagulation produce large amounts of contaminated sludge, which needs further handling (Gavazza et al., 2015; Singh et al., 2015; Solanki et al., 2013). Moreover, some technologies involved in the physical-chemical treatment of these wastes (e.g. membranes and filtering media) involve high costs (Santos et al., 2007; Sharma et al., 2016). Biological degradation of azo dyes has been proposed as a cost-effective and environmentally sustainable alternative to those conventional techniques and has the potential to reduce or even eliminate the biotoxicity of these effluents (Amaral et al., 2014; Menezes et al., 2019; Oliveira et al., 2020).

The main known mechanisms of decolorization of azo dyes are: i) reductive decolorization, in which azo bonds are reduced under anaerobic or anoxic conditions; and ii) processes involving lignin-modifying enzymes or enzymes from the oxidoreductase enzyme system (including azoreductases), which can be carried in environments with varying redox potential conditions (i.e. anaerobic, anoxic or aerobic). This review is going to cover particularly reductive decolorization due to the aims of this work and applicability to continuous bioreactor systems using mixed microbial culture technology.

6.1. Reductive decolorization of azo dyes

In the reductive decolorization process, azo dyes are directly reduced by biological enzymes, or indirectly, in the presence of redox mediators (RM). Reductive decolorization only occurs in anaerobiosis, in which the azo dye is the final electron acceptor. In aerobic conditions, oxygen is the final electron acceptor (Santos, 2001; Singh et al., 2015; Van Der Zee et al., 2003).

Figure 2. 2-A shows the mechanism of reductive decolorization of azo dyes by reducing equivalents. Reducing equivalents are produced during the metabolization of a co-substrate, which is an easily biodegradable compound, and are used by bacterial enzymes which catalyze the reductive cleavage of the azo bond (Imran et al., 2016). The main class of enzymes supposedly involved is *azoreductase*, but many other enzymes from the oxidoreductase enzyme system were reported to have a substantial contribution in color removal under anaerobic or anoxic conditions (Jadhav et al., 2010; Pandey et al., 2007; Phugare et al., 2011; Telke et al., 2010).

The use of RMs in enhancing the enzymatic reduction of azo dyes was addressed in several studies (Dos Santos et al., 2003; Santos et al., 2007, 2004). These compounds act as electron carriers by channeling electrons from reducing equivalents produced inside the microbial cells to the azo compounds, as shown in Figure 2. 2-B (Imran et al., 2016; Rau and Stolz, 2003). In spite of the good results obtained with batch experiments, the use of RMs showed little impact on the decolorization of azo dyes in continuous bioreactor systems (Braúna et al., 2009; Dos Santos et al., 2003). However, good performance was obtained by applying RMs and thermophilic anaerobic treatment (Dos Santos et al., 2005).

Figure 2. 2. Mechanism of azo dye decolorization in anaerobic systems. A) direct enzymatic electron transfer; and B) indirect electron transfer by redox mediators. E_{red}/E_{ox} are, respectively, the reduced and oxidized forms of an enzyme, and M_{red}/M_{ox} are the reduced and oxidized forms of a low molecular weight electron carrier (mediator).

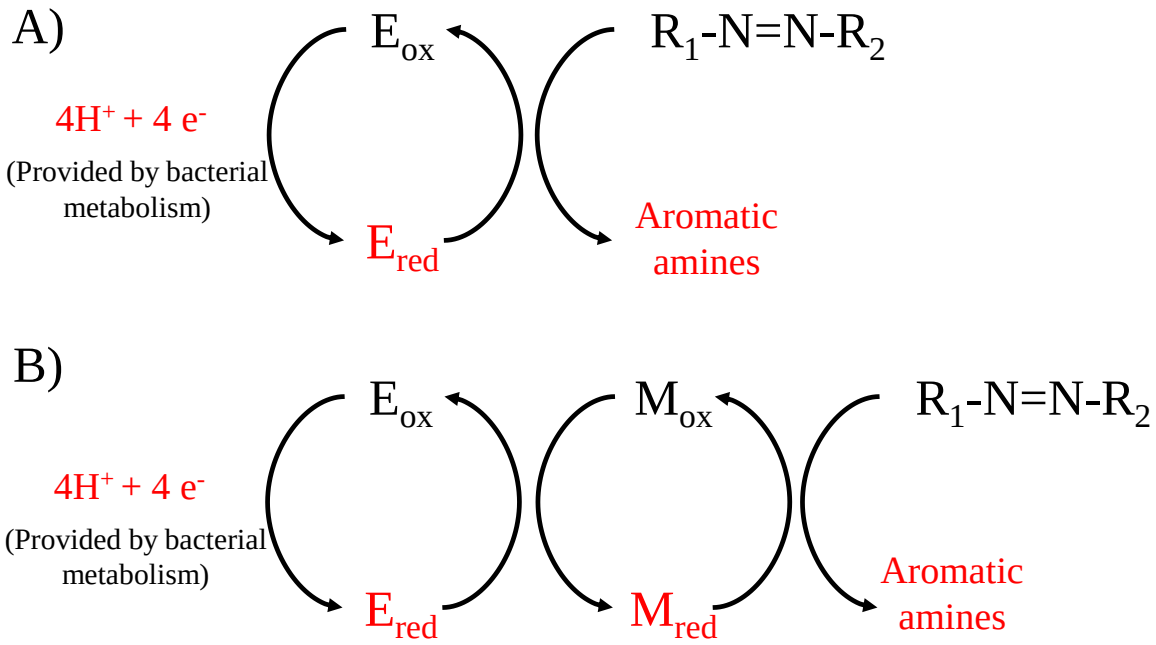

Source: adapted from Van Der Zee et al. (2003).

6.2. Sulfidogenesis interference on reductive decolorization

Azo dyes can also be reduced chemically in bioreactors operating under sulfidogenic conditions. In this mechanism, hydrogen sulfide (H_2S) produced by sulfate-reducing bacteria (SRB) abiotically transfer electrons to the azo compound. H_2S is then oxidized to elementary sulfur (S^0), whereas the azo dye is reduced leading to the formation of aromatic amines (Pandey et al., 2007; Van Der Zee et al., 2003). However, the abiotic mechanism was found to have a less relevant contribution to reductive decolorization of azo dyes compared to the mechanism mediated by biological enzymes (Van Der Zee et al., 2003).

On the other hand, the contribution of biogenic sulfide can be counterbalanced by the interference of the sulfidogenic pathway on reductive decolorization. Amaral et al. (2014) observed that high concentrations of sulfate ions (>300 mg L^{-1} SO_4^{2-}) led to significant inhibition of color removal in a system operated with real textile effluent. In another study, the increase in the hydraulic retention time (HRT) resulted in better sulfate removal efficiencies, but decolorization efficiency was not improved (Amaral et al., 2017). It was hypothesized that reducing equivalents are preferentially used to reduce sulfate rather than azo dyes, in a competition mechanism similar to that observed between SRB and methanogens (Bijmans et al., 2011).

6.3. Azo dyes and reduction products interference on methanogenesis

The role of methanogens on the reductive decolorization process is still not a consensus in the literature. A few authors have stated that methanogenic archaea contribute in reductive decolorization (Pandey et al., 2007; Plumb et al., 2001; Santos et al., 2006). Other studies have shown that methanogens and azo reducers may compete for electron donors, and high concentration of azo dyes can inhibit methane production (Cervantes et al., 2005; Dai et al., 2018, 2016). Moreover, it was previously observed that azo dyes are more toxic to methanogenic archaea than their respective aromatic byproducts (Donlon et al., 1997).

7. Azo dye biodegradation in continuous systems: reactor configuration, biomass and support material

Several reactor configurations were previously proposed for the treatment of azo dye wastewaters. Table 2. 3 shows a summary of the main continuous reactor systems used in studies involving the complete or partial biodegradation of azo dyes. In the reductive decolorization process, the cleavage of the azo chromophore occurs as a result of electron transfer to the dye

molecule in the absence of molecular oxygen. Therefore, anaerobic process units are usually designed as the first stage in these bioreactor systems.

The upflow anaerobic sludge blanket reactor (UASB) and the expanded granular sludge bed reactor (EGSB) are common choices among bioreactors in studies involving the reductive decolorization of azo dyes. However, the performance of these systems relies on a good granulation of the biomass (Fuess, 2017). In anaerobic treatment processes with phase separation, i.e., acidogenic and methanogenic stages occurring in distinct units, acidogenesis is expected to predominate in the 1st-stage reactor. The characteristics of the acidogenic biomass differ from those of the anaerobic granular sludge conventionally used in UASB and EGSB systems, although stable performance has been achieved in acidogenic UASB reactors before (Braga et al., 2016; Ribeiro et al., 2022). Among the innovative reactor configurations, anaerobic fixed-bed reactors with structured or randomic biomass immobilization are often preferred for the treatment of high-strength wastewaters (de Aquino et al., 2017). The main examples of technologies using these media arrangements are the anaerobic packed-bed reactor (APBR) and the anaerobic structured-bed reactor (AnSTBR), respectively.

In previous studies, an acidogenic APBR reactor was applied for the treatment of an effluent rich in sulfate (Fuess et al., 2017, 2016). In spite of the good performance initially obtained, the system struggled with excessive growth of biomass and required periodic discharge of the excessive sludge. The study further mentions several APBR systems which collapsed over a period of 50 – 60 days of operation. In a complex system as the one proposed in this work, the collapse of the preliminary unit would threaten the integrity of the whole system.

The AnSTBR reactor built with polyurethane (PU) foam has been widely used in studies conducted in the Biological Processes Laboratory – LPB (São Carlos School of Engineering, University of São Paulo). According to Mockaitis et al. (2014), the AnSTBR has advantages over the APBR regarding the excessive accumulation of solids and continuous growth of biomass, which lead to clogging and channeling effects. Microbial colonization in the PU foam matrix was found to occur in the form of both micro-granules entrapped in the porous medium, thin multi-cellular layers attached to the inner surface and individual cells (Varesche et al., 1997). In the context of the biodegradation of azo dyes, the AnSTBR configuration was recently evaluated for the treatment of DB22 and sulfate removal using single-stage AD (Florêncio et al., 2021). DB22 decolorization and sulfate removal efficiencies achieved were 66.4 and 77.3%, respectively. The authors attributed the relatively low efficiencies to the competition between azo dyes and sulfate for reducing equivalents.

Table 2. 3. Main continuous reactor systems applied to the biodegradation of azo dyes in real or synthetic textile effluents.

Reference	Reactor configuration / effluent type	HRT (h)	OLR (g-COD L^{-1} d^{-1})	Average color removal
Amaral et al. (2014)	UASB-SAB/ real effluent	UASB: P1: 12 P2: 12 P3: 8 SAB: P1: 9 P2: 9 P3: 6	UASB: P1: 1.84 P2: 2.42 P3: 2.7 SAB: P1: 1.74 P2: 1.66 P3: 4.5	UASB: P1: 30% P2: 37% P3: 52% SAB: P1: 92% P2: 62% P3: 52%
Amaral et al. (2017)	UASB-SAB/ real effluent	UASB: P1: 16 P2: 96 SAB: P1: 12 P2: 72	UASB: P1: 1.77 P2: 1.41 SAB: P1: 1.33 P2: 0.73	UASB: P1: 67% P2: 55%
Braúna et al (2009)	EGSB/ synthetic effluent	10	2.5	R1[a]: P1: 89% P2: 92% P3: 87% R2: P1: 83% P2: 91% P3: 88% P.S.: similar performance in both the reactors
Ferraz-Junior et al. (2011)	UASB-SAB/ real effluent	UASB: P1: 24 P2: 16.6 P3: 12.3 SAB: P1: 18 P2: 12.5 P3: 9.2	UASB: P1: 1.3 P2: 1.2 P3: 3.2 SAB: P1: 1.0 P2: 0.9 P3: 2.6	UASB: P1: 64% P2: 40 (55%)[b] P3: 10 (50%)[b]
Firmino et al. (2010)	UASB (single and two-stage/ synthetic and real effluent	SS: P1-6: 24 P7: 12 AS: P1-6: 4 P7: 6 MS: P1-6: 20 P7: 10		<u>Synthetic effluent</u> SS: 93.4-98.1% AS: 49-93.2% AS+M: 92.6-98.5% <u>Textile effluent</u> SS: 57.1% AS: 44.8% AS+M: 50.1%
Gavazza et al. (2015)	UASB/ synthetic effluent	16	1,7	R1[c]: 80% R2: 80% P.S.: significant decrease after exhaustion of the adsorption sites
Santos et al. (2003)	EGSB/ synthetic effluent	10	2,5-5	R1[a]: 54-98% R2: 46-93% P.S.: similar performance in both the reactors
Santos et al. (2005)	EGSB/ real effluent	2,5-10	5	R1: 13-86% (30ºC) R2[a]: 47-88% (30ºC) R3: 69-91% (55ºC) R4[a]: 79-95% (55ºC)

Notes: [a] reactor supplemented with redox mediator AQDS; [b] measurements in between parenthesis indicate color removal efficiencies after acclimation to the new conditions; [c] reactor coupled with electrode systems.

Abbreviations: EGSB = expanded granular sludge bed reactor; SAB: submerged aerated biofilter; UASB = up-flow anaerobic sludge blanket reactor; HRT = hydraulic retention time; OLR = organic loading rate; SS = single stage; AS = acidogenic stage; MS = methanogenic stage; AS+M: acidogenic and methanogenic stages combined.

The competition between sulfate and azo dyes for reducing equivalents was previously reported in a study conducted by Amaral et al. (2014) in a UASB reactor fed with real textile wastewater. In the system proposed in this study, i.e. two stage AD system, it is expected that

azo reduction will occur predominantly in the 1st-stage reactor, where electrons produced during the organic matter conversion will be transferred to the azo compound in reactions mediated by oxidoreductase enzymes (Imran et al., 2016). In this way, competing reactions such as sulfate reduction and conversion of carbon dioxide to methane will be avoided, as they are expected to occur in the 2nd-stage of the AD system.

8. Concluding remarks

Reductive decolorization of azo dyes is a feasible alternative to the physical-chemical treatment processes from both the economic and environmental perspectives. The proposed strategy aims at enhancing the decolorization performance by using multiple stage anaerobic treatment. In the 1st-stage reactor, electron-competing processes such as methanogenesis and sulfidogenesis would be of lesser importance due to the environmental conditions typical of the fermentative metabolism, e.g. low pH and high applied organic loading rates.

Chapter 3

Broken into pieces: the challenges of determining sulfonated azo dyes in biological reactor effluents using LC-ESI-MS/MS

Abstract: Most studies on biodegradation of textile azo dyes use color as parameter for measuring the efficiency of degradation. Although widely employed, spectrophotometric methods are susceptible to the interference of metabolites or degradation products from the biological treatment. We propose a method for determination of a model sulfonated azo dye (Direct Black 22, DB22) in wastewater using solid-phase extraction (SPE) and liquid chromatography – electrospray ionization tandem mass spectrometry (LC-ESI-MS/MS). MS analysis in negative electrospray ionization mode showed DB22 as the most abundant precursor ion, corresponding to $[M–3Na+H]^{2-}$, which yields two radical anions of *m/z* 370.1 and *m/z* 645 after MS/MS fragmentation by collision-induced dissociation (CID). Calibration curve presented adequate linearity and precision in the range of 120–1500 ng mL^{-1}, and recovery and detection limit were appropriate to the typically employed working concentrations. Nevertheless, we observed that standard heating of DB22 under alkaline conditions to simulate the production of wastewater during dye-baths resulted in loss of MS/MS signal, without affecting color. Further analysis showed that DB22 undergoes hydrolysis and does not remain unaltered in solution. Alternative methods of hydrolysis evaluated resulted in no MS/MS signal as well. SPE-LC-ESI-MS/MS analysis evidenced the structural change of DB22 in aqueous solution while the dyeing-capacity was preserved. This technique has also the potential of being tailored to consider the detection of the hydrolyzed fragments of azo dyes in wastewater for appropriate quantification, but it was not the scope of the current step of this research. Color remains as a more reliable parameter for monitoring azo compounds which are unstable in aqueous solution, while a more robust and holistic method needs to be developed for the speciation of the DB22 products of thermal hydrolysis.

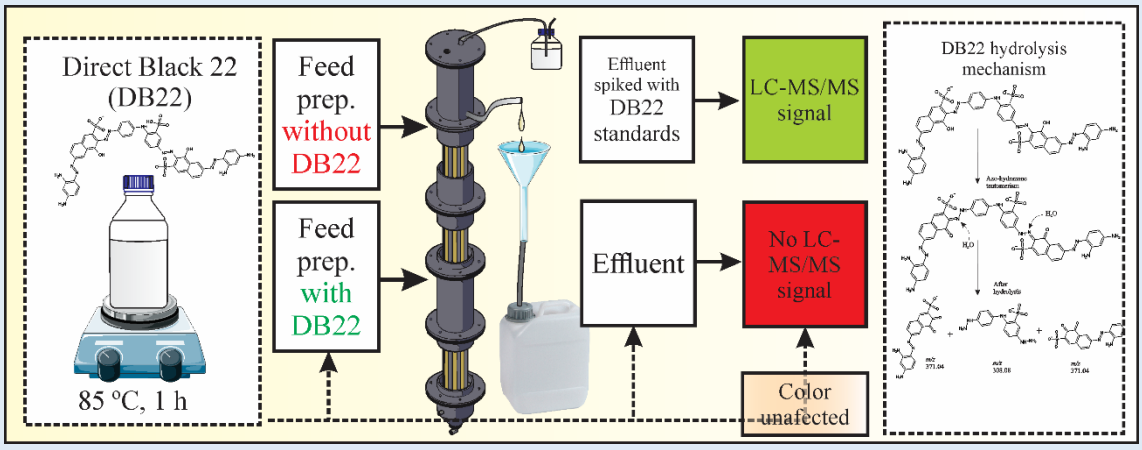

A modified version of this chapter was submitted to a journal published by Elsevier:

Oliveira, J.M.S., Sabatini, C. A., Santos-Neto, A.J., Foresti, E., 2022. Broken into pieces: the challenges of determining sulfonated azo dyes in biological reactor effluents using LC-ESI-MS/MS.

1. Introduction

Most studies on biodegradation of azo dyes use color to monitor the removal of these compounds. Nevertheless, spectrophotometric methods are susceptible to interference caused by metabolites produced in biological reactors. These interferences are even more significant in processes carried by mixed microbial consortia, which is the case of anaerobic digestion. Beyond that, color analysis is non-specific, and therefore this analysis is not appropriate for determining the concentration of azo dyes in wastewaters which contain multiple colorants. In this context, chromatography with tandem mass spectrometry is more suitable for quantification of azo compounds in complex matrices due to its high selectivity (Chiaradia et al., 2008).

The main disadvantage associated with quantification of azo compounds using chromatographic techniques lies in the difficulty of developing methods for the multitude of azo dyes that can be found in dye-related wastes, and which possess distinct physical and chemical characteristics (Voyksner et al., 1993). Extraction of these compounds from complex matrices to minimize matrix effect is another bottleneck. However, methods based on solid-phase extraction (SPE) may offer good results in terms of elimination of interferences from these matrices (Franca et al., 2019). Regarding detection, mass spectrometers interfaced with electrospray ionization (ESI-MS) have been successfully implemented for identification of sulfonated azo dyes in particular cases, and ionization in negative mode (ESI^-) is often preferred due to the presence of sulfonic acid groups in these compounds (Ding et al., 2009; Holčapek et al., 2001, 1999; Reemtsma, 2003).

In this study, we developed a method for the determination of the sulfonated azo dye Direct Black 22 (DB22) in effluents from biological reactors using SPE and liquid chromatography – electrospray ionization tandem mass spectrometry (LC-ESI-MS/MS). Determination of DB22 using LC-ESI-MS/MS is particularly challenging because the commercial dye used by the textile industries has low purities ($\leq 50\%$), and DB22 standards with higher purities are not available in the market. Despite the good results initially obtained, as revealed by analytical performance parameters, we demonstrate that the heating of a dye solution commonly performed by textile industries to increase solubility in water may severely interfere in the quantification of these compounds.

2. Materials and Methods

2.1. Chemicals and synthetic textile wastewater

DB22 (CAS 6473-13-8) was acquired from the dye supplier Aupicor Quimica© (Pomerode – SC, Brazil) and had a molecular weight of 1083.97 g mol^{-1} and a 42% purity. DB22 is a tetra-azo dye with maximum absorbance wavelength of 481 nm and charge of -3 at pH 5-9 (http://chemicalize.com). Dye hydrolysis was conducted by increasing pH to 11 and heating at 85 ºC for 1 hour (Santos et al., 2004). Synthetic textile wastewater contained: glucose (1.50 g-COD.L^{-1}), KH_2PO_4 (0.25 g.L^{-1}), NaCl (0.5 g.L^{-1}), Na_2SO_4 (0.5 g.L^{-1}), yeast extract (0.2 g.L^{-1}), $NaHCO_3$ (0.15 g.g-COD^{-1}) and 1 mL L^{-1} of trace elements solution (Appendix A).

2.2. Liquid chromatography – electrospray ionization tandem mass spectrometry (LC-ESI-MS/MS)

DB22 precursor ions were identified using the high resolution micrOTOF QII mass spectrometer (Bruker Daltonics, Bremen, Germany), a hybrid quadrupole time-of-flight mass spectrometer, coupled with an electrospray source operating in negative mode. A standard solution of DB22 at 50 mg L^{-1} (acetonitrile:H_2O 1:1) was directly introduced in the mass spectrometer at a flow rate of 3 µL.min^{-1}. The source parameters were as follows: spray voltage, -4 kV; temperature, 180 ºC; drying N_2 flow, 4 mL min^{-1}; nebulizer N_2, 1 bar.

For DB22 quantification, we used a hybrid triple quadrupole-linear ion trap mass spectrometer QTRAP 5500 (AB SCIEX, Foster, CA) with a turbo ion spray source coupled to the LC system described above. Source-dependent parameters were optimized by flow injection analysis. The QTRAP was operated in negative ionization mode with selected reaction monitoring (SRM). All data was collected and processed in Analyst 1.6.1 software. Source parameters were optimized by direct introducing DB22 at 1 mg L^{-1} (acetonitrile:$AcNH_4$ 50 mmol L^{-1} 1:1) in the QTRAP system at a flow rate of 10 µL min^{-1}. System was set to ESI^- and optimized parameters were as follows: spray voltage, -4.5 kV; source temperature, 350 ºC; N_2 curtain gas, 20 psi; nebulizer and heater N_2, 50 psi.

The analytical column was a Poroshell 120 EC-18 50.0 mm x 3.0 mm; 2.7 µm (Agilent, Melbourne, Australia), maintained at 30 ºC and at a flow of 0.3 mL min^{-1}. Solvents were A = $AcNH_4$ 5 mM and B = acetonitrile:methanol (9:1), and the gradient program was: linear gradient from 5% B to 70% B, 1-21 min; then increased to 90% B within 2 min and kept at 90% B for 1 min; return to initial condition within 1 min. Injection volume was 10 µL.

2.3. Solid-phase extraction (SPE)

SPE extraction was conducted in 6 mL Chromabond® cartridges packed with endcapped octadecyl silica (500 mg). Conditioning was accomplished by passing 6 mL of acetonitrile followed by 6 mL of H_2O through the column. Subsequently, 10 mL of sample was loaded onto the cartridge. Washing step involved the addition of 1 mL of H_2O followed by vacuum for 30 s. The elution step was done with 2 mL of acetonitrile and sample extracts were diluted with H_2O to a 10 mL final volume.

2.4. Analytical performance parameters

Recovery was calculated following the protocols of Matuszewski et al. (2003). Briefly, two calibration curves were constructed in the effluent of an acidogenic bioreactor (pH 5.0) fed with dye-free synthetic textile wastewater. The effluent was composed mainly of volatile organic acids and solvents, whose total concentration in terms of chemical oxygen demand (COD) was 1264.8 mg L^{-1} COD. DB22 standards (120-1500 ng mL^{-1}) were spiked either *after* (Curve A) or *before* (Curve B) SPE extraction. True recovery was calculated by using the ratio between slopes of the respective calibration curves (*B/A x 100*).

Linearity, precision, and accuracy were evaluated following the protocols of ANVISA RDC 166/2017. A signal-to-noise ratio of 10 was considered for the calculation of the limit of detection.

3. Results

3.1. ESI-MS spectra

High resolution full-MS scan (50 – 3000 Da) results obtained in the micrOTOF QII mass spectrometry showed that DB22 forms molecular ions with the general expression $[M–xNa+yH]^{x-y}$, in which the maximum values of *x-y* are equal to or lower than the number of sulfonic acid groups in the molecule (Figure 3. 1). This fragmentation pattern in negative ionization mode was observed in other studies on identification of azo dyes using ESI-MS (Ding et al., 2009; Holčapek et al., 2001, 1999). The charges of the molecular ions were determined from the mass difference of the isotopic ions, i.e. three-charged ions have isotopes wi th $\Delta m/z = 0.33$ (Figure 3. 2).

Figure 3. 1. High-resolution ESI$^-$/MS spectrum of Direct Black 22 obtained in fullMS-scan mode in the range 50 – 3000 Da using a hybrid quadrupole time-of-flight mass spectrometer (micrOTOF QII).

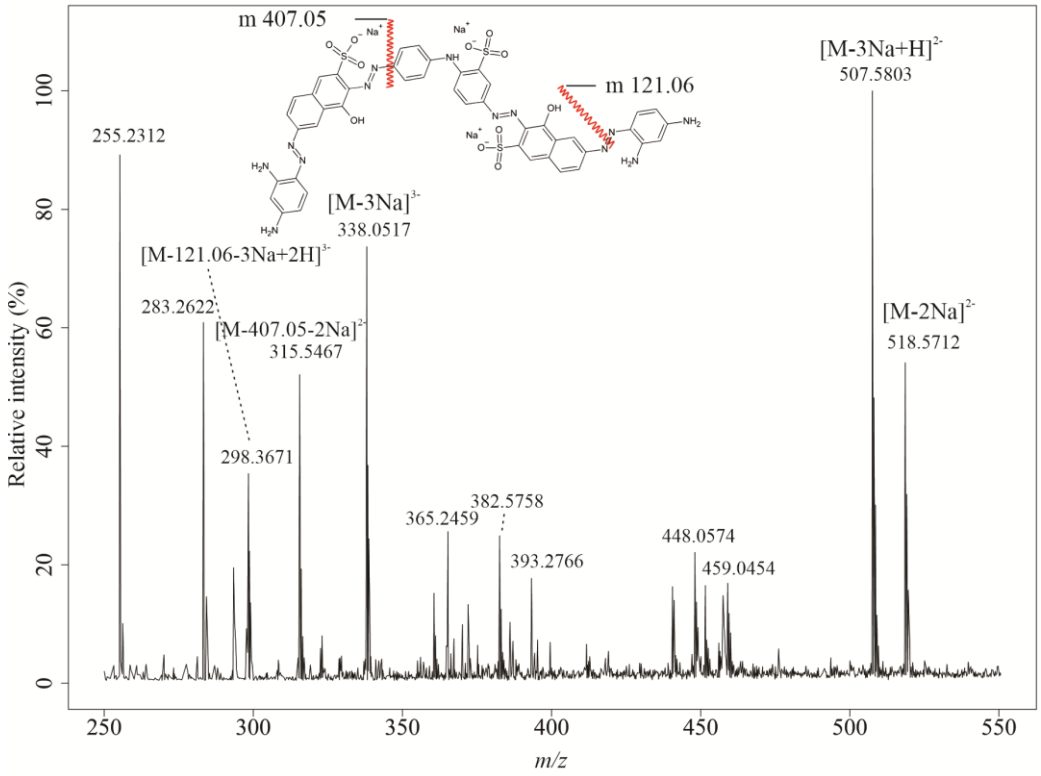

3.2. ESI-MS/MS spectra

Focusing on the quantitative purpose, DB22 ESI-MS/MS spectra was also evaluated in the QTRAP 5500 system by collision-induced dissociation of the precursor ion of *m/z* 507.6. Results revealed the acquisition of fragment ions at *m/z* 370.1, *m/z* 645.0 and *m/z* 356.0. It is worth noting that these fragments result from the cleavage of an azo bond from the precursor ion, yielding radical anions with two unpaired electrons (Figure 3. 3). This fragmentation pattern, i.e. in which cleavage occurs in the N=N double bond, was also observed by Franca et al. (2019) for a similar compound. Nevertheless, most studies within this scope have proposed a distinct MS/MS fragmentation pattern for sulfonated azo dyes (Ding et al., 2009; Reemtsma, 2003; Richardson et al., 1992; Sullivan et al., 1998). According to them, azo compounds undergo a hydrazo-azo tautomerization and split at the C-N bond on either side of the azo bonds; or even at the N-N single bond of the resulting hydrazo form. No other studies on the determination or identification of DB22 using LC-ESI-MS were found in the current literature.

Figure 3. 2. Isotopic profile of the most abundant precursor ions of Direct Black 22: **A)** isotopes of $[M-3Na+H]^{2-}$, with $\Delta m/z = 0.50$; and **B)** isotopes of $[M-3Na]^{3-}$, with $\Delta m/z = 0.33$. High resolution ESI^-/MS spectra were obtained using a hybrid quadrupole time-of-flight mass spectrometer (micrOTOF QII).

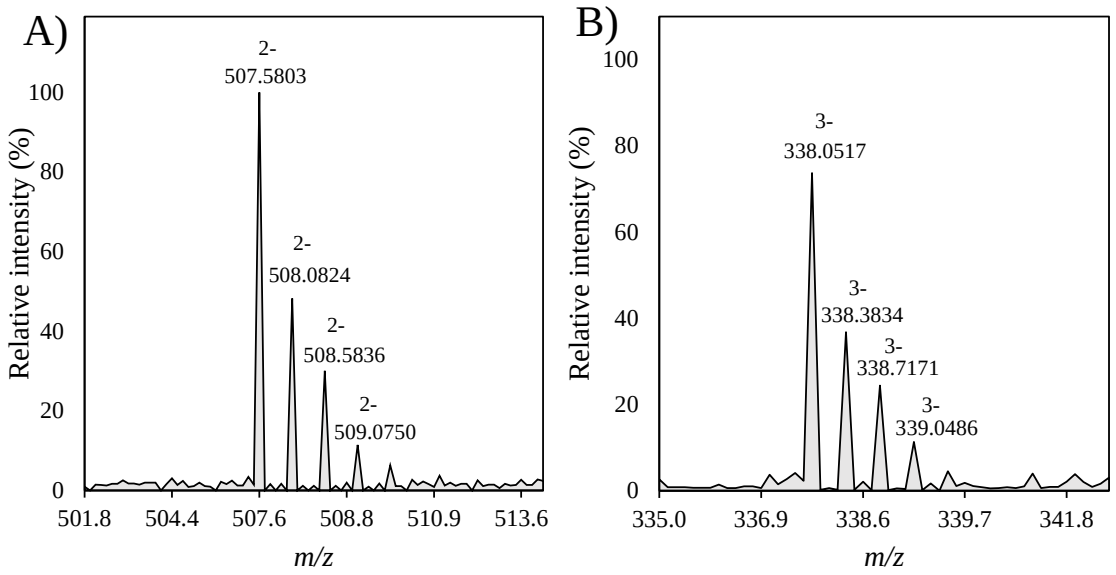

Figure 3. 3. Scheme of the proposed fragmentation pattern of DB22.

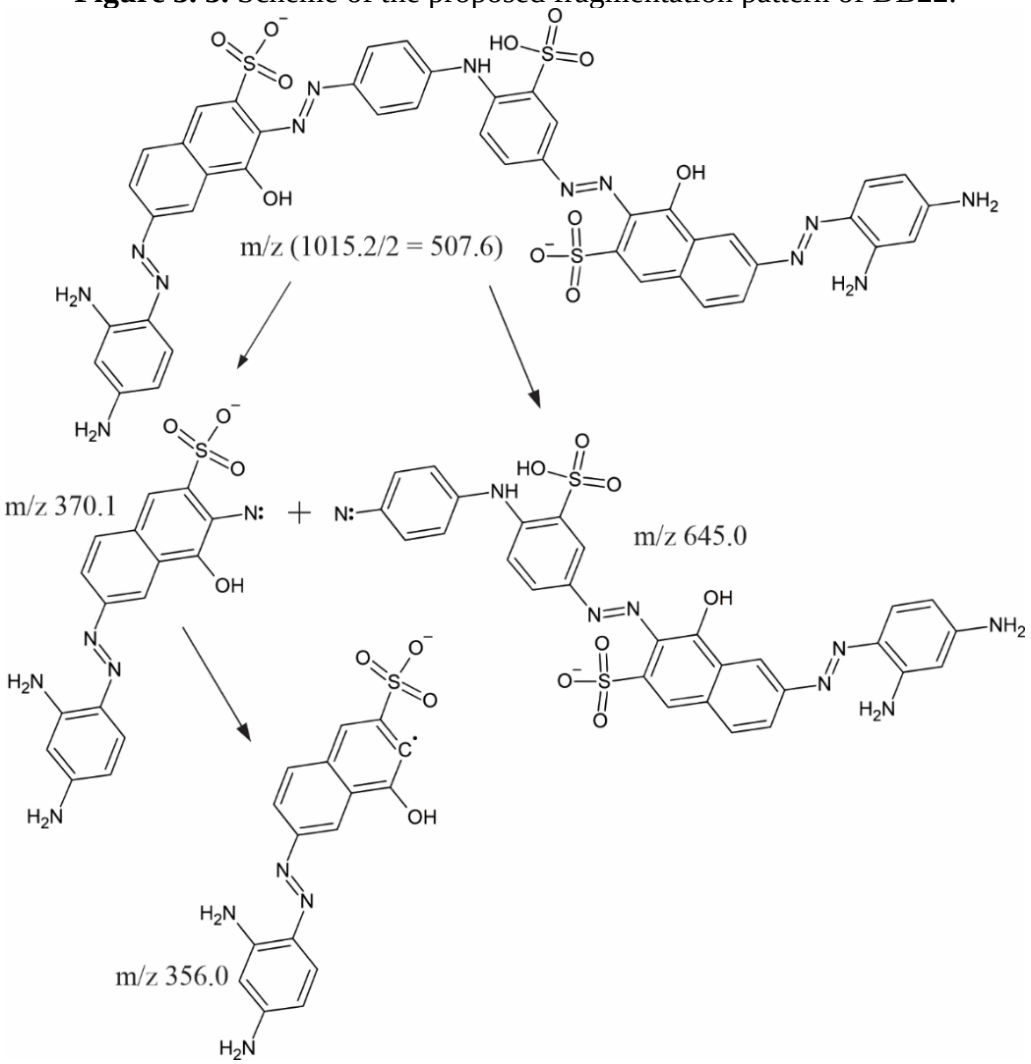

3.3. LC-MS Analysis

Detection parameters used in the LC-ESI-MS/MS analysis of DB22 are shown in the Table 3. 1. Ion pairs *m/z* 507.6 → *m/z* 370.1 were selected for quantification of DB22 due to the greater formation of product ions of *m/z* 370.1, whereas product ion *m/z* 645 was used as confirmation ion. The LC-ESI-MS/MS chromatogram of the sample matrix spiked with 1200 ng mL^{-1} of DB22, subjected to SPE extraction, is shown in the Figure 3. 4.

Table 3. 1. Optimized parameters used for the analysis of DB22 by offline SPE LC- MS/MS in ESI- ionization mode in quadrupole ion trap mass spectromer.

RT (min)	Q1		Q3		DP (eV)	EP (eV)	CE (eV)	CXP (eV)
	Precursor ion	*m/z*	Product ion	*m/z*				
12.61	$[M-3Na+H]^{2-}$	507.6	$C_{16}H_{12}N_5O_4S^{-(2\bullet)}$	370.1	-130	-10	-28	-15
			$C_{28}H_{21}N_8O_7S_2^{-(2\bullet)}$	645	-130	-10	-22	-27
			$C_{16}H_{12}N_4O_4S^{-\bullet}$	356	-130	-10	-34	-15

Figure 3. 4. LC-ESI-MS/MS chromatogram of DB22 extracted from the effluent of a biological reactor using SPE.

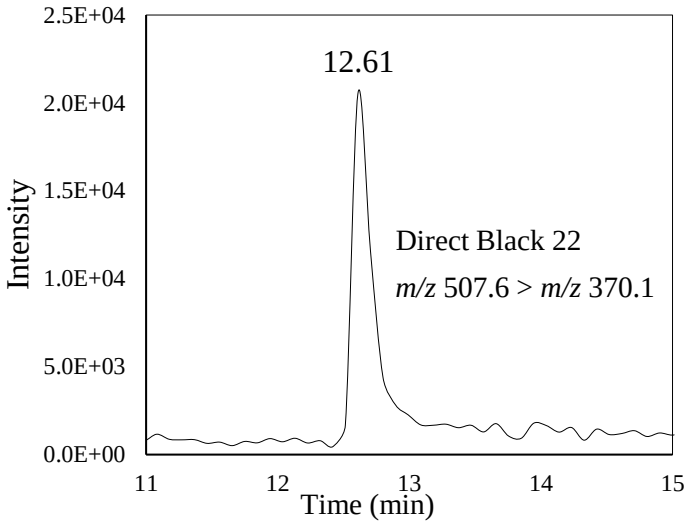

3.4. Analytical method evaluation

Linearity of the SPE LC-ESI-MS/MS method was evaluated according to Brazilian Health Surveillance Agency (ANVISA) RDC 166/2017. Eight different concentrations of DB22 (120-1500 ng mL^{-1}) were spiked in the biological reactor effluent and triplicate samples were processed using offline SPE. The calibration curve is shown in Figure 3. 5.

Figure 3. 5. Calibration curve constructed with DB22 standards extracted from the matrix by offline SPE **(A)** and residual plot for the weighted (*1/X*) linear regression model **(B)**.

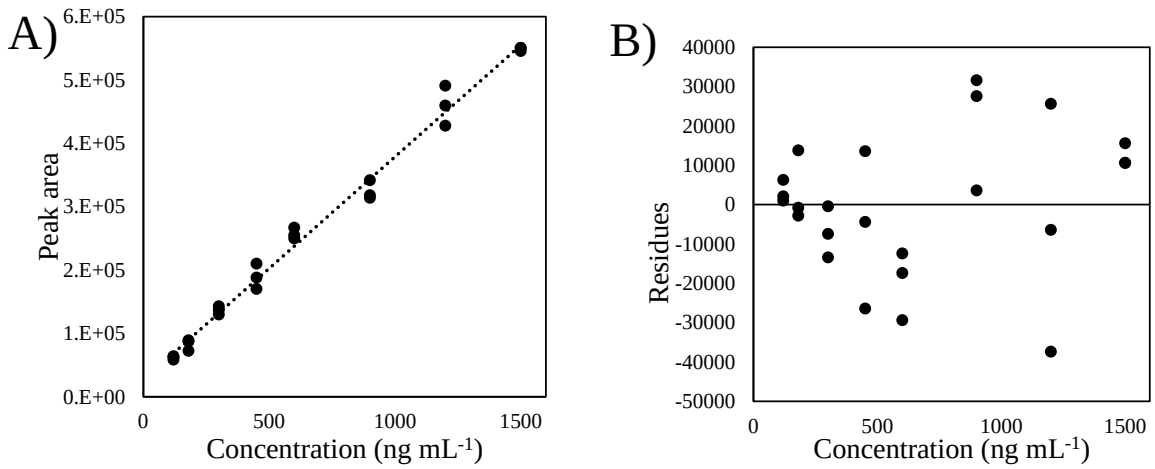

The weighted (*1/X*) linear regression model fitted better to the values of peak area. The correlation coefficient obtained for samples spiked with DB22 before SPE (Curve B) was R = 0.9947 for the working concentrations ranging from 120 to 1500 ng mL^{-1} (Table 3. 2). LoD found was 12 ng mL^{-1}. The concentrations of 30 and 60 ng mL^{-1} were also evaluated but were discarded due to the low accuracy values (% bias) of these determination points.

Table 3. 2. Parameters of the calibration curve constructed by spiking DB22 standards to the study matrix either after (Curve A) or before (Curve B) offline SPE extraction.

	LoD (ng mL^{-1})	Linear range (ng mL^{-1})	Slope	Intercept	Correlation co-efficient	Calibration
Samples spiked after extraction (Curve A)	N/A	120-600	912	41200	0.9714	1/X
Samples spiked before extraction (Curve B)	12	120-1500	360	21600	0.9947	1/X

Regression was considered statistically significant in the goodness of fit test far beyond the 5% level ($p < 0.0001$). Calculated F-value ($F_{calc} = 710.7$) is far greater than the F-distribution ($F_{crit} = 4.30$), showing that the regression is highly predictive (Box and Wetz, 1973). The ration between the lack of fit mean square and the pure error mean square was 2.4 – lower than the

F_{crit} of 2.74 –, indicating that the model fitted well to the data. The residual plot shown in Figure 3. 5-B further supports that there is no evidence of lack of fit, as points are randomly distributed.

Table 3. 3. ANOVA for the fit of a weighted (*1/X*) linear regression model to chromatographic area of DB22 peaks for samples spiked before offline SPE extraction at 5% significance level.

	Sum of squares	DF[a]	Mean square	F-value	p-value
Regression	227316940555.6	1	227316940555.6	710.7	< .00001
Residues	7037100000.0	22	319868181.8		
Lack of fit	3357213333.3	6	559535555.6	2.4	0.075762
Pure error	3679886666.7	16	229992916.7		
Total	234354040555.6	23			

[a] DF: degrees of freedom

The precision (CV) of the method was determined by triplicate analysis at all levels used in the construction of the calibration curve. The range of CV values was 0.5-15% for the set of samples spiked before extraction. Accuracy values ranged from -7.2 to 9.3%, falling within the acceptable limits, i.e. from 80 to 120% of the nominal concentration.

Table 3. 4. Precision, measured as a percentage relative standard deviation (CV), and accuracy assessments of the analythical method developed for determining DB22 in biological reactor effluents.

Expected concentration	Mean	Standard deviation	CV (%)	Accuracy (% bias)
120	111.4	7.8	7.0	-7.2
180	170.8	25.3	14.8	-5.1
300	319.4	17.6	5.5	6.5
450	467.0	55.3	11.8	3.8
600	655.7	24.6	3.8	9.3
900	841.8	42.4	5.0	-6.5
1200	1217.9	87.7	7.2	1.5
1500	1466.1	7.8	0.5	-2.3

Recovery of the proposed offline SPE protocol was obtained from the ration between the slopes of the calibration curves constructed with samples spiked before (Curve B) and after (Curve A) extraction (Figure 3. 6). A 39.5% recovery was obtained for concentrations ranging from 100 to 600 ng mL^{-1} DB22. Recovery at higher concentrations (above 600 ng mL^{-1}) could not be estimated because the response is not linear for peak areas higher than 6.0 x 10^5.

Although partial, recovery did not affect the precision and linearity of the analytical method. It should be emphasized that azo dyes are usually found in textile effluents at concentrations much higher than those used in the construction of the calibration curve in this study (120 – 1500 ng mL^{-1}). According to Amorim et al. (2013), textile wastewater containing mainly DB22 presents a color index corresponding to approximately 65 mg L^{-1} DB22. Therefore, optimization of this method to improve the SPE method aiming at higher recoveries is not necessary.

Figure 3. 6. Comparinson between calibration curves constructed with samples spiked either after (Curve A) or before (Curve B) offline SPE processing to estimate the true recovery.

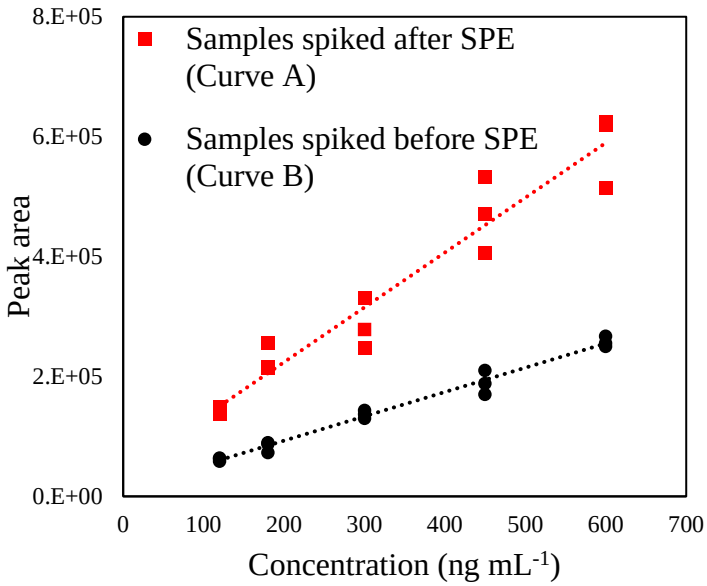

3.5. Determination of DB22 in biological reactor effluents

The anaerobic structured-bed reactor was fed with synthetic textile wastewater containing DB22 (32.5 mg L^{-1}). During the feeding preparation, DB22 in solution was heated at 85 ºC for 1 h to increase solubility in water, as this is a common step in the textile wet processing chain and dye-baths are performed at high temperatures (Santos et al., 2007). However, no DB22 signal was observed in either the feed or effluent of the bioreactor. A series of trouble-shooting procedures performed to diagnose the problem revealed that heating of DB22 was the cause of the loss in LC-MS/MS signal (Figure 3. 7).

Alternative solubilization of DB22 at lower temperatures or with sonication gave no LC-MS/MS signal as well. ESI^-/MS spectrum of the modified DB22 obtained in Full-Scan mode revealed a high abundance of single-charged fragments with *m/z* 308.1 and *m/z* 371.0, which correspond to smaller fragments of DB22 (Appendix A).

Previous research has showed that azo dyes containing naphthyl groups are expected to undergo tautomerization, as resulting hydrazone tautomers are more stable over the azo forms (Özen et al., 2007). However, double bonds of the N-N=C hydrazone groups are susceptible to hydrolytic cleavage (Itoh et al., 2008), and hydrolysis of hydrazone compounds under either acidic or basic conditions has been reported in several studies (Buss and Ponka, 2003; Kalia and Raines, 2008; Richardson et al., 1989). The mechanism of Schiff bases hydrolysis (including hydrazones) was postulated by Bruylants and Feytmants-de Medicis (2010) and involves a pre-ionization equilibrium followed by nucleophilic attack on the protonated Schiff base. Moreover, the rate of hydrolysis increases with pH as a consequence of the ionization of hydroxyl groups, further supporting that DB22 undergoes transformation under alkaline conditions. The proposed mechanism of DB22 hydrolysis is shown in Figure 3. 8.

Figure 3. 7. Troubleshooting procedures to diagnose failures in LC-MS/MS detection of Direct Black 22 (DB22) in wastewater. **A)** steps performed in the contruction of the calibration curve; **B)** steps involved in the bioreactor feeding preparation, including several methods of DB22 solubilization assessed; and **C)** further actions taken to test whether SPE was the cause of failure in the DB22 detection.

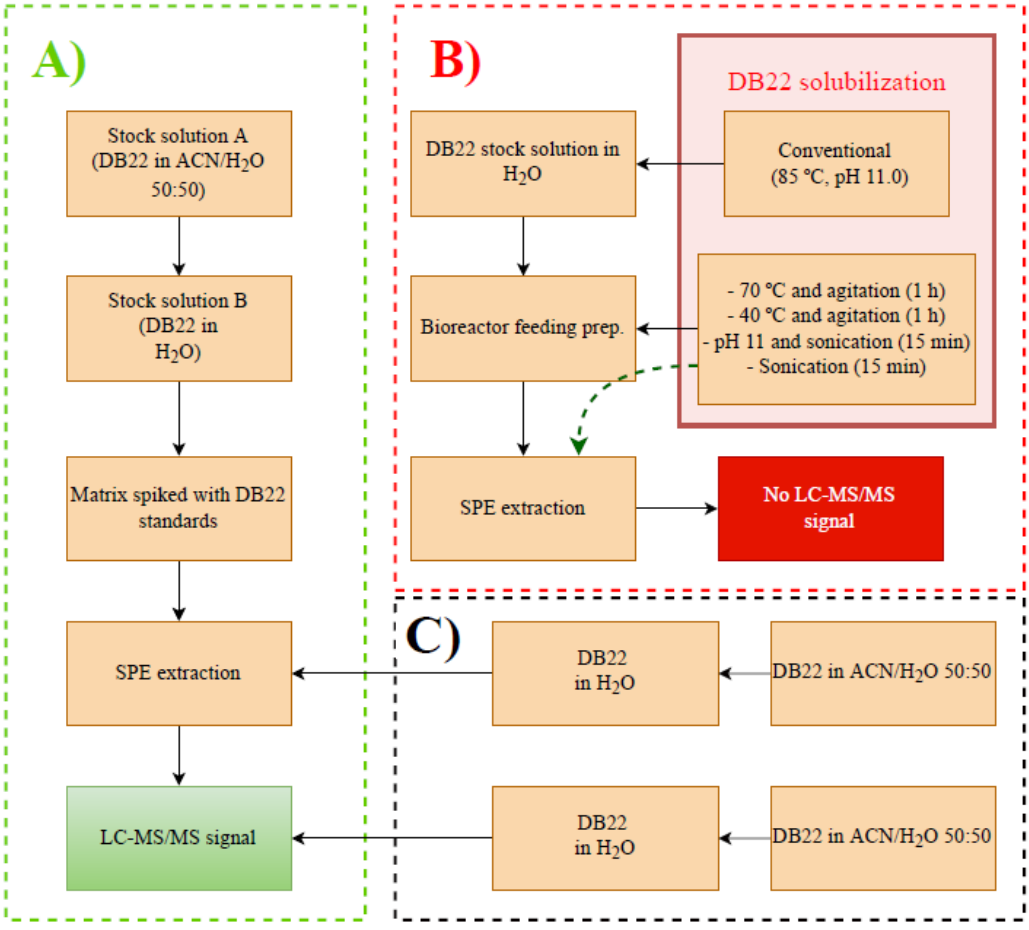

4. Discussion

Reactive dyes are known to react with either cellulose or water at high temperatures and under alkaline conditions (Weber and Stickney, 1993). For this reason, studies on degradation of reactive azo dyes are often conducted after hydrolysis of these compounds to simulate their actual states in wastewater. Hydrolysis is usually conducted at pH 10-12, temperatures ranging from room- to boiling-temperature (usual range is 70-85 ºC) and for the period of 1-3 h (de Souza et al., 2010; Dos Santos et al., 2003; Gottlieb et al., 2003; Rehorek et al., 2004; Weber and Stickney, 1993; Zhang et al., 2007).

Figure 3. 8. Proposed mechanism of hydrolysis of the azo dye Direct Black 22 (DB22) at high temperature and alkaline conditions, yielding smaller fragments with *m/z* 308.08 and *m/z* 371.04.

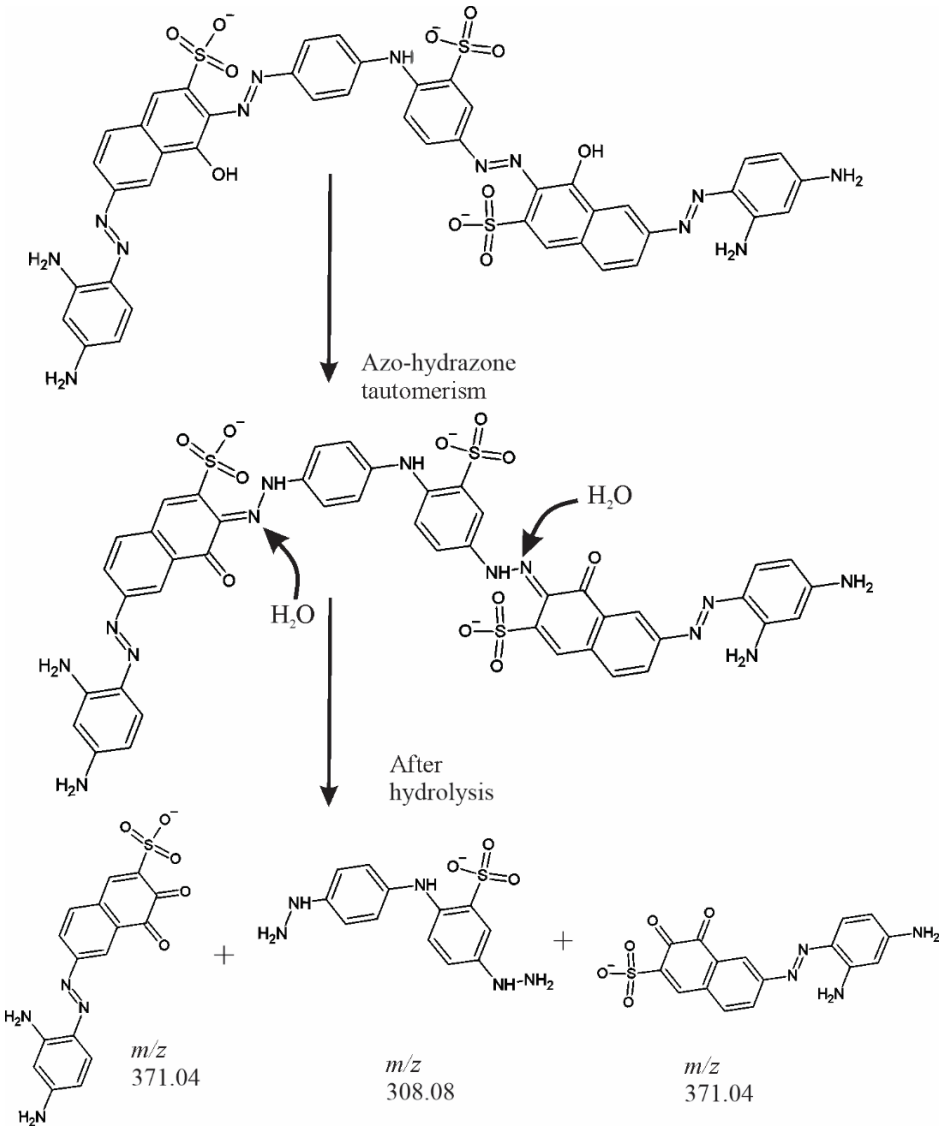

However, reactivity is not a proven attribute among direct dyes. Many studies conducted with this class of dyes do not use any type of thermal or alkaline treatment prior to experiments (Malik and Saha, 2003; Rehorek et al., 2004; Shi et al., 2007). Our observations with DB22 seems to be controversial, as this dye was found to be relatively insoluble in water unless it undergoes thermal treatment. Heating of the dye solution at 85 ºC and pH 11 was also performed in other studies using DB22 to increase its solubility in water (Amorim et al., 2013; Carvalho et al., 2020; Florêncio et al., 2021; Gavazza et al., 2015; Menezes et al., 2019; Oliveira et al., 2020).

A previous evidence of hydrolysis among direct dyes was observed by Byberg et al. (2013). According to their findings, several dyes belonging to this class were transformed after heating at 80 ºC for 90 min, and modified direct dyes were more recalcitrant to photocatalytic degradation. Although the authors used the term *hydrolysis* to refer to the transformation in the azo dyes, chemical structure of the modified compounds was not assessed. In the case of DB22, we observed that the dye was partially fragmented upon solubilization at temperatures ranging from 40–85 ºC or sonication and under pH 11 or natural pH (pH 10.4 in solution). We proposed a mechanism of DB22 hydrolysis in which the compound is subjected to an azo-hydrazone tautomerism followed by hydrolytic cleavage of the resulting C=N double bonds. Hydrolysis was less significative in freshly prepared solutions of DB22 in acetonitrile:H_2O 1:1.

DB22 hydrolysis raises a question on whether MS based techniques are more appropriate than conventional color analysis for monitoring the azo dye biodegradation in biological reactors, in spite of the limitations of the later regarding the selectivity. Dye impurities, which result mainly from incomplete reactions during the dye synthesis, may have similar properties as the dye's itself and cannot be targeted by the LC-ESI-MS method as well. However, this analysis can be tailored to consider the detection of representative hydrolyzed fragments of azo dyes in wastewater, of whom the removal is an indicative of the overall removal efficiency of azo dye fragments in the system.

5. Conclusions

The extraction method and sample preparation, although without thorough optimization, met the needs of the analysis, particularly because working concentrations are high. Recovery was partial but did not affect the performance of the analytical parameters (particularly precision and linearity). However, no LC-ESI-MS/MS signal was observed after solubilization of DB22 using standard procedures to simulate the steps involved in the textile wet processing

chain. Further analysis showed that DB22 is unstable and undergoes hydrolysis at high temperatures and under alkaline conditions. These results show that the LC-ESI-MS/MS analysis should be tailored to consider the detection of the hydrolysed fragments of azo dyes in wastewater for appropriate detection. Color remains as a reliable method for the monitoring of direct azo dyes which are unstable in solution, but azo dye concentrations cannot be determined based on the reflection properties of these dyes solely.

Acknowledgment

This work was supported by the Fundação do Amparo à Pesquisa do Estado de São Paulo (process numbers 2015/06246-7 and 2018/24269-2) and the Coordenação de Aperfeiçoamento de Pessoal de Nível Superior (CAPES) – Brazil (Finance Code001). The authors also would like to thank Dr. Guilherme Miola Titato for his technical and scientific support.

Chapter 4

Two-stage anaerobic digestion system for biotransformation of an azo dye in the presence of sulfate: minimizing competition for reducing equivalents

Abstract. Anaerobic treatment of azo dyes is particularly challenging in the case of wastewaters containing sulfate. We studied the use of multiple stage anaerobic system to minimize the impacts of sulfidogenesis and methanogenesis on the decolorization and biotransformation of an azo dye. The system was composed of a 1st-stage anaerobic structured-bed reactor (R1), designed for removal of color, followed by a 2nd-stage upflow anaerobic sludge blanket reactor (R2) intended for organic matter and sulfate removals. Results showed that near complete decolorization was achieved in R1 when a dye loading rate of 222 ± 9 mg L^{-1} d^{-1} was applied. Sulfidogenic activity in this reactor was negligible due to the low pH and did not impair reductive decolorization. After increasing dye load, decolorization efficiency in R1 decreased, but gradually recovered in the following weeks. R2 kept decolorization around 90% even when R1 presented decreased efficiencies, keeping up with overall performance. Residual organic matter in the system's final effluent consisted of aromatic amines and other dye fragments recalcitrant to anaerobic digestion (AD), whose concentrations further increased after treatment in R2. The average volumetric methane production rate achieved in R2 was 472 ± 111 mL L^{-1} d^{-1}. The two-stage AD system provided enhanced removals of color, organic matter and sulfate by eliminating issues related to the competition for reducing equivalents.

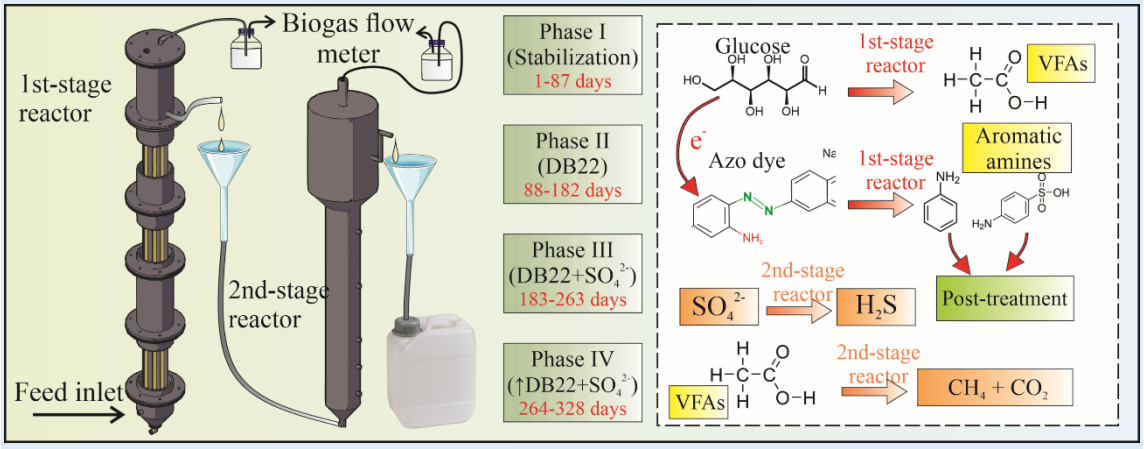

A modified version of this chapter was published in:

Oliveira, J.M.S., Damianovic, M.H.R.Z., Foresti, E., 2022. Two-stage anaerobic digestion system for biotransformation of an azo dye in the presence of sulfate: Minimizing competition for reducing equivalents. J. Water Process Eng. 47, 102819. https://doi.org/10.1016/j.jwpe.2022.102819

1. Introduction

Bioremediation has proven to be a cost-effective and environmentally sustainable solution for the treatment of wastewaters containing azo dyes (Menezes et al., 2019; Oliveira et al., 2020). Reductive decolorization is a common choice among the biological processes due to advantages such as reduced sludge generation, potential for biogas production and applicability in continuous systems using mixed microbial consortium. Nevertheless, textile wastewaters are usually rich in sulfate, which were found to negatively affect color removal in anaerobic systems in the case of specific azo dyes (Amaral et al., 2017, 2014).

Sulfate reduction is not desired in biodigesters treating azo dye due to the consumption of electrons that are not associated with reductive decolorization (Santos et al., 2007), in a mechanism similar to the competition that occurs between sulfate reducing bacteria and methanogens (Bijmans et al., 2011). Dai et al. (2018) observed that methanogens may also compete with azo reducers for the electrons released from the organic matter oxidation. AD in multiple stages seems appropriate for solving this issue by providing environments with singular characteristics.

In a two-stage AD system, sulfidogenesis and methanogenesis can be partially inhibited by either the low pH or the high organic loading rate (OLR) in the 1st-stage reactor (Ripley et al., 1986; Sharma et al., 2014; Wang and Yin, 2017), while stimulated in the following unit. Then, electrons from the co-substrate could be preferentially used to reduce azo compounds. A few studies have used two-stage anaerobic systems for removal of azo dyes before (Firmino et al., 2010; Talarposhti et al., 2001), but these experiments were not carried under sulfidogenic conditions. To the best of our knowledge, the use of multiple stages aiming at minimizing the impacts of both sulfidogenesis and methanogenesis on reductive decolorization was not investigated before.

The use of a preliminary unit specially designed for decolorization and conversion of carbohydrates has additional advantages. Shorter hydraulic retention times (HRTs) and higher azo dye loads can be applied in these reactors, reducing capital and operating costs. Moreover, this system's configuration can ease our understanding on the role of distinct groups of microorganisms on anaerobic treatment of azo dye wastewaters. For instance, there is evidence that acidogens play a major role in decolorizing processes (Cervantes et al., 2005; Firmino et al., 2010), while the involvement of methanogenic archaea is

rather controversial. A few authors have stated that methanogenic archaea contribute in reductive decolorization (Pandey et al., 2007; Plumb et al., 2001; Santos et al., 2006). Other studies have shown that methanogens and azo reducers may compete for electron donors, and high concentration of azo dyes can inhibit methane production (Cervantes et al., 2005; Dai et al., 2018, 2016).

In this study, we assessed the use of a two-stage AD system for enhanced biotransformation of a model azo dye, Direct Black 22 (DB22), in the presence of sulfate ions. DB22 is extensively used in the Brazilian textile industry (Amaral et al., 2014) and was proven to be toxic to several bioindicators (Carvalho et al., 2020; Oliveira et al., 2020). Although the ability of azo dyes to be outcompeted depends on the dye's redox potential (Dubin and Wright, 1975), DB22 was showed to be affected in an experiment using single-stage anaerobic treatment (Amaral et al., 2014). The 1st-stage consisted of an anaerobic structured-bed reactor (AnSTBR), a configuration that was previously studied for simultaneous removal of azo dyes and sulfate (Florêncio et al., 2021); and the 2nd-stage was an upflow anaerobic sludge blanket reactor (UASB). The system was operated under electron-limiting conditions, as showed by mass balance analysis. We further monitored biogas production, organic matter conversion, and the concentration of total aromatic amines (TAA) in the system, providing a comprehensive view of the proposed system.

2. Material and Methods

2.1. Chemicals and synthetic textile wastewater

DB22 (CAS 6473-13-8) was acquired from the dye supplier Aupicor Quimica© (Pomerode, SC) and had a molecular weight of 1083.97 g mol^{-1} and a 42% purity. Physical-chemical properties of the dye are shown in Appendix B. Dye hydrolysis was conducted by increasing pH to 11 and heating at 80 ºC for 1 hour (Santos et al., 2004). Synthetic textile wastewater was based on the composition of real textile effluent (Amorim et al., 2013) and contained: DB22 (0-65 mg L^{-1}), glucose (1.60 g COD L^{-1}), KH_2PO_4 (0.25 g L^{-1}), NaCl (0.50 g L^{-1}), Na_2SO_4 (0-0.50 g L^{-1}), yeast extract (0.20 g L^{-1}), $NaHCO_3$ (0.15 g g^{-1} COD) and 1 mL L^{-1} trace elements solution (composition is shown in the Appendix B section). The pH of the feed was kept at 7.0 ± 0.1.

2.2. Two-stage system setup and operational strategies

The two-stage AD system was composed of an AnSTBR, R1, designed for removal of color, followed by an UASB, R2, intended for organic matter and sulfate removals. R1 was built with a cylindrical shape (internal diameter = 64 mm and height = 650 mm), a conical bottom (height = 80 mm) and a headspace 150 mm tall. Total working volume was 2.45 L. The fixed-bed was constructed with seven polyurethane foam rods (10x10x650 mm) strategically placed along a vertical axis made with galvanized wire. R2 had a cylindrical shape (internal diameter = 52 mm and height = 400 mm) and a gas-solid-liquid triphasic separator (height = 151 mm), with a total working volume of 1.35 L. Details for both the reactors design are shown in the Appendix B section.

R1 and R2 were operated in series and in continuous flow mode for a period of 328 days at mesophilic temperature (30 ºC). Applied OLRs, expressed as chemical oxygen demand (COD), were 11.7 and 2.0 g L^{-1} d^{-1}, respectively, in reactors R1 and R2. Corresponding HRT values were 3.5 and 16 h. R1 was fed with the synthetic textile wastewater described in Section 2.1. R2 was fed with the effluent from R1 after the addition of $NaHCO_3$ (0.70 g L^{-1}) to keep pH at around 6.0. Bioreactors were inoculated with anaerobic sludge from a full scale UASB reactor (Pereira – SP, Brazil) processing wastewater from a poultry slaughterhouse. For R1, the sludge was previously heat-treated at 100 ºC for 1 h for inactivation of methanogenic archaea (Wang and Yin, 2017). Strategies used in the operation of the AD system are shown in **Table 4. 1**.

Table 4. 1. Strategies used in the operation of the two-phase AD system.

Operational phase	Operation days	Description
PI	1-87	Start-up and stabilization
PII	88-182	32.5 mg L^{-1} DB22
PIII	183-263	32.5 mg L^{-1} DB22 + 338 mg L^{-1} SO_4^{2-}
PIV	264-328	65 mg L^{-1} DB22 + 338 mg L^{-1} SO_4^{2-}

2.3. Physical-chemical analysis

COD, sulfate (SO_4^{2-}), sulfide (S^{2-}), pH and volatile suspended solids (VSS) were measured according to the protocols of the APHA Standard Methods (2005). For SO_4^{2-} and S^{2-} analysis, liquid samples were collected using a syringe to avoid exposure to the atmosphere and preserved in flasks containing hydrochloric acid (1 M) and zinc acetate (1 M), respectively. Sulfide interference on COD test was eliminated by adding zinc sulfate in excess to the samples. Soluble carbohydrates (CH) and lactic acid concentrations were determined according to DuBois et al. (1956) and Taylor (1996), respectively. Color removal was evaluated using the spectra record method (Wu et al., 1998; APHA, 2005), after diluting samples with phosphate buffer (10.86 g L^{-1} NaH_2PO_4 e 5.98 g L^{-1} Na_2HPO_4) (Firmino et al., 2010). DB22 biodegradation was qualitatively assessed using the UV-VIS spectrophotometric method (Pinheiro et al., 2004). TAA were determined colorimetrically (Jayapal et al., 2018), and results were expressed in terms of concentration of sulfanilic acid.

2.4. Gas phase monitoring

Biogas composition in R1 (H_2, CH_4 and CO_2) was measured using a Shimadzu GC-2010 with thermal conductivity detector (TCD), a Carboxen®-1010 PLOT column (0.53 mm x 30 m x 30 µm) and using argon as carrier gas (Perna et al., 2013). In R2, biogas composition (H_2S, CH_4 and CO_2) was analyzed using a Shimadzu GC-2014 equipped with TCD, a HP-PLOT/Q column (0.53 mm x 30 m x 40 µm) and using H_2 as carrier gas (Lebrero et al., 2016). Biogas flow rate (BFR) was continuously measured using a system composed of a glass column (U-tube) filled with NaCl 3.4 mol L^{-1} (pH 2.0) and an Arduino® microcontroller (Gyalai-Korpos et al., 2014).

2.5. Performance evaluation

Response variables used to assess the performance of the two-phase AD system included decolorization (in %), COD and SO_4^{2-} removals (in %), conversion of total CH (CE_{CH}, in %), volumetric hydrogen production rate (VHPR, in mL H_2 L^{-1} d^{-1}), volumetric methane production rate (VMPR, in mL CH_4 L^{-1} d^{-1}) and molar methane flow (MMF, in mmol CH_4 d^{-1}). Equations for calculating these variables are shown below:

$$Decolorization = \frac{\int_{400\,nm}^{700\,nm} A_{feed} \cdot \mathrm{d}\lambda - \int_{400\,nm}^{700\,nm} A_{effl} \cdot \mathrm{d}\lambda}{\int_{400\,nm}^{700\,nm} A_{feed} \cdot \mathrm{d}\lambda} \cdot 100 \quad \text{(Eq. 1)}$$

in which A_{feed} is the absorbance of the feed; A_{effl} is the absorbance of the effluent; and dλ is an infinitesimal wavelength interval.

$$\mathrm{VHPR} = \frac{\mathrm{BFR} \cdot \%\mathrm{H_2} \cdot P_{local} \cdot T_{standard}}{V_R \cdot T_{local} \cdot P_{standard}} \quad \text{(Eq. 2)}$$

$$\mathrm{VMPR} = \frac{\mathrm{BFR} \cdot \%\mathrm{CH_4} \cdot P_{local} \cdot T_{standard}}{V_R \cdot T_{local} \cdot P_{standard}} \quad \text{(Eq. 3)}$$

in which BFR is the biogas flow rate; $\%H_2$ and $\%CH_4$ are, respectively, the hydrogen and methane contents in the biogas; P_{local} and $P_{standard}$ are, respectively, the local and standard atmospheric pressure (atm); T_{local} and $T_{standard}$ are, respectively, the temperature measured in the gasometer and the standard temperature (K); and V_R is the working volume of the reactor (L).

$$MMF = \frac{\mathrm{BFR} \cdot \%\mathrm{CH_4} \cdot P_{local}}{T_{local}\,\mathrm{R}} \quad \text{(Eq. 4)}$$

in which R is the universal gas law constant (0.082 atm L mol^{-1} K^{-1}).

The mass balance for R2 was calculated using the Eq. (5).

$$Mass\ balance\ (\%) = \frac{(COD_{CH4,b} + COD_{CH4,d} + COD_{VSS} + COD_{sulf} + COD_{residual})}{COD_{applied}} \cdot 100 \quad \text{(Eq. 5)}$$

in which $COD_{CH4,b}$ and $COD_{CH4,d}$ (in mg d^{-1}) are the COD corresponding to both the fraction of methane in the biogas and the fraction of methane dissolved in the liquid phase, respectively; COD_{VSS} (in mg d^{-1}) is the COD removed for cell synthesis; COD_{sulf} (in mg d^{-1}) is the COD requirement for sulfate reduction; $COD_{residual}$ (in mg d^{-1}) is the remaining COD in the effluent from R2; and $COD_{applied}$ (in mg d^{-1}) is the total COD applied to R2. Parameters were calculated using the Eq. (4), (6), (7) and (8), as well as the following COD conversion factors: (i) 4.00 g COD g^{-1} CH_4, given by the oxidation reaction (1); (ii)

1.42 g COD g^{-1} VSS, given by reaction (2); and (iii) 1.5 g SO_4^{2-} g^{-1} COD (Deng et al., 2016).

$$CH_4 + 2O_2 \rightarrow CO_2 + 2H_2O \quad (Reaction\ 1)$$

$$C_5H_7O_2N + 5O_2 \rightarrow 5CO_2 + 2H_2O + NH_3 \quad (Reaction\ 2)$$

$$X_{CH4} = M_{CH4} \cdot P_{CH4} \cdot K_H \quad (\mathrm{Eq.}\ 6)$$

in which X_{CH4} is the dissolved methane concentration (g L^{-1}); P_{CH4} is the methane partial pressure in the biogas (atm); and K_H is the Henry's law constant for methane in water at 25 ºC ($1.34 \cdot 10^{-3}$ mol L^{-1} atm^{-1}) (Godoi et al., 2015).

$$COD_{applied} = COD_{feed} \cdot \mathrm{Q} \quad (Eq.\ 7)$$

$$COD_{residual} = COD_{effl} \cdot \mathrm{Q} \quad (Eq.\ 8)$$

in which COD_{feed} is the total COD concentration in the feed (mg L^{-1}), COD_{effl} is the soluble COD concentration in the effluent (mg L^{-1}) and Q is the flow rate in the bioreactor (L d^{-1}).

A more detailed step-by-step calculation is provided in the published dataset (Oliveira, 2022).

2.6. Statistical analysis

Statistical analysis was performed to compare TAA values in the effluents from R1 and R2 within the same operational phase. Data normality was previously assessed using the Shapiro-Wilk test. Since some of the data subsets presented skewed distribution, the non-parametric Kruskal-Wallis test was used to test for differences between TAA values at a significance level of $p \leq 0.05$. Calculations were performed using the PAST 4 software (Hammer et al., 2001).

3. Results and Discussion

3.1. First-stage reactor: organic matter conversion and biogas production

An average OLR of 11.70 ± 0.93 g L^{-1} d^{-1} was applied to R1 during the 328 days of continuous operation (Figure 4. 1-A). The average OLR in the effluent was 9.80 ± 0.77 g L^{-1} d^{-1}, which represented an average COD removal efficiency of 16.1 ± 5.0%. Similar performances were observed in other studies involving the use of acidogenic systems for the treatment of industrial effluents (Oktem et al., 2006; Saddoud et al., 2007; Talarposhti et al., 2001). Organic matter removal in acidogenic systems is related to cell synthesis and therefore are typically low. COD removal was stable through all operation and was not affected by either the addition of DB22 (PII) or sulfate (PIII).

CE_{CH} was around 99% during most of the operation (Figure 4. 2-B). Nevertheless, we observed a drop in CE_{CH} to nearly 70% after the addition of 32.5 mg L^{-1} DB22 in PII (residual concentration of CH in the effluent was around 500 mg L^{-1}). This was likely caused by a toxic effect of the azo compound to the microorganisms involved in the acidogenesis process. CE_{CH} above 90% was reestablished in R1 in the 14th day after transition to PII, suggesting that microorganisms became acclimated to the dye and to intermediates of the reductive decolorization.

There was a correlation between the BFR and the VHPR in the beginning of R1 operation (Figure 4. 2). In the 7th day, biohydrogen ($bioH_2$) content reached 45.9%. Maximum BFR and VHPR values were, respectively, 3376 mL d^{-1} and 633 mL L^{-1} d^{-1}. This was followed by a drop in bioH2 production, which was nearly zero during the rest of the operation. Since then, VHPR was not correlated with BFR and carbon dioxide was the main biogas component.

Instability in $bioH_2$ production is one of the main challenges encountered by those studying energy recovery from wastewater. Some of the largest problems reported are shifts in the structure of the microbial community – which causes changes in the end products of the microbial metabolism –, and the presence of both hydrogen-consuming microorganisms and organisms that compete for the organic substrate, e.g. lactic acid bacteria (Castelló et al., 2019). However, we did not observe an increase in methane production concurrently with the drop in the hydrogenogenic activity; and lactic acid concentration was below 32.4 mg L^{-1} during all system's operation. Therefore, the decrease in VHPR was possibly a result of the increase in activity of homoacetogens and/or

propionic fermenters (Castelló et al., 2019; Madigan et al., 2014). In fixed-bed continuous bioreactors, this can be seen as a consequence of the drop in the specific organic loading rate (Del Pilar Anzola-Rojas et al., 2015). Because hydrogen is a good electron donor for dye reduction (Li et al., 2014), it is important that it remains in the system and is not released as a biogas component, as it was observed in this experiment.

Figure 4. 1. Load and conversion of organic matter in the first-stage reactor (R1) as a function of time. **A)** Influent and effluent organic loading rate (OLR) and removal of chemical oxygen demand (COD); and **B)** carbohydrates (CH) conversion efficiency.

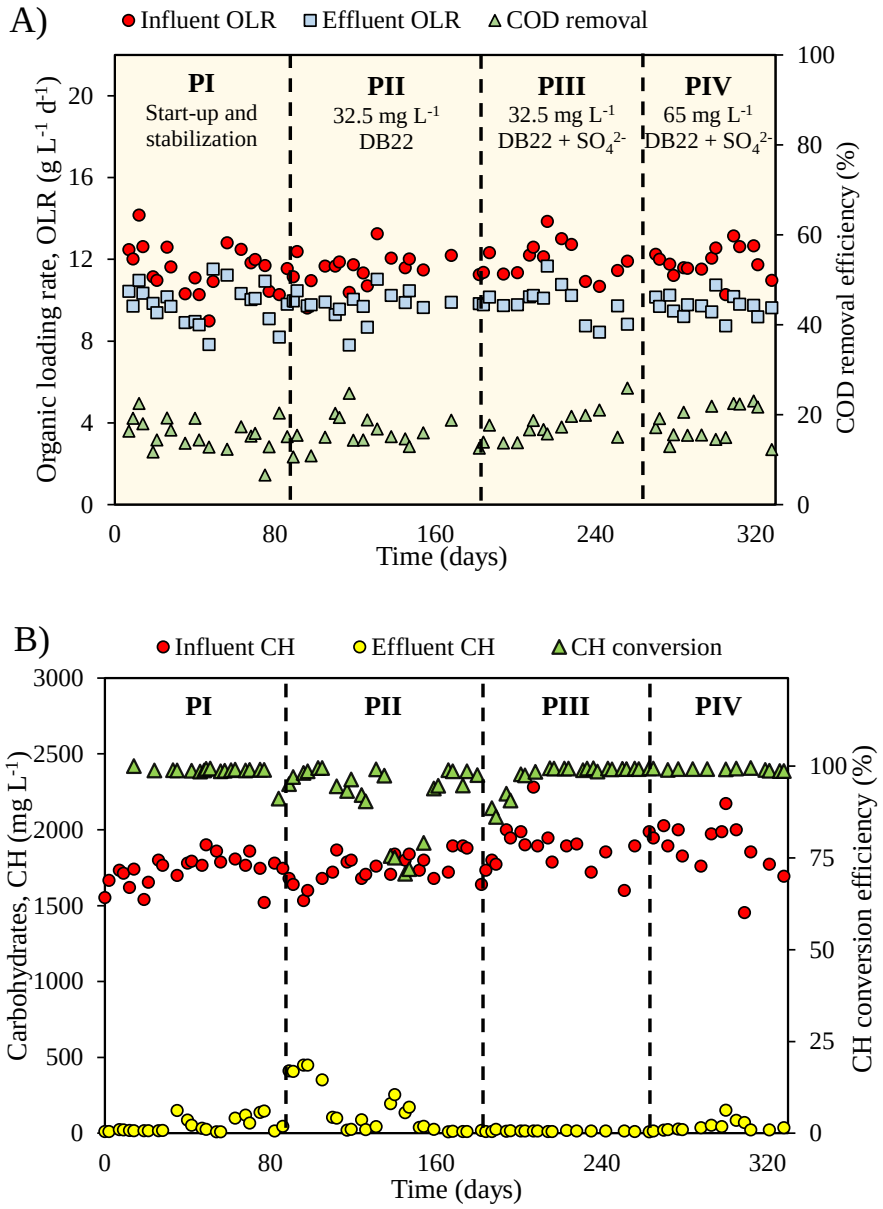

Figure 4. 2. Biogas flow rate (BFR) and volumetric hydrogen production rate (VHPR) as a function of time in the first-stage reactor (R1). Parameters were calculated at standard temperature and pressure (273.15 K and 1 atm).

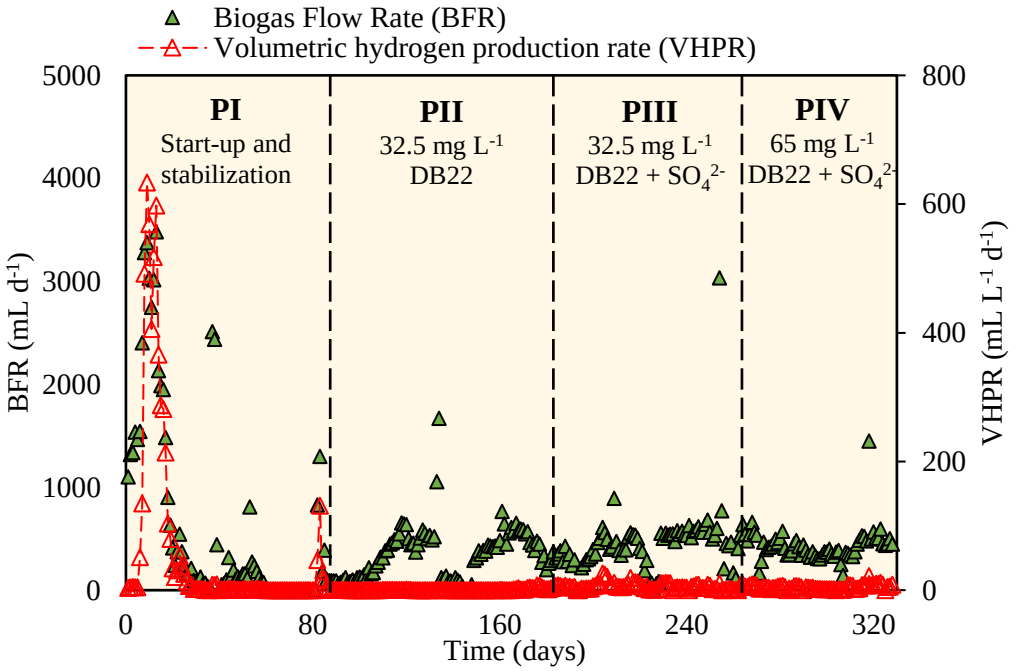

3.2. Second-stage reactor: organic matter conversion and biogas production

R2 was fed with the effluent from R1 after the addition of $NaHCO_3$ (0.70 g L^{-1}) for alkalinity correction. The average OLR applied to R2 was 1.96 ± 0.15 g L^{-1} d^{-1}. In phase PI, R2 presented a COD removal efficiency close to 100% (residual COD < 10 mg-O_2 L^{-1}), as shown in Figure 4. 3. COD remaining in the system's effluent increased to 28.0 ± 5.3 mg-O_2 L^{-1} after the addition of DB22 (32.5 mg L^{-1}) in phase PII, meaning that this residual organic matter consists of recalcitrant byproducts from the azo reduction (Pandey et al., 2007). Residual organic matter concentration fluctuated to 25.1 ± 7.3 mg-O_2 L^{-1} after establishment of sulfidogenesis, in phase PIII, which is assumed to be a negligible difference when considering the standard deviation of the mean values. In phase PIV, the increase in DB22 concentration to 65 mg L^{-1} led to a proportional increase in the average COD level to 40.3 ± 6.7 mg-O_2 L^{-1}, reinforcing that the remaining organic compounds are byproducts from the DB22 decolorization.

R2 stable operation and efficient performance can also be inferred from analysis of data from biogas contents (Figure 4. 4-A). We observed low variations in the fractions of methane (84.1 ± 2.8%) and carbon dioxide (15.9 ± 2.8%) in the biogas during the startup phase (days 1–47). After the addition of DB22 (phase PII), there was a drop in the

methane content (days 48–62) from approximately 89 to 76%, with a subsequent increase in the fractions of carbon dioxide. At the time, CH_4/CO_2 ratio lowered to values below 3.0. A similar trend was observed for the VMPR, which decreased from 537 ± 88 to as lows as 154 mL L^{-1} d^{-1} on transition to phase PII (Figure 4. 4-B). These results show that DB22 and/or intermediates from azo reduction negatively affect the microorganisms involved in methanogenesis. Methane production gradually increased back to initial levels as of the 89th day of system's operation, stabilizing at approximately 550 mL L^{-1} d^{-1}, showing that R2 is resilient to the azo dye. After sulfidogenesis was stablished (phase PIII), we did not observe further fluctuations in the methane production, while sulfide content in the biogas oscillated from 0.60 to 1.48% in this period, which corresponded to volumetric production rates from around 4 to 12 mL L^{-1} d^{-1}. This low fraction of sulfide is expected due to the pH of the effluent from R2 (pH 7.4-8.3), condition in which the predominant sulfide specie is the HS^- ion, therefore remaining in solution (Vismann, 1996). Further increasing DB22 concentration to 65 mg L^{-1} also did not affect methanogenesis.

Figure 4. 3. Residual chemical oxygen demand (COD) and COD removal eficiency in the second-stage reactor (R2) as a function of time.

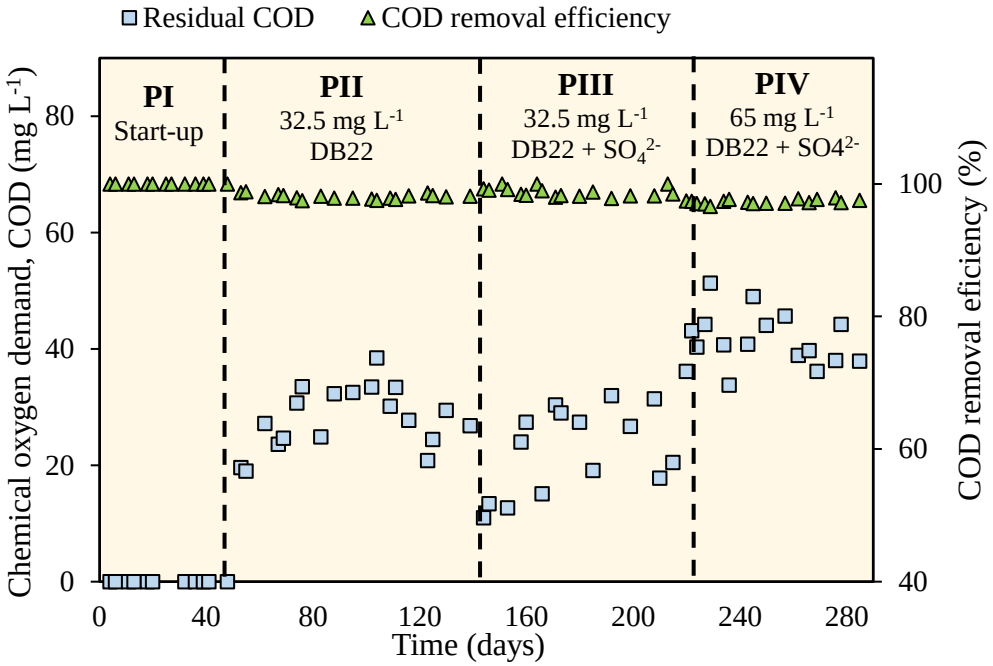

Figure 4. 4. Biogas production in the second-stage reactor (R2) as a function of time. **A)** carbon dioxide, methane, and hydrogen sulfide contents in the headspace. **B)** biogas flow rate (BFR) and volumetric methane production rate (VMPR). Parameters were calculated at standard temperature and pressure (273.15 K and 1 atm).

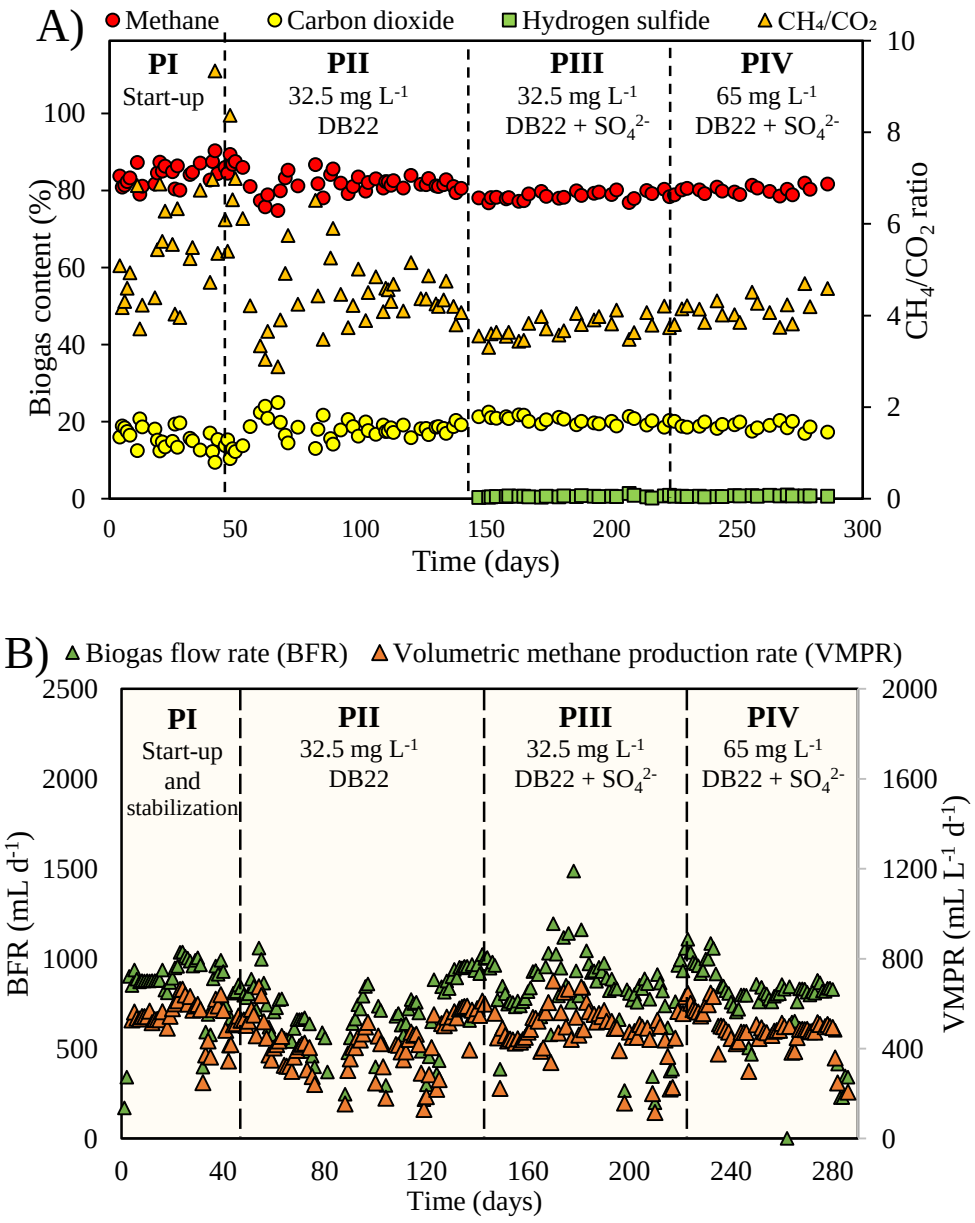

3.3. Dynamics of sulfate reduction and sulfide production

Concentration of sulfate ions in R1 was monitored during phases PIII and PIV of the experiment, after which this salt was added to the system. Figure 4. 5 shows that sulfate concentration in the effluent from R1 ranged from 211 to 334 mg L^{-1}, and there was little or no sulfate removal. This negligible sulfate removal can be explained by analysis of the pH in the 1st-stage reactor (Appendix B).

In spite of the different strategies assessed, there were little fluctuations in effluent pH values of R1, in which the average pH (considering phases PI, PII, PIII and PIV) was 4.1 ± 0.1. Although acidic conditions are unfavorable for bioH_2 production (Carrillo-Reyes et al., 2014), the maintenance of pH at values below 5.0 was intentional and aimed at investigating whether the inhibition of the sulfidogenesis process in R1 would prevent the competition between sulfate and azo for the available reducing equivalents. Therefore, achievement of low sulfate removals in the first-stage reactor was a required condition in order for reductive decolorization to occur without interference from sulfidogenesis.

R2 was fed with the effluent from R1 containing an average sulfate concentration of 312 ± 29 mg L^{-1}. In the beginning of the phase PIII operation, sulfate removal fluctuated between 66.9 and 77.4%, and further reached approximately 100% as from the 201st system's operation day (including in phase PIV). Measured sulfide concentrations were close to those calculated stoichiometrically (Appendix B). Theoretical estimates were calculated considering a stoichiometry coefficient of 0.33 mg of sulfide produced per mg of sulfate reduced, and further considering that sulfide remained in solution due to the high pH in R2. The average measured sulfide concentrations, in the liquid phase, were 94.4 ± 8.6 and 104 ± 7 mg L^{-1} in phases PIII and PIV, respectively. The proposed system was proved effective for the removal of sulfate from wastewaters containing azo dyes.

Figure 4. 5. Sulfate removal in the two-stage anaerobic digestion system as a function of system operation time. **A)** First-stage reactor (R1) and **B)** second-stage reactor.

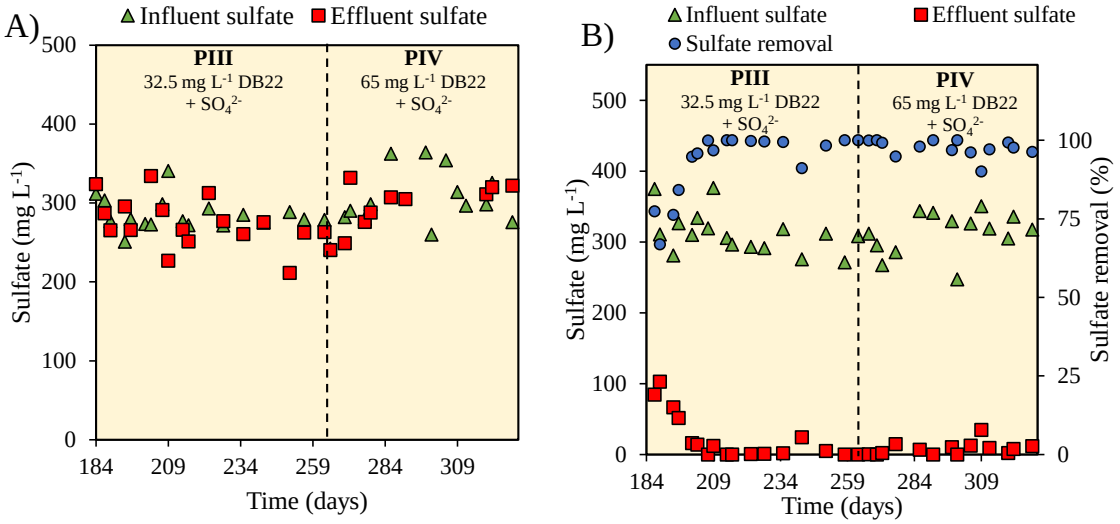

3.4. Color removal in the two-stage AD system

Color removal efficiency was monitored in the two-stage anaerobic digestion system for 328 days. DB22 loading rate applied to R1 and color removal efficiencies are shown in Figure 4. 6. In initial days after the addition of DB22 to the system's feed, color removals in R1 ranged from 65 to 73%, and further decreased to 55% in the second week of phase PII (145th operation day). This suggests that adsorption had a significant contribution in color removal in the initial days of operation with the DB22. Decolorization efficiency gradually increased in the following weeks, showing that the microbial biomass became acclimated to the azo dye and that there was an enrichment of azo dye reducers in the first-stage reactor.

Addition of sulfate, in phase PIII, did not affect decolorization of the DB22 in R1. This is because the low pH of the acidogenic unit (pH 4.3-4.5) inhibited the activity of sulfate reducing bacteria, as shown by results of sulfate removal in the first-stage reactor, which were below 8% (see Section 3.3). Results show that electrons from the co-substrate were preferentially used to reduce the azo chromophore rather than to reduce sulfate, a problem that was addressed in earlier studies which were conducted using single-stage continuous reactors (Amaral et al., 2017, 2014). This confirms our hypothesis that two-stage anaerobic digestion is an effective strategy to enhance decolorization of azo dyes.

Applied DB22 loading rate was increased from 222 ± 9 to 438 ± 13 mg L^{-1} d^{-1} in phase PIV, which resulted in a gradual decline in the color removal efficiencies in R1 (from approximately 90 to 50%). The acidogenic system progressively recovered as from the 307th operation day, showing that the first-stage reactor is resilient to fluctuations in the dye loading. In situations in which R1 presented decreased efficiencies, the 2nd-stage reactor kept decolorization in the final effluent above 90%, playing a key role in keeping the system's performance.

Exceptionally in phase PIII, at times, color removal efficiencies in the final effluent were lower than those obtained after treatment in the 1st-stage reactor solely. This increase in color in the effluent of R2 may be due to the presence of dissolved sulfide species (99.0 ± 9.1 mg L^{-1}), which can interfere in certain colorimetric assays (Pomeroy, 1954). This was later corrected by adding zinc acetate to the sample to precipitate sulfide (Pomeroy, 1954). Interference due to sulfide species was not observed in R1 due to the low sulfidogenic activity in this stage.

Figure 4. 6. Applied DB22 loading rate and color removal efficiencies in the first- (R1) and second-stage (R2) reactors as a function of system operation time.

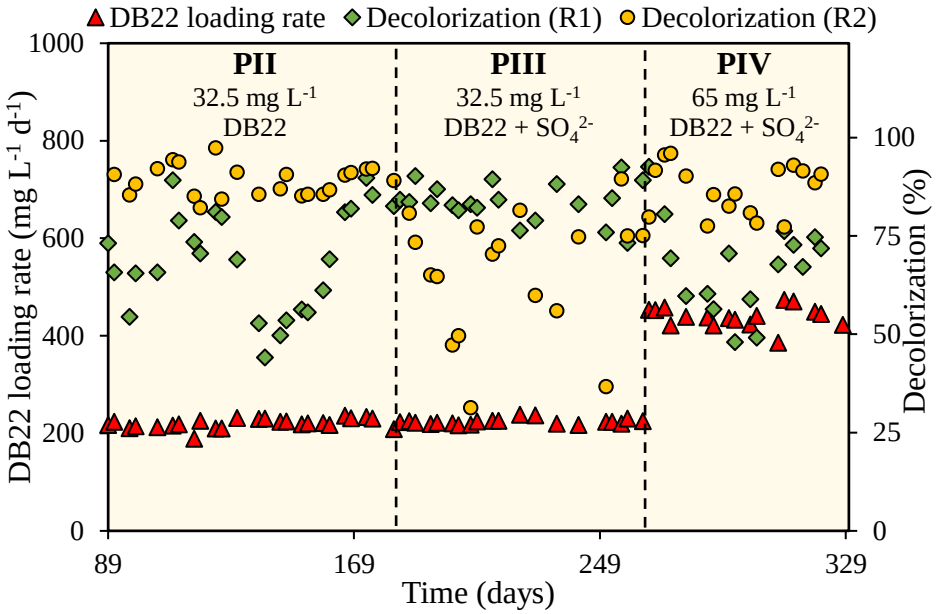

3.5. DB22 biotransformation and production of aromatic amines

TAA were determined colorimetrically to evaluate the DB22 biotransformation. While TAA were not detected in samples from the feed and also in effluent samples collected during phase PI, median concentrations increased to 13.4 (interquartile range = 0.9) and to 12.5 (interquartile range = 1.4) mg.L^{-1} in effluents from reactors R1 and R2, respectively, after the addition of 32.5 mg L^{-1} DB22 (Figure 4. 7). Moreover, we observed an increase in TAA concentration in the effluent from R2 to 17.3 (interquartile range = 4.4) mg.L^{-1} after the establishment of sulfidogenesis, which did not occur in R1 (sulfidogenesis was not stablished in this reactor). This increment was statistically significant according to Kruskal-Wallis test at 95% probability. A similar trend can be observed in results from UV-VIS analysis (Appendix B). While new peaks emerged in the UV spectrum after biological treatment for all operational strategies, a higher peak in the region of 297-300 nm was observed in samples collected from the effluent of R2 during phases PIII and PIV, i.e. after addition of sulfate to the feed. These results show that residual DB22 and/or its fragments undergo further biotransformation in the presence of sulfide species, resulting in the production of new aromatic amines. In fact, it is known that the azo chromophore can be chemically reduced by sulfide in sulfidogenic bioreactors, even though the abiotic mechanism of dye reduction is less significant than that of the biological processes (Van Der Zee et al., 2003).

After increasing DB22 concentration in phase PIV, TAA concentrations further increased to 22.7 (interquartile range = 9.2) and 28.5 (interquartile range = 9.6) mg L^{-1}, respectively, in R1 and R2, and remained higher in the final effluent when compared to samples taken after treatment in the 1st-stage reactor alone. Kruskal-Wallis test performed to compare results from R1 and R2, in phase PIV, was also statistically significant.

Figure 4. 7. Total aromatic amines (TAA) concentration in effluents from the 1st- (R1) and 2nd-stage (R2) reactors of the anaerobic digestion system. Results are expressed as sulfanilic acid concentration.

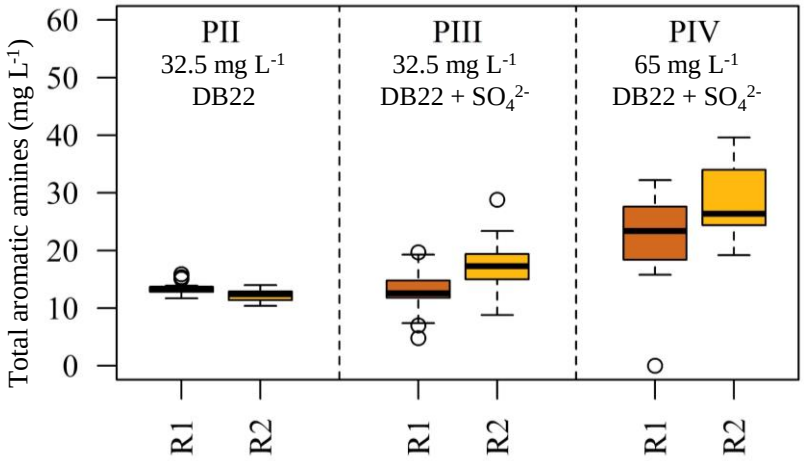

3.6. Mass balance on electrons in the 2nd-stage reactor

Four reducing equivalents are required to reduce one azo bond, accounting for 32 mg COD per mmol of mono-azo dye (Van Der Zee and Villaverde, 2005). Since DB22 is a tetra-azo dye, the required amount of electron-donating co-substrate increases to 128 mg COD $mmol^{-1}$ DB22, meaning that approximately 7.7 mg COD L^{-1} is needed to reduce 65 mg L^{-1} DB22. Nevertheless, this amount will increase due to the demand for electrons by other reactions, justifying the typical use of primary substrates in amounts that largely exceeds the stoichiometric quantity required for azo reduction (Van Der Zee and Villaverde, 2005), otherwise the system will experience decreased decolorization performance (Kapdan and Alparslan, 2005; Oliveira et al., 2020). For example, the theoretical COD demand for reducing 338 mg L^{-1} SO_4^{2-} via the acetic pathway is 226 mg L^{-1} (considering the COD conversion factor of 1.5 g SO_4^{2-} g^{-1} COD) or 458 mg d^{-1} for a reactor with the same HRT and working volume of R2, i.e. 16 h and 1.35 L. In phase PI, an average organic matter removal of 2470 ± 212 mg d^{-1} was achieved in R2 (Table 4. 2), of which at least 94% was converted to methane. In phase PIV, an additional 458 mg d^{-1}

COD is necessary for total sulfate reduction, decreasing the fraction of organic matter removed via methanogenesis to 79.6%. These routes direct approximately 100% of the electron flux in R2, meaning that any additional demand will compete with both the processes for reducing equivalents. A further amount of 16 mg d^{-1} COD would be necessary to reduce 65 mg L^{-1} DB22 in R2 if this unit was not preceded by a 1st-stage reactor. In the presence of both DB22 and sulfate, the oxygen demand required by reactions in R2 exceeded the available amount (biodegradable COD) more often, resulting in an average mass balance of 101.4 ± 8.8%. It is important to highlight that the COD requirement for reducing DB22 azo bonds is the only hypothetical demand in this mass balance analysis, given the fact that reductive decolorization mostly occurred in R1. The 1st-stage reactor not only mitigated this demand but could also uptake a higher azo dye load due to its 5-fold shorter HRT. A more detailed mass balance showing the step-by-step calculation is provided in the published dataset (Oliveira, 2022).

It is worth noting that sulfidogenesis can also contribute in reductive decolorization of azo dyes in two possible ways. The first case is a consolidated mechanism in which the azo bond is chemically reduced by sulfide. However, this mechanism was found to be negligible compared to the biotic one (Van Der Zee et al., 2003).

The other way is a mechanism proposed by Albuquerque et al. (2005) to explain good decolorization efficiencies by a *Desulfovibrio* species in batch experiments fed with lactate as primary substrate and sulfate. The authors attributed the decolorization to a chemically mediated reaction coupled to biological sulfate reduction. Nevertheless, given the experimental design, it is not possible to assess whether decolorization was coupled to sulfate reduction or if it happened in spite of the competition between sulfate and azo molecules for reducing equivalents.

Moreover, co-metabolic decolorization of azo dyes are related to the azo dye reduction potential (Dubin and Wright, 1975), and therefore the ability of the azo dye to be preferentially reduced over sulfate is dye-specific. Amaral et al. (2014) stated that sulfate levels higher than 300 mg L^{-1} SO_4^{2-} significantly impaired dye reduction in a single-stage UASB reactor operated with real textile wastewater which contained DB22 as major dye component. In another experiment conducted with synthetic textile effluent, DB22 decolorization under sulfidogenic conditions was 69 ± 9% and COD and sulfate-

Table 4. 2. Mass balance on electrons in the 2nd-stage reactor showing the fraction of the organic matter removed via methanoegenesis and sulfidogenesis and the oxygen requirements for reducing DB22 azo bonds in phases PI (0 mg L^{-1} DB22, 0 mg L^{-1} SO_4^{2-}) and PIV (0 mg L^{-1} DB22, 338 mg L^{-1} SO_4^{2-}).

	$COD_{applied}$ (mg d^{-1})	COD_{rem} (mg d^{-1})	$COD_{residual}$ (mg d^{-1})	COD_{VSS} (mg d^{-1})	$COD_{CH4,biogas}$ (mg d^{-1})	$COD_{CH4,dissolved}$ (mg d^{-1})	$COD_{sulfate}$ (mg d^{-1})	COD_{DB22} (mg d^{-1})	COD_{demand} (mg d^{-1})	Mass balance (%)
PI	2671	2671	BDL[1]	114	2169	116	0	0	2399	89.8
PI	2333	2333	BDL	99	2053	118	0	0	2270	97.3
PI	2293	2293	BDL	98	2044	113	0	0	2254	98.3
PI	2155	2155	BDL	92	2100	116	0	0	2307	107.1
PI	2291	2291	BDL	98	2310	123	0	0	2531	110.5
PI	2641	2602	39	111	2309	121	0	0	2541	97.6
PI	2613	2587	25	110	2201	120	0	0	2430	93.9
PI	2797	2797	BDL	119	2393	129	0	0	2640	94.4
PI	2500	2500	BDL	107	2197	117	0	0	2421	96.8
Average	2477	2470	7	105	2197	119	0	0	2421	98.4
SD	218	212	15	9	121	5	0	0	132	6.5
PIV	2609	2530	79	108	2103	118	458	16	2802	110.8
PIV	2668	2578	90	110	2300	117	458	16	3000	116.4
PIV	2462	2404	58	102	1920	112	458	16	2607	108.5
PIV	2612	2540	72	108	1824	116	458	16	2522	99.3
PIV	2700	2622	78	112	1717	116	458	16	2419	92.3
PIV	2811	2768	43	118	1767	118	458	16	2477	89.5
PIV	2809	2727	81	116	1852	119	458	16	2561	93.9
PIV	2548	2491	57	106	1928	97	458	16	2604	104.5
PIV	2549	2478	72	106	1871	117	458	16	2567	103.6
PIV	2762	2698	64	115	1871	118	458	16	2577	95.5
Average	2653	2583	69	110	1915	115	458	16	2614	101.4
SD	118	118	14	5	170	7	0	0	169	8.8

Abbreviations:

$COD_{applied}$ – total COD applied in the bioreactor; $COD_{residual}$ – residual COD in the effluent of the bioreactor; COD_{rem} – total COD removed in the bioreactor, COD_{VSS} – COD used for cell synthesis; $COD_{CH4,b}$ – COD corresponding to the fraction of methane measured in the biogas; $COD_{CH4,d}$ – COD corresponding to the fraction of methane dissolved in the liquid; COD_{sulf} – theoretical COD for achieving complete sulfate removal in the bioreactor; COD_{DB22} – theoretical COD for achieving complete reduction of azo bonds; COD_{req} – total COD requirements in the bioreactor.

[1]BDL – below detection limits (10 mg L^{-1} COD).

removals were approximately 70 and 60%, respectively (Carvalho et al., 2020). Florêncio et al. (2021) obtained an average decolorization efficiency of 68 ± 5%, and sulfate and COD removal efficiencies both below 78% in a single-stage AnSTBR reactor. These results suggest that reductive decolorization of DB22 undergoes competition with sulfidogenesis and methanogenesis. On the other hand, the two-stage AD system achieved nearly total color, COD and sulfate removal efficiencies, showing that this strategy is not only effective for enhancing decolorization, but also for improving the organic matter and sulfate removals from textile wastewaters.

4. Conclusion

1st-stage reactor could uptake high loads of dye and achieve good decolorization performance, exhibiting resilience to fluctuations in dye concentration. Sulfidogenic and methanogenic activities were minimal in this reactor and did not impair reductive decolorization. 2nd-stage reactor kept decolorization performance high even when R1 presented decreased efficiencies, and therefore overall system's performance was shown to be stable. Remaining COD in the system's final effluent was attributed to recalcitrant aromatic amines. The proposed strategy was proven effective in the removal of color, organic matter, and sulfate from wastewaters containing azo dyes by minimizing competition between azo dye and other processes for reducing equivalents. This system's configuration showed feasibility for industrial application due to its stable performance and higher azo dye load capacity when compared to single-stage systems.

Acknowledgments

This work was supported by the Fundação do Amparo à Pesquisa do Estado de São Paulo (process numbers 2015/06246-7 and 2018/24269-2) and the Coordenação de Aperfeiçoamento de Pessoal de Nível Superior (CAPES) – Brazil (Finance Code001). The authors also would like to thank Dr. Carolina Sabatini, Dr. Eloisa Pozzi, Dr. Maria Angela Adorno, Dr. Isabel K. Sakamoto and Dr. Savia Gavazza for their technical and scientific support.

Chapter 5

Microbial communities and metabolic pathways involved in reductive decolorization of an azo dye in a two-stage AD system

Abstract. Multiple stage anaerobic system was found to be an effective strategy for reductive decolorization of azo dyes in the presence of sulfate. Bulk color removal (56 – 90%) was achieved concomitant with acidogenic activity in the 1st-stage reactor (R1), while organic matter removal (≤ 100%) and sulfate reduction (≤ 100%) occurred predominantly in the 2nd-stage reactor (R2). However, azo dye reduction mechanism and metabolic routes involved remain unclear. The involved microbial communities and conditions affecting the azo dye removal in a two-stage anaerobic digestion (AD) system were elucidated using amplicon sequencing (*16S rRNA*, *fhs*, *dsrB* and *mcrA*) and correlation analysis. Reductive decolorization was found to be co-metabolic and mainly associated with hydrogen-producing pathways. We also found evidence of the involvement of an azoreductase from *Lactococcus lactis*. Bacterial community in R1 was sensitive and shifted in the presence of the azo dye, while microorganisms in R2 were more protected. Higher diversity of syntrophic-acetate oxidizers, sulfate reducers and methanogens in R2 highlights the role of the 2nd-stage in organic matter and sulfate removals, and these communities might be involved in further transformations of the azo dye reduction products. The results improve our understanding on the role of different microbial communities in anaerobic treatment of azo dyes and can help in the design of better solutions for the treatment of textile effluents.

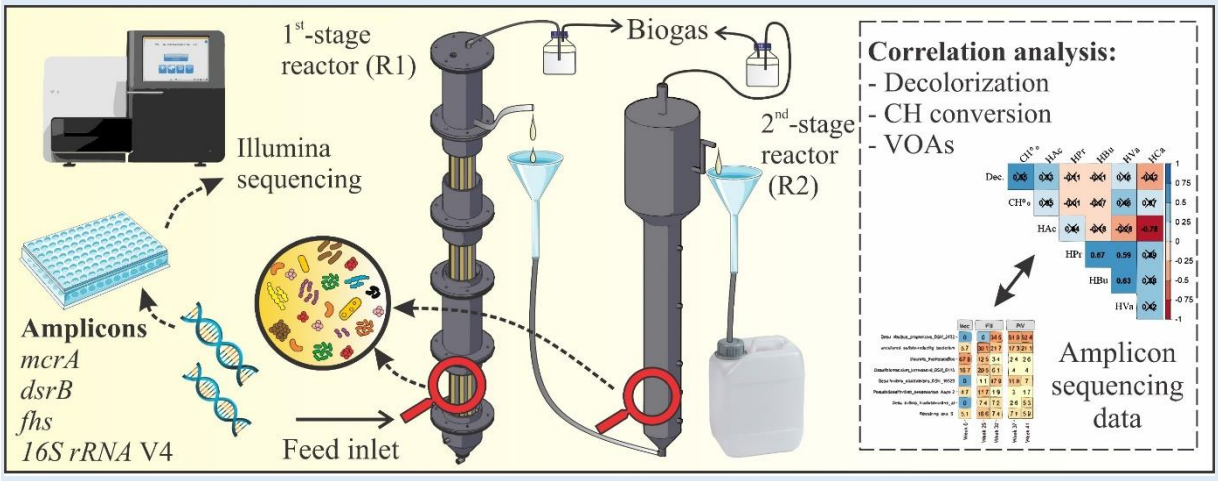

A modified version of this chapter was published in:

Oliveira, J.M.S., Poulsen, J.S., Foresti, E., Nielsen, J.L. 2022. Microbial communities and metabolic pathways involved in reductive decolorization of an azo dye in a two-stage AD system. Chemosphere, 136731. https://doi.org/10.1016/j.chemosphere.2022.136731

1. Introduction

Use of multiple stage anaerobic systems can improve reductive decolorization of azo dyes by channeling electrons to preferentially reduce azo bonds in the 1st-stage of the anaerobic digestion (AD), whereas organic matter and sulfate removals are achieved in the following unit with enhanced performance (Oliveira et al., 2022). In this system's configuration, it is expected that distinct microbial communities will stablish in each stage as a result of the different operating conditions applied (Baldi et al., 2019; Demirel and Yenigün, 2002). Acidogens, acetogens and methanogens grow at their optimal ecophysiological conditions, resulting in a better overall process stability compared to single stage anaerobic treatment (García-Depraect et al., 2022). Understanding the role of these microbial communities on the biodegradation of azo dyes can help in the designing of better solutions for the treatment of textile wastewaters.

The conversion of carbohydrates into organic acids occurs in the earliest stage of AD in reactions carried by acidogenic bacteria (Cohen et al., 1980; García-Depraect et al., 2022). In the following step, acetogens and methanogens form syntrophic associations to produce methane (Stams and Plugge, 2009). Under specific conditions, aceticlastic methanogens are inhibited and the Wood–Ljungdahl pathway is inversed (Müller et al., 2013). This rather results in formation of H_2+CO_2 from acetate by the syntrophic acetate oxidizing bacterial (SAOB) community. All these communities are possibly involved in reductive decolorization of azo dyes to a greater or lesser extent.

Some microbial populations play a controversial role in anaerobic treatment of azo dyes. Sulfate-reducing bacterial (SRB) community was found to compete for electrons with azo reducers (Oliveira et al., 2022; Santos et al., 2007), sometimes impairing the reductive decolorization process (Amaral et al., 2014). Nevertheless, decolorization coupled to sulfate reduction was observed before (Albuquerque et al., 2005) and biogenic sulfide can chemically reduce the azo bonds (Prato-Garcia et al., 2013; Zeng et al., 2021). It was hypothesized that whether SRB populations act opposing or in favor of reductive decolorization rather depends on the microbial interspecies interactions and on the biochemical reactions that they are mediating in the system.

Moreover, it is not clear whether mixed microbial cultures rely on specialized enzymes for biodegrading azo dyes. More than a decade ago, Santos et al. (2007) stated that the main mechanism is likely a co-metabolic reaction in which reducing equivalents, as well as reduced cofactors, work as secondary electron donors to cleave the azo bonds. By that time, there were evidence of azoreductases among aerobic bacteria, but no proof in anaerobic microorganisms

(Santos et al., 2007; Stolz, 2001). Later on, Morrison et al. (2012) isolated and characterized an anaerobic azoreductase from *Clostridium perfringens*. Decolorization of azo dyes by other enzymes from the oxidoreductase enzyme system, including laccases, NADH–DCIP reductases, veratryl alcohol oxidases, tyrosinases, riboflavin reductases, and lignin and manganese peroxidases was recently reported among pure and co-cultures of microorganisms (Ali et al., 2020; Kurade et al., 2017; Saratale et al., 2013; Waghmode et al., 2019, 2011). Additionally, synergistic action of different oxidoreductase enzymes was proved to enhance decolorization efficiency (Mendes et al., 2011), suggesting that many microbial communities degrade azo dyes through distinct metabolic routes.

This study proposes to bridge the gap between the microbial communities involved in the decolorization of azo dyes in anaerobic treatment systems and the underlying mechanism. The overall bacterial, SAOB, methanogenic, SRB communities were monitored using amplicon sequencing of the 16S rRNA and functional genes. Efficiency parameters were correlated with the production of volatile fatty acids (VFAs) and metabolites in the system to elucidate the main pathways involved. Sulfidogenic conditions were further applied because sulfate is a common constituent of textile wastewater (Amaral et al., 2014). We provide valuable insights into the anaerobic treatment of azo dyes that can help to better understand how syntrophic microbial communities degrade azo dyes.

2. Materials and Methods

2.1. Reactor setup and operational strategies

Two anaerobic reactors were operated continuously over a period of 328 days. The two-phase anaerobic digestion system was composed of a 1st-stage anaerobic structured-bed reactor (R1) and a 2nd-stage upflow anaerobic sludge blanket reactor (R2) running in series and under mesophilic conditions (30 ºC). In R1, the fixed-bed was built with polyurethane foam strips (10x10x650 mm). R1 was operated with a theoretical chemical oxygen demand (COD) of 28.7 gCOD d^{-1} (organic loading rate = 11.7 gCOD L^{-1} d^{-1}) and R2 was operated with 2.7 gCOD d^{-1} (organic loading rate = 2.0 gCOD L^{-1} d^{-1}). Respective hydraulic retention times were 3.5 and 16 h.

R1 was fed with synthetic textile wastewater composed of: Direct Black 22, DB22 (0-65 mg L^{-1}), glucose (1.70 gCOD L^{-1}), KH_2PO_4 (0.25 g L^{-1}), Na_2SO_4 (0-0.50 g L^{-1}), NaCl (0.50 g L^{-1}), yeast extract (0.20 g L^{-1}), $NaHCO_3$ (0.15 g g^{-}1 COD) and 1 mL L^{-1} trace elements solution (Appendix C). The pH of the feed was kept at 7.0 ± 0.1. R2 was fed with the effluent from

R1 after the addition of $NaHCO_3$ (0.70 g L^{-1}) to raise pH to 6.0. Bioreactors were inoculated with anaerobic sludge from a full scale upflow anaerobic sludge blanket reactor, located in the city of Pereira – SP, processing wastewater from a poultry slaughterhouse. For R1, methanogenic archaea were inactivated by heat-treating the sludge (100 ºC, 1 h) previously to inoculation (Wang and Yin, 2017).

Strategies used in the operation of the AD system were as following: startup and stabilization period with no addition of DB22 or SO_4^{2-} (Phase PI); addition of 32.5 mg L^{-1} DB22 (Phase PII); addition of both 32.5 mg L^{-1} DB22 and 338 mg L^{-1} SO_4^{2-} (Phase PIII); and addition of 65.0 mg L^{-1} DB22 and 338 mg L^{-1} SO_4^{2-} (Phase PIV).

2.2. Microbial sampling and DNA extraction

Biofilm from R1 and R2 was sampled at different times of each phase after system's performance was stable. In R1, samples were harvested from the bottom biomass of the polyurethane foam used as support for growth. In R2, samples were collected from the sludge blanket (lower portion). Genomic DNA was extracted using the FastDNA® Spin Kit for Soil (MP Biomedicals, Santa Ana, USA) and following the manufacturer's protocols. DNA quantification was assessed using the Quant-iT™ High-Sensitivity DNA Assay Kit on a plate reader (TECAN Infinite M1000) and integrity was evaluated using the TapeStation 2200 with genomic DNA ScreenTapes (Agilent, USA).

2.3. Amplicon sequencing

PCR reactions targeting the V4 variable region of the bacterial 16S rRNA gene and the functional genes formyltetrahydrofolate synthetase (*fhs*), dissimilatory sulfite reductase β-subunit (*dsrB*), and methyl coenzyme-M reductase (*mcrA*) were further conducted to investigate the SAOB, SRB and methanogenic communities, respectively. Corresponding primer sets are shown in the Table 5. 1. Thermocycler settings were as following: initial denaturation at 95 ºC for 2 min; amplification for 25 cycles at 95 ºC for 15 s, 50 ºC for 15 s, and 72 ºC for 60 s; and a final extension of 5 min at 72 ºC. Number of cycles, annealing temperature and extension time were appropriately adjusted according to the target gene. Sample preparation was conducted similarly to that described elsewhere (Agneessens et al., 2017), except that for *fhs* a 200 ng of extracted DNA was used as template.

Table 5. 1. Primer sets used in the amplicon sequencing analyses.

Name	Target gene	Function sequences (5'-3')	Adaptations	Reference
515F 806R	*16S rRNA*, Region V4	GTGCCAGCMGCCGCGGTAA GGACTACHVHHHTWTCTAAT	--	Caporaso et al., (2011)
3-SAO4I-fw 3-SAO4I-rev SAO-rev	*fhs*	CCIACICCISYIGGNGARGGNAA ATITTIGCIAAIGGNCCNSCNTG ATRTTNGCRAADGGNCCNCCRTG	35 cycles; 52 ºC annealing; 60 s extension	Müller et al. (2013); Singh et al. (2020)
dsrB-F1 dsrB-4RSI1	*dsrB*	CAYACNCARGGNTGG CAGTTDCCRCAGWACAT	30 cycles; 51 ºC annealing; 60 s extension	Müller et al. (2015)
mcrA-fw mcrA-rev	*mcrA*	GGTGGTGTMGGAT-TCACACARTAYGCWACAGC TTCATTGCRTAGTTWGGRTAGTT	35 cycles; 50 ºC annealing; 60 s extension	Luton et al. (2002)

2.4. Bioinformatics processing and statistical analysis

Bioinformatic processing was conducted using the AmpProc 5.1 pipeline (https://github.com/eyashiro/AmpProc), based on USEARCH11 (Edgar, 2013) and QIIME 1.9.1 (Caporaso et al., 2010). For 16S rRNA gene, *fhs* and *dsrB* amplicons, taxonomy was assigned using MiDAS 4.8.1 (Dueholm et al., 2021), AcetoBase (Singh et al., 2019) and a database of *dsrAB* sequences (Müller et al., 2015). For *mcrA*, a custom database of representative reference sequences was obtained from the Functional Gene Repository (FunGene; http://fungene.cme.msu.edu/). Statistical analysis were performed in R version 4.0.1 via RStudio version 2021.09.0 (http://www.rstudio.com) using the R CRAN package ampvis (v2.7.11) (Albertsen et al., 2015). Structure and differences between microbial communities were assessed using heatmaps and non-metric multidimensional scaling (NMDS) analysis. Sequences were deposited in the European Nucleotide Archive (ENA) database under accession number PRJEB52299.

2.5. Analytical methods and performance evaluation

COD, pH and standard reduction potential (E_0') were measured according to APHA Standard Methods (2005). Sulfide interference on COD analysis was previously eliminated with zinc sulfate addition. For color analysis, samples were appropriately diluted with phosphate buffer (10.86 g L^{-1} NaH_2PO_4 and 5.98 g L^{-1} Na_2HPO_4) (Firmino et al., 2010) and assessed according to the spectra record method (Wu et al., 1998; APHA, 2005). Soluble carbohydrates (CH) and lactic acid were determined as previously described (DuBois et al., 1956; Taylor, 1996). For E_0' profiling in R1, samples were collected at different heights (155, 305, 455, 630 and 750 mm) with the aid of a syringe and transferred to vacuum blood collection tubes. Samples were handled in an anaerobic chamber with N2 atmosphere. VFAs (C2-C6) and solvents were analyzed by gas chromatography (Adorno et al., 2014).

COD removal (in %) and conversion of CH (CH%, in %) were calculated using Eq. (1).

$$X\ (\%)\ =\ \frac{(X_{feed}\ -\ X_{effl})}{X_{feed}}\ \ 100 \qquad (Eq.1)$$

in which X is either COD removal or CH conversion, X_{feed} is the concentration of X in the feed, and X_{effl} is the concentration of X in the effluent.

Decolorization (in %) was calculated using Eq. (2):

$$Decolorization = \frac{\int_{400\ nm}^{700\ nm} A_{feed}\ \mathrm{d}\lambda - \int_{400\ nm}^{700\ nm} A_{effl}\ \mathrm{d}\lambda}{\int_{400\ nm}^{700\ nm} A_{feed}\ \mathrm{d}\lambda}\ \ 100 \qquad (Eq.2)$$

in which A_{feed} is the absorbance of the feed; A_{effl} is the absorbance of the effluent; and $\mathrm{d}\lambda$ is an infinitesimal wavelength interval.

3. Results and Discussion

3.1. Two-stage AD system's overall performance

The two-stage AD system was operated for 328 days to investigate how the performance was affected by loading of color and exposure to sulphate. In R1, COD removal efficiencies were below 20% during the entire operation (Table 5. 2) and the volumetric methane production rate rarely exceeded 50 mL L^{-1} d^{-1}. R1 achieved decolorization efficiencies in the range of 80-90% when a DB22 loading rate of approximately 222 mg L^{-1} d^{-1} was applied in phase PII. Although sulfate was added to the feed as from phase PIII (338 mg L^{-1} SO_4^{2-}), sulfidogenic

activity in R1 was minimal (median sulfate removal = 3.5%, IQR = 8.3) and did not impair color removal performance. R2 achieved over 97% of COD and almost 100% sulfate removal efficiencies. Mass balance analysis showed that methanogenesis and sulfidogenesis demanded nearly all the electrons in R2, meaning that the use of a two-stage anaerobic system was important to alleviate the demand of both these processes for reducing equivalents in R1, driving electrons preferentially to reduce the azo dye. Further information on the performance of the two-stage AD system had been published elsewhere (Oliveira et al., 2022).

Table 5. 2. Overview of the performance of the two-stage AD system treating azo dye and sulfate.

Phase	Description	Operation days	Average decolorization (%)	Average carbohydrates removal (%)	Average COD removal (%)	Effluent pH
1st-stage reactor (R1)						
PI	No DB22 or SO_4^{2-}	1-87	-	97.6 ± 2.6	14.9 ± 5.0	4.4 ± 0.1
PII	32.5 mg L^{-1} DB22	88-182	69 ± 13	91.5 ± 9.7	15.3 ± 5.2	4.4 ± 0.1
PIII	32.5 mg L^{-1} DB22 + 338 mg L^{-1} SO_4^{2-}	183-263	84 ± 5	99.2 ± 0.2	17.5 ± 3.4	4.5 ± 0.5
PIV	65 mg L^{-1} DB22 + 338 mg L^{-1} SO_4^{2-}	264-328	67 ± 12	97.6 ± 1.8	18 ± 3.8	4.4 ± 0.1
2nd-stage reactor (R2)						
PI	No DB22 or SO_4^{2-}	1-87	-	N/A	99.8 ± 0.5	7.7 ± 0.3
PII	32.5 mg L^{-1} DB22	88-182	89 ± 4	N/A	98.1 ± 0.4	7.6 ± 0.2
PIII	32.5 mg L^{-1} DB22 + 338 mg L^{-1} SO_4^{2-}	183-263	66 ± 16	N/A	98.5 ± 0.7	7.7 ± 0.3
PIV	65 mg L^{-1} DB22 + 338 mg L^{-1} SO_4^{2-}	264-328	87 ± 6	N/A	97.4 ± 0.5	8.0 ± 0.3

3.2. Azo dye decolorization is mediated by electron shuttles

Color removal profiling in R1 was assessed after performance was stable (Figure 5. 1-A). The highest increment in color removal was observed between the sampling points *a* and *b*, where decolorization increased from 33 to 90% (as compared to the system's influent). Surprisingly, color removal efficiency decreased in samples taken in sampling point *c* (decolorization = 67%), and further fluctuated across the reactor's profile. This suggests that intermediates produced after the cleavage of the azo bonds were reoxidized in particular zones of the reactor, resulting in the formation of newer azo bonds. It is well known that exposure of byproducts from reductive decolorization to atmospheric oxygen causes the formation of color (Menezes et al., 2019; Oliveira et al., 2020), since hydrazine groups and/or azo anion free radicals in the molecules react with oxygen (Zimmermann et al., 1982). However, there are no studies reporting the reoxidation of aromatic amines inside anaerobic digestors themselves, causing cyclic increases and decreases in color removal across the reactor's profile.

Figure 5. 1. Association between decolorization efficiency and reduction potential (E_0') in the 1st-stage reactor (R1). **A)** Vertical profiling for decolorization and E_0' in R1; and **B)** Pearson's correlation analysis (R = -0.64, $p < 0.05$) for both the variables. Decolorization in each sampling port (a, b, c, d, e and effluent) was calculated relatively to the color of the synthetic wastewater in the feed tank.

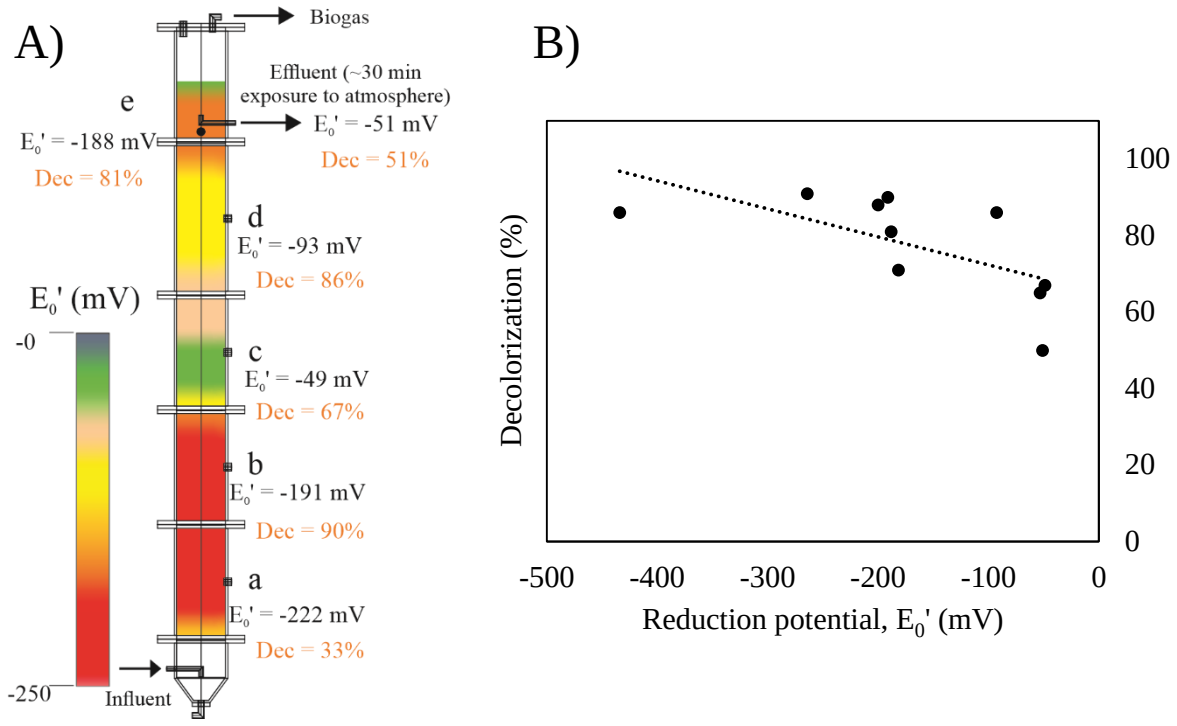

Sampling along R1 further revealed strong zonation with different redox potentials. This reduction potential (E_0') profiling in R1 provided valuable insight into the mechanism of color removal across the 1st-stage reactor's vertical profile. The lower portion of R1, which includes sampling points *a* and *b*, presented more reduced conditions (E_0'~ -200 mV). This is probably because CH conversion reactions into VFAs occurred in the bottom of the reactor (Appendix C). Moreover, it was previously observed that biohydrogen ($bioH_2$) production from sugars mainly occurs in the basal portion of fixed-bed reactors (Fuess et al., 2021), supporting the hypothesis that the DB22 reduction mechanism is governed by – but not limited to – co-metabolic reactions, in which reducing equivalents or reduced cofactors such as NADH act as secondary electrons donors to cleave azo bonds (Santos et al., 2007).

In the intermediary zone (sampling point *c*), E_0 increased to -49 mV, and DB22 intermediates reoxidized as a result of the less reduced conditions. E_0 values decreased to -93 mV, and further to -188 mV in sampling points *d* and *e*, respectively, causing color removal efficiencies to rise again, oscillating between 81 and 86%. Upon exposure of the effluent to the atmosphere for approximately 30 min, E_0 increased to -51 mV and decolorization decreased to 51%. After repeated measurements were taken across the R1's profile (Figure 5. 1-B), we confirmed that color removal is negatively correlated with E_0 in the system ($R = -0.64$; $p = 0.045$).

The rate of azo reduction has previously been shown to depend on the dye redox potential if the rate-limiting step involves a redox equilibrium between the azo molecule and a reducing agent (Dubin and Wright 1975). The mechanism hypothesized involves a redox cycle in which a redox mediator transfer electrons between the enzyme and the substrate (Figure 5. 2). Reduction of the azo dye (R_1-N=N-R_2) to its hydrazo intermediate (R_1-HN-NH-R_2) will only occur if the mediator is present in sufficient concentrations and shifted toward a reduced form (Dubin and Wright, 1975). High concentrations of the reduced mediator will result in decreased E_0 values, and electron transfer to azo compounds will happen once the redox potential in the environment approach that of the dye. However, this last reaction is reversible as long as the hydrazo intermediate is not further degraded. It can be hypothesized that the equilibrium shifted towards re-oxidation of DB22 intermediates (e.g., hydrazo to azo) as reduction potential in the system increased due to consumption of mediators in the reduced form, causing reappearance of color in the upper portion of R1.

Figure 5. 2. Postulated mechanism of azo dye decolorization in anaerobic systems by redox mediators. E_{red}/E_{ox} are, respectively, the reduced and oxidized forms of an enzyme, and M_{red}/M_{ox} are the reduced and oxidized forms of a low molecular weight electron carrier (mediator). Green arrows represent a shift in the equilibrium towards reoxidation of the hydrazo intermediate and generation of newer azo bonds. Adapted from Dubin and Wright (1975).

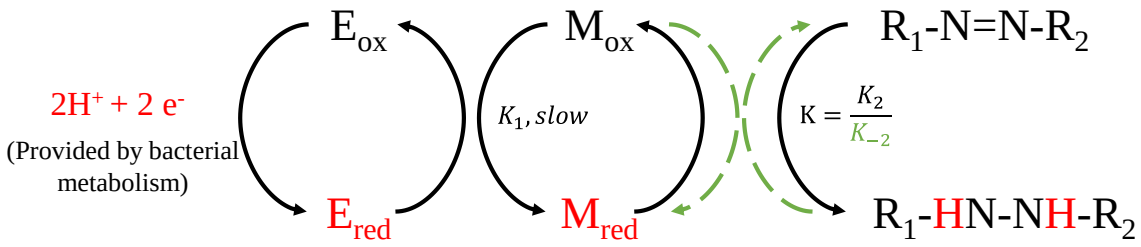

3.3. Co-metabolic routes involved in reductive decolorization

Conversion of carbohydrates occurred in R1 with efficiencies of approximately 99% throughout the 328 days of operation. Production of VFAs and metabolites in the effluent after R1 was monitored and is shown in Figure 5. 3.

Butyrate-type fermentation was the main pathway observed during the stabilization phase. Median concentrations of HBu and HAc were, respectively, 295 mg L^{-1} (IQR = 245) and 154 mg L^{-1} (IQR = 220) in this period, which accounts for a HBu/HAc ratio of 1.91. In phases PII and PIII (32.5 mg L^{-1} DB22), HBu/HAc ratios decreased to 0.79 and 0.98, while HPr concentrations remained similar (PI: median 132 mg L^{-1}, IQR= 117; PII: median 118 mg L^{-1}, IQR = 46; and PIII: median 156 mg L^{-1}, IQR = 82). These results indicate the predominance of the acetic pathway (Table 5. 3, Eq. 2) during most of the operation with the azo dye, which is usually associated with higher bioH_2 production rates from CH when compared to other more reduced metabolites (Fernandes et al., 2010; Fuess et al., 2016).

The involvement of the acetic fermentation pathway on reductive decolorization is further supported by results from Pearson's correlation test (R = 0.48, p = 0.001) performed with samples collected all over the operation (Figure 5. 4-A). Butyrate fermentation (Table 5. 3, Eq. 3), another hydrogen-producing reaction, was also significant for color removal (R = 0.35, p = 0.021). Since bioH_2 was not released in the biogas phase (Oliveira et al., 2022), some of the reducing power generated via these metabolic routes might have been consumed during co-metabolic decolorization of DB22.

The strongest correlation was found to be between decolorization and CH% (R = 0.60, $p < 0.001$). In fact, the catabolism of glucose to pyruvate yields two NADH molecules, which can serve as reducing power for the cleavage of azo bonds (Table 5. 3, Eq.1). Moreover,

glycolysis is the precursor of all mixed acid fermentation reactions and acidogenesis was found to be a critical step in AD of azo dyes (Firmino et al., 2010; Li et al., 2014).

Figure 5. 3. Concentration of volatile organic acids (VFAs) in the effluent of the 1st-stage reactor (R1). **A)** PI: stabilization period; **B)** PII: 32.5 mg·L^{-1} DB22; **C)** PIII: 32.5 mg·L^{-1} DB22 and 338 mg·L^{-1} SO_4^{2-}; and **D)** PIV: 65 mg·L^{-1} DB22 and 338 mg·L^{-1} SO_4^{2-}. Nomenclature: Ace – acetone; MeOH – methanol; EtOH – ethanol; n-BuOH – n-buthanol; HAc – acetic acid; HPr – propionic acid; HIsoBu – isobutyric acid; HBu – n-butyric acid; HIsoVa – isovaleric acid; HVa – n-valeric acid; HCa – n-caproic acid.

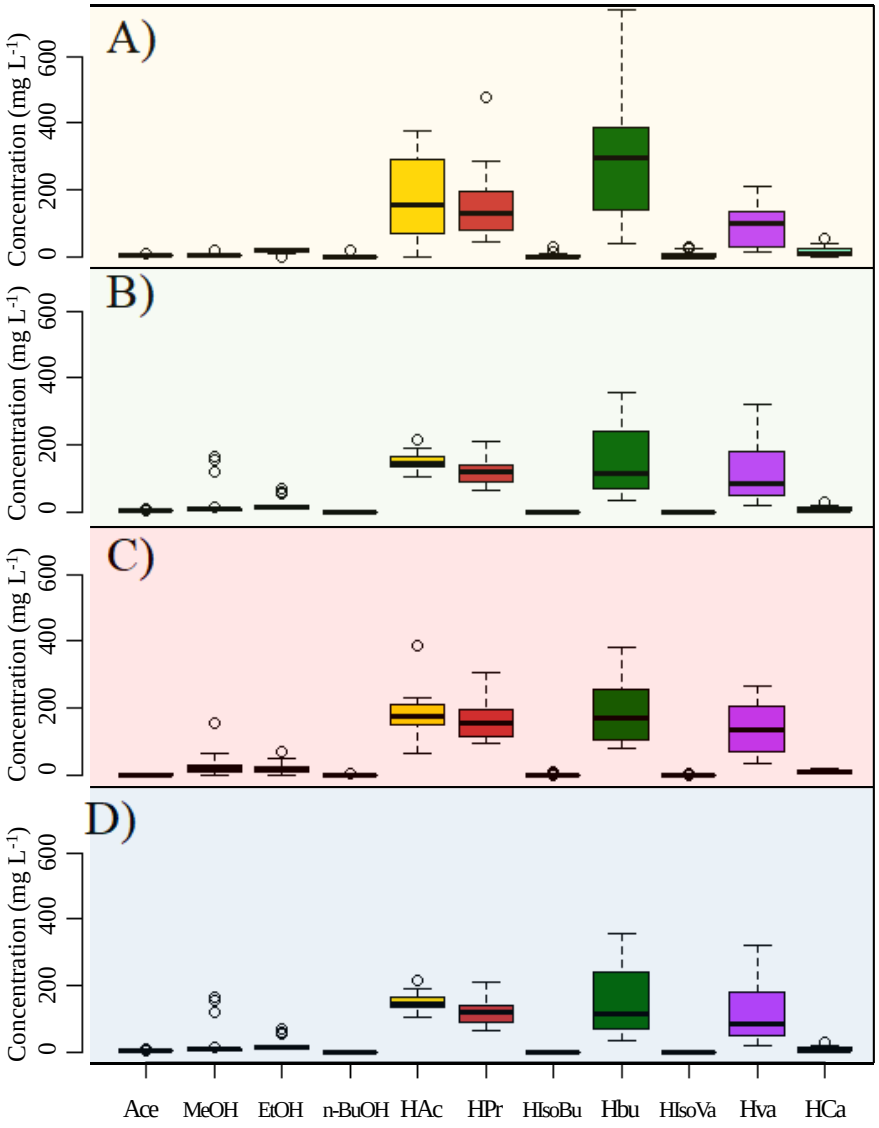

Interestingly, metabolites produced via hydrogen-consuming reactions such as n-valeric acid (Table 5. 3, Eq. 9), ethanol (Table 5. 3, Eq. 10) and methanol (Table 5. 3, Eq. 11) were also positively correlated with color removal. For instance, n-valerate elongation from propionate consumes six mols of H_2. Both ethanol and methanol formation obtain reducing power from $NADH+H^+$. Nevertheless, the correlations between these metabolites and reductive decolorization may reflect the fermentative diversity in R1 rather than causation directly. Several

studies have shown the benefits of metabolic diversity on decolorization of azo dyes by mixed microbial cultures due to the synergistic action of different enzymes from the oxidoreductase system. Observed increases in the activities of NADH-DCIP reductases, azoreductases, veratryl alcohol oxidases and laccases after decolorization of textile effluents by microbial consortiums rather than in controls with the respective individual isolates were previously observed (Kurade et al., 2017; Phugare et al., 2011). In another study, decolorization was found to be correlated with higher microbial diversity in batch experiments, further supporting the relevance of metabolic diversity in the biodegradation of azo dyes (Oliveira et al., 2020). Finally, production and accumulation of metabolites such as ethanol may stimulate other hydrogen-producing routes, e.g., chain elongation to n-caproic acid production (Cavalcante et al., 2017), therefore explaining the positive correlation between ethanol and decolorization.

Table 5. 3. Main fermentation pathways involved in co-metabolic decolorization of the azo dye Direct Black 22. Adapted from Cavalcante et al. (2017); Mariano et al. (2011); Saady (2013); and Xin et al. (2004).

Pathway	Reaction	No.
I - Hydrogen-producing reactions (as H_2 or $NADH+H^+$)		
Glucose to pyruvate formation	Glucose $\rightarrow$ 2pyruvate + 2 $NADH+H^+$	(1)
Glucose to acetic acid formation	Glucose + $2H_2O \rightarrow$ 2acetic acid + $4H_2$ + $2CO_2$	(2)
Glucose to butyric acid formation	Glucose $\rightarrow$ butyric acid + $2H_2$ + $2CO_2$	(3)
Ethanol to n-caproic acid generation	12ethanol + 3acetic acid $\rightarrow$ 5n-caproic acid + $4H_2$ + $8H_2O$	(4)
Lactic acid to n-caproic acid generation	15lactic acid $\rightarrow$ 5n-caproic acid + $5CO_2$ + $10H_2$ + $5H_2O$	(5)
Glucose to acetone formation	Glucose + $2H_2O \rightarrow$ 1acetone + $4H_2$ + $3CO_2$	(6)
n-Butyric acid oxidation	n-Butyric acid + $2H_2O \rightarrow$ 2acetic acid + $2H_2$	(7)
II - Hydrogen-consuming reactions (as H_2 or $NADH+H^+$)		
Pyruvate to acid lactic formation	Pyruvate + $NADH+H^+ \rightarrow$ Lactic acid + NAD^+	(8)
Propionic acid to n-valeric acid elongation	Propionic acid + $2CO_2$ + $6H_2 \rightarrow$ n-valeric acid + $4H_2O$	(9)
Glucose to ethanol formation*	Glucose $\rightarrow$ 2ethanol + $2CO_2$	(10)
Methane to methanol formation	CH_4 + $1/2O_2$ + $NADH+H^+ \rightarrow$ Methanol + NAD^+	(11)

*No net hydrogen production/consumption.

Figure 5. 4. Pearson's correlation matrix (significance level $p \leq 0.05$) for DB22 decolorization (Dec, in %), carbohydrates conversion efficiency (CH%, in %), volatile organics acids (acetic acid – HAc, propionic acid – HPr, n-butyric acid – HBu, n-valeric acid – HVa, n-caproic acid – HCa, in mg L^{-1}) and solvents (methanol – MeOH, ethanol – EtOH, acetone – Ace, in mg·L^{-1}). **A)** All operational phases, n = 43 obs.; **B)** PII: 32.5 mg·L^{-1} DB22, n = 14 obs.; **C)** PIII: 32.5 mg·L^{-1} DB22 and 338 mg·L^{-1} SO_4^{2-}, n = 17 obs.; and **D)** PIV: 65 mg·L^{-1} DB22 and 338 mg·L^{-1} SO_4^{2-}(n = 43).

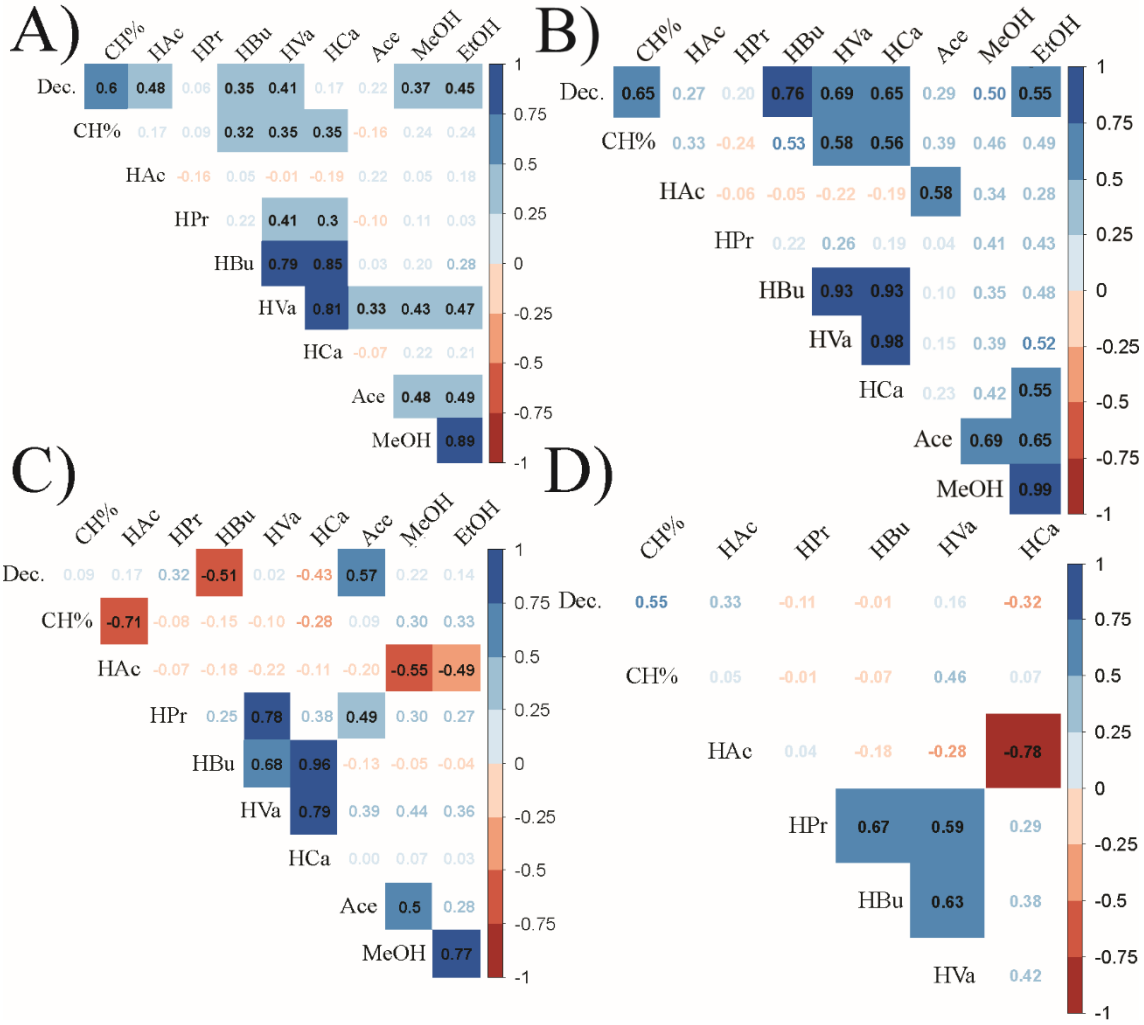

Pearson's correlation analysis was also performed separately for each system's operational strategy. In phase PII (32.5 mg·L^{-1} DB22), decolorization was significantly correlated with CH% and the production of HBu, HVa, HCa and ethanol (Figure 5. 4-B). Production of n-caproic acid from both ethanol and lactic acid yields bioH_2 that can be used as reducing power for reductive decolorization (Table 5. 3, Eq. 4-5). Ethanol elongation to n-caproic acid likely occurred because both ethanol and acetic acid were present in phase PII, and ethanol concentrations were strongly correlated with those of n-caproic acid (R = 0.55, p = 0.040). Moreover,

lactic acid was detected in samples collected all over PII operation at concentrations ranging from 10 to 32 $mg \cdot L^{-1}$. Given the high abundance of homolactic bacteria in R1 (see Topic 3.6), lactic acid was probably utilized to generate n-caproic acid. It can therefore be hypothesized that decolorization of DB22, in phase PII, was mainly driven by reactions involved in chain elongation for n-caproate production.

Addition of sulfate (338 $mg \cdot L^{-1}$ SO_4^{2-}), in phase PIII, did not appear to affect decolorization and CH% efficiencies in R1 (Figure 5. 4-C). Effluent sulfate concentrations remained similar and, sometimes, slightly higher than those measured in the feed tank. In fact, the 1st-stage reactor was designed with the aim of preventing sulfidogenesis, thus avoiding competition between the azo dye and sulfate for reducing equivalents. Although no sulfate removal occurred in R1, Pearson's correlation analysis results showed that distinct metabolic routes were involved in DB22 decolorization in phase PIII. Decolorization was positively correlated with acetone formation ($R = 0.57$, $p = 0.018$), which is a bioH_2 producing reaction (Table 5. 3, Eq. 6), and negatively associated with HBu concentration ($R = -0.51$, $p = 0.035$) in this period. The later suggests that the decrease in HBu/HAc ratio occurred as a result of butyrate oxidation (Table 5. 3, Eq. 7), which leads do the production of bioH_2 that can serve as additional electron donor for reductive decolorization. The findings agree with previous studies in which the presence of an azo dye led to higher decomposition of VFAs (propionate and butyrate) into acetate, compared to a control without azo dye (Li et al., 2014). The authors hypothesized that bioH_2 produced in acetification of VFAs served as additional reducing power for reductive decolorization. This was further supported by results from enzymatic assays, which showed that azoreductase activity was higher in the presence of butyrate and propionate than acetate.

After applied DB22 loading rate was increased to 438 ± 13 $mg \cdot L^{-1} \cdot d^{-1}$ (65 $mg \cdot L^{-1}$, Phase PIV), we observed a lower metabolic diversity in R1 (Figure 5. 4-D). Methanol, ethanol and acetone were not detected as from the 5th day after transition to phase PIV, and HBu/HAc ratio increased to 1.70. Moreover, no correlations were found between the produced metabolites and decolorization. This period of operation was marked by a decrease in decolorization efficiencies in R1, with later stabilization at lower removal rates. This further supports our hypothesis that a higher metabolic diversity is beneficial for reductive decolorization of azo dyes.

3.4. Overall bacterial community and sensitivity of acidogens towards azo dye

After a DB22 loading rate of 222 ± 9 $mg \cdot L^{-1} \cdot d^{-1}$ (32.5 $mg \cdot L^{-1}$, Phase PII) was applied to R1, CH% had a sudden drop from approximately 99 to 70%, with gradual recovery in the following weeks (Oliveira et al., 2022). This suggests that microorganisms adapted to the dye and to intermediates of the reductive decolorization. However, this could also mean that a microbial community with different structure was stablished in the system. Molecular identification of microorganisms based on the 16S rRNA and functional genes was further conducted to understand the possible causes.

Amplicon sequencing of the 16S rRNA gene targeting the V4 region revealed a significant shift in the bacterial community structure in R1 after DB22 was added to the system, in phase PII (Figure 5. 5-A). Samples clustered into four groups, of which each one represented a different operational strategy. DB22 was found to be the main source of variation in the dataset, since samples from phase PI (operation without the azo dye) clustered separately on the left side of NMDS1 axis, apart from the other phases, which grouped to the right side. Within this main group, samples from phase PII (operation with no sulfate addition) clustered in the upper-right quadrant, while samples from phases PIII and PIV (338 $mg \cdot L^{-1}$ SO_4^{2-} added to the feed) grouped in the lower-right portion. These results indicate that sulfate is the second largest source of variation in the gradient analysis. Calculated stress-value was 0.05, which suggests a relative strong separation of the microbial communities (Paliy and Shankar, 2016).

Some members of the family *Clostridiaceae* and of the genera *Lactococcus*, *Prevotella* and *Atopobium* increased in proportion in the presence of the azo dye, while members of *Ruminococcaceae* and *Clostridium sensu stricto 1* were negatively affected. Members of Firmicutes predominated in all conditions, with relative abundance values of 66-80% (PI), 53-67% (PII), 72-76% (PIII) and 76-81% (PIV) (Appendix Cs). This phylum is often favored under acidogenic conditions (Ribeiro et al., 2022) and was recently associated with azo-reducing activity in the gut microbiota (Zahran et al., 2021).

Figure 5. 6-A shows the most abundant genera in R1 as a function of operational phase. *Lactococcus*, an homolactic bacteria belonging to Firmicutes, increased in proportion from 0.9-9.2% (PI) to 16.9%, in PII, and up to 26.7% after DB22 loading rate was further increased (PIV). In a study conducted by Pérez-Díaz and McFeeters (2009), several lactic acid bacteria were able to modify an azo dye under anaerobic and even aerobic conditions, and therefore *Lactococcus* is a potential azo degrader.

Figure 5. 5. Non-metric multidimensional scaling (NMDS) analysis based on Bray-Curtis distance for the overall bacterial community in the **A)** 1st-stage (R1) and **B)** 2nd-stage (R2) reactors. Low abundant amplicon sequencing variants (ASVs) were removed from the analysis using a 1.5 % threshold.

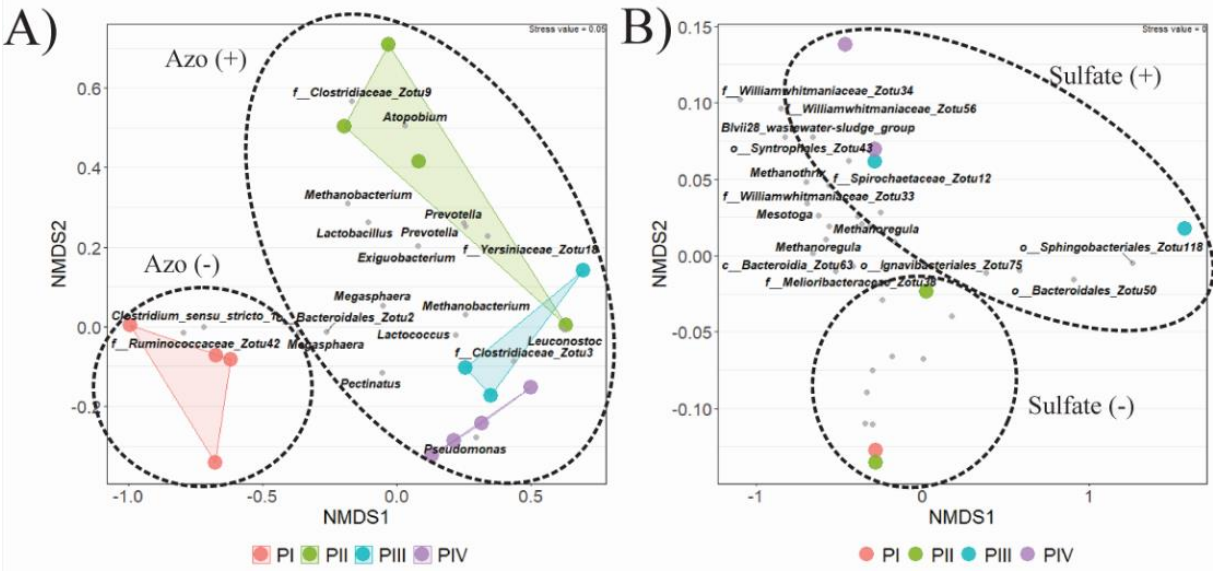

Clostridium was also positively selected in the presence of the azo dye, accounting for 19.5% of the overall bacterial community in the end of the operation (day 328). An anaerobic azoreductase capable of reducing high molecular weight sulfonated azo dyes has been recently described in a member of *Clostridium* (Morrison and John, 2015), meaning that this bacterium might be involved in the biodegradation of DB22 (Morrison and John, 2015).

Prevotella and *Atopobium*, which have no previous records regarding azo decolorization, were also among the genera that were positively selected in the presence of DB22. *Prevotella* can produce acetate from glucose (Takahashi and Yamada, 2000) and major end-products of *Atopobium* include lactic acid and acetate (Acevedo Monroy and Kizilova, 2006; Burton et al., 2004). Since acetate formation presented a strong correlation with color removal (Section 3.3), these bacteria could be involved in decolorization of DB22 via inter-species hydrogen transfer.

On the contrary, samples from R2 rather grouped by either the absence (PI and PII) or presence (PIII and PIV) of sulfate ions in the feed (Figure 5. 5-B), suggesting that azo dyes and/or intermediates from reductive decolorization had little impact on the bacterial community structure in R2. This is likely because microorganisms in R2 were less exposed to the dye, since most of the decolorization occurred in R1, which also received a higher DB22 load.

Nevertheless, these microorganisms were still exposed to aromatic amines and other DB22 fragments recalcitrant to the AD.

Figure 5. 6. Heatmap of the top 18 amplicon sequencing variants (ASVs) in the **A)** 1st-stage (R1) and **B)** 2nd-stage (R2) reactors identified after targeting the bacterial *16S rRNA* V4 region. Samples are faceted by the operational strategies used in the operation of the AD system.

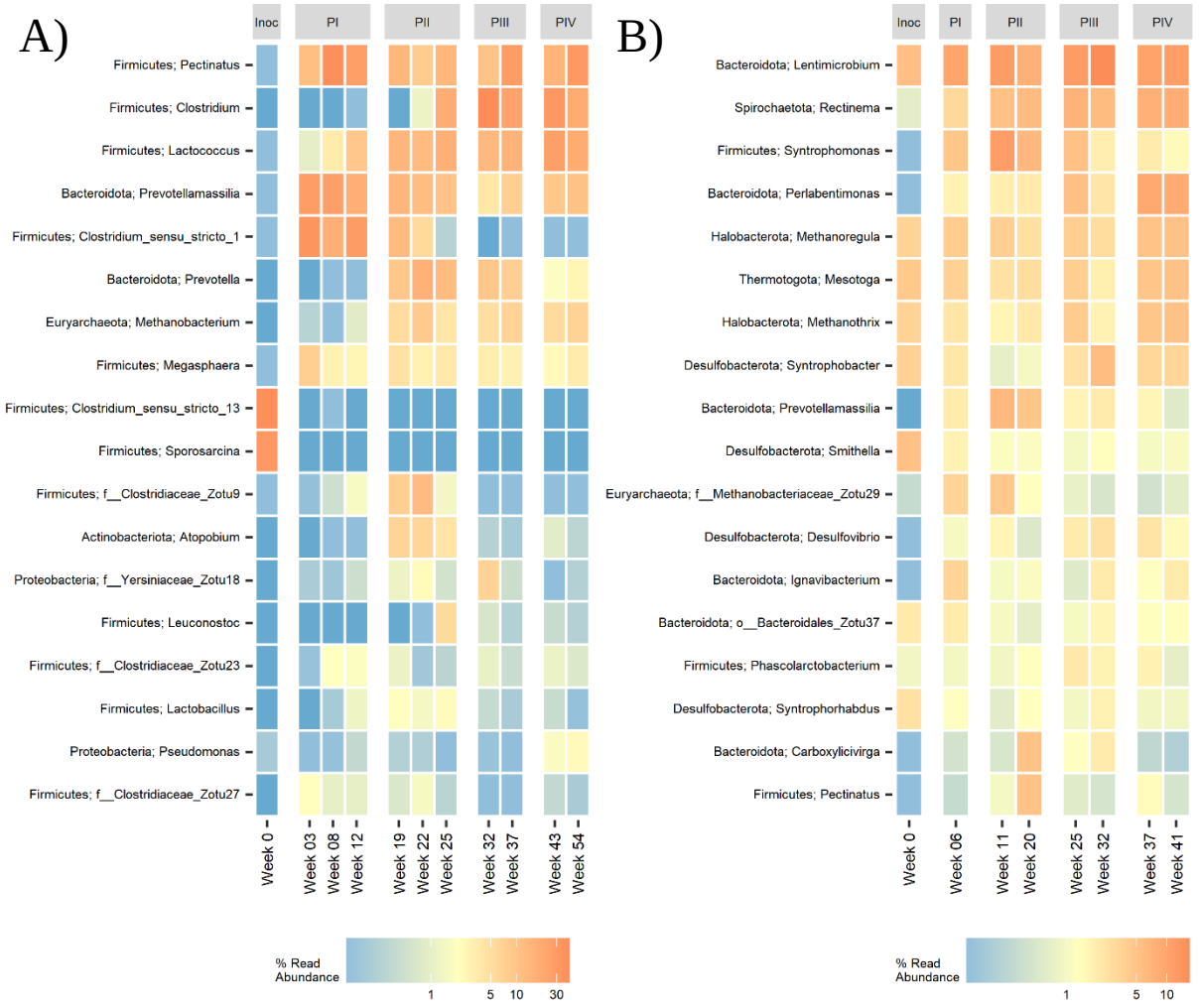

Syntrophobacter and *Desulfovibrio* were among the genera that were enriched in the presence of sulfate. *Syntrophobacter* increased in proportion from 0.7-1%, in phase PII, to 2.5-5.8% after sulfate was introduced into the system (Figure 5. 6-B). *Desulfovibrio* increased its relative abundance from 0.5-1.6 to up to 2.6% under the same conditions. Both are sulfate reducers with fermentation ability (Muyzer and Stams, 2008). SRB community in the two-stage AD system will be covered with more detail in the next section.

3.5. Sulfate reducing bacterial (SRB) and methanogenic communities in the two-stage AD system

No sequences of the *dsrB* and few sequences of the *mcrA* genes were obtained in samples from R1. Indeed, SRB and methanogens were not expected in this reactor due the low pH (pH 4.3-4.5). In R2, methanogenic community presented minor variations during the system's operation (Figure 5. 7-A). Uncultured *Methanobacteriales archaeon*, *Methanosaeta concilii GP-6*, and *Methanosaeta concilii* were the only taxa enriched in the presence of DB22 (Phases PII, PIII and PIV). Members of the order *Methanobacteriales* generally use $H_2 + CO_2$ to produce methane (Acevedo Monroy and Kizilova, 2006), therefore uncultured *Methanobacteriales archaeon* is likely to compete with azo reducers, especially since it accounted for nearly 50% of the methanogenic community in R2. *Methanosaeta concilii*, which comprised up to 20.6% of the *mcrA* sequences in phase PIV, is the only methanogen in R2 capable of utilizing acetate as substrate for methanogenesis (Barber et al., 2011). The increased proportion of hydrogenotrophic methanogens shows that production of methane derived primarily from hydrogen and carbon dioxide, but competition between azo reducers and hydrogen-utilizing methanogens was minimized because bulk color removal occurred in the preceding unit, i.e. R1.

It is important to point out that R2 was inoculated with sludge from a UASB reactor processing wastewater from a poultry slaughterhouse, which are enriched with hydrogenotrophic methanogens. Ammonia released in the biodegradation of protein-rich effluents leads to inhibition of aceticlastic methanogens and in inversion of the Wood–Ljungdahl pathway by SAOB community (Müller et al., 2013). DB22 biodegradation may result in increasing concentrations of ammonia as well. Both the source of the inoculum and the presence of DB22 might have influenced the predominance of hydrogen-utilizing methanogens.

SRB community structure in samples from phases PIII and PIV – which correspond to the operation with added sulfate – did not present a significant shift after the increment in DB22 loading rate (Figure 5. 7-B). Although *Desulfobulbus propionicus* demonstrated a large increase in proportion in phase PIV (approximately 52%), this enrichment had started in the previous phase, at lower concentrations of the azo dye. *Desulfobulbus propionicus* is capable of oxidizing propionate in the presence of sulfate, sulfite or thiosulfate as terminal electron acceptors (Widdel and Pfennig, 1982). Sulfide produced (Reaction 1) can be involved in further transformation of DB22 reduction products in R2, as well as in additional removal of color, since an increase in the concentration of total aromatic amines was observed in this reactor (Oliveira et al., 2022). This is because chemical reduction of azo bonds by sulfide can be expected under

sulfidogenic conditions, but the contribution of this mechanism was found to be little compared to biological reduction (Van Der Zee et al., 2003). Propionate oxidation lead to formation of acetate (Reaction 1), and therefore *D. propionicus* can establish syntrophic interactions with *Methanosaeta concilii* instead of competing for acetate.

$$4propionate^- + 3SO_4^{2-} \rightarrow 4acetate^- + 4HCO_3^- + 3HS^- + H^+ \qquad (Reaction\ 1)$$

Figure 5. 7. Heatmaps of the top amplicon sequencing variants (ASVs) in the 2nd-stage reactor (R2) identified after targeting the functional genes: **A)** *mcrA*; and **B)** *dsrB*. Organisms are listed at the highest taxonomic level.

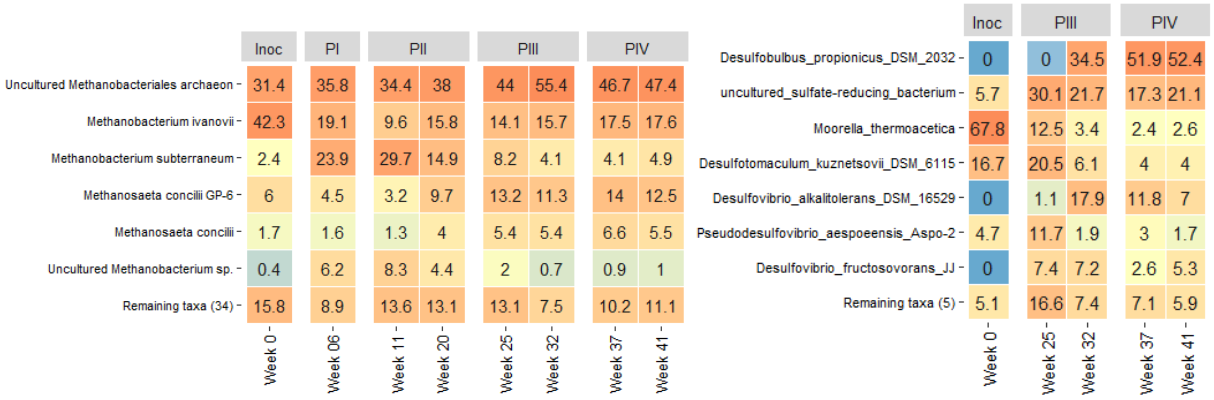

3.6. Syntrophic acetate-oxidizing bacterial (SAOB) and acetogenic communities in the two-stage AD system

Amplicon sequencing targeting the *fhs* gene was conducted in samples from the two-stage AD system to investigate the SAOB and acetogenic communities. A low diversity of these populations was observed in R1, where *Leuconostoc mesenteroides* predominated in all operational phases (62-95%), regardless of the presence of DB22 or sulfate (Figure 5. 8-A). *L. mesenteroides* is an heterolactic lactic acid bacterium (LAB) that produces lactic acid, ethanol and/or acetate as main fermentation end-products (Özcan et al., 2019).

On the other hand, the homolactic LAB *Lactococcus lactis* was clearly selected in the presence of the azo dye, increasing its relative abundance from 0-2.4% in the stabilization phase to up to 11.5% at 32.5 mg·L^{-1} DB22 (Phases PII and PIII), and further to 16.1% when DB22 concentration was further increased to 65 mg·L^{-1} DB22 (Phase PIV). These results are compatible with those from the 16S rRNA gene amplicon sequencing analysis (Section 0) and suggests that *L. lactis* is involved in reductive decolorization of DB22 through the pathway in Eq. 8 (Table 5. 3). However, it is not clear whether decolorization mediated by *L. lactis* is a typical co-metabolic reaction carried by redox mediators. NADH+H$^+$ produced in glycolysis is

recycled during lactate formation from pyruvate, resulting in no net hydrogen production. Other studies reported azo dye reduction by *L. lactis* (You and Teng, 2009) and LAB (Pérez-Díaz and McFeeters, 2009). We hypothesize that azo dye decolorization by *L. lactis* occurs through the action of enzymes with high specificity to azo dyes, since genes encoding the production of the enzyme FMN-dependent NADH-azoreductase were found in the genome of *L. lactis* isolated from this same reactor (unpublished data).

SAOB and acetogenic communities were more diverse in R2 (Figure 5. 8-B). *Prevotella melaninogenica* was remarkably enriched at higher DB22 concentrations (Phase PIV), accounting for up to 41.1% of the *fhs* sequences. This bacterium is able to produce acetic and succinic acids as primary end products of glucose or lactose fermentation (Shah and Gharbia, 1992). On the other hand, *Sporolituus thermophilus* (Ogg and Patel, 2009), which utilizes both malate and citrate, decreased in proportion throughout R2 operation, particularly under sulfidogenic conditions (Phases PIII and PIV). Probably, this apparent drop in the relative abundance is rather a consequence of the enrichment of *P. melaninogenica*.

Figure 5. 8. Heatmaps of the top 15 amplicon sequencing variants (ASVs) in the **A)** 1st-stage reactor (R1) and **B)** 2nd-stage reactor (R2) identified after targeting the *fhs* gene. Organisms are listed at the highest taxonomic level.

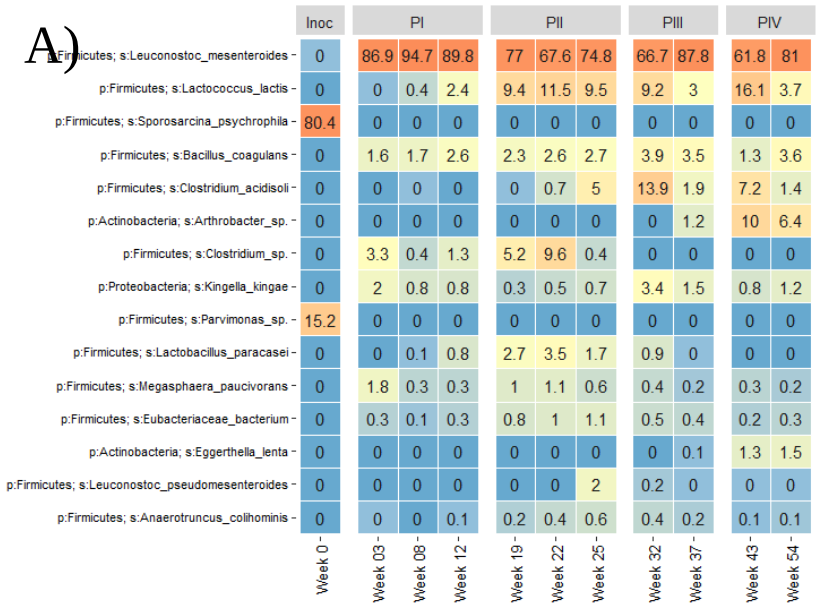

B)

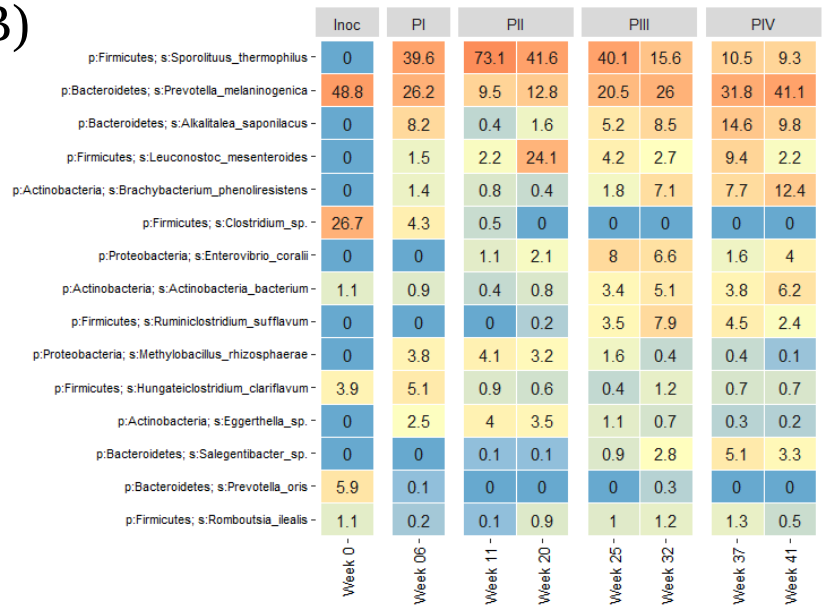

	Inoc	PI	PII		PIII		PIV	
p:Firmicutes; s:Sporolituus_thermophilus	0	39.6	73.1	41.6	40.1	15.6	10.5	9.3
p:Bacteroidetes; s:Prevotella_melaninogenica	48.8	26.2	9.5	12.8	20.5	26	31.8	41.1
p:Bacteroidetes; s:Alkalitalea_saponilacus	0	8.2	0.4	1.6	5.2	8.5	14.6	9.8
p:Firmicutes; s:Leuconostoc_mesenteroides	0	1.5	2.2	24.1	4.2	2.7	9.4	2.2
p:Actinobacteria; s:Brachybacterium_phenoliresistens	0	1.4	0.8	0.4	1.8	7.1	7.7	12.4
p:Firmicutes; s:Clostridium_sp.	26.7	4.3	0.5	0	0	0	0	0
p:Proteobacteria; s:Enterovibrio_coralii	0	0	1.1	2.1	8	6.6	1.6	4
p:Actinobacteria; s:Actinobacteria_bacterium	1.1	0.9	0.4	0.8	3.4	5.1	3.8	6.2
p:Firmicutes; s:Ruminiclostridium_sufflavum	0	0	0	0.2	3.5	7.9	4.5	2.4
p:Proteobacteria; s:Methylobacillus_rhizosphaerae	0	3.8	4.1	3.2	1.6	0.4	0.4	0.1
p:Firmicutes; s:Hungateiclostridium_clariflavum	3.9	5.1	0.9	0.6	0.4	1.2	0.7	0.7
p:Actinobacteria; s:Eggerthella_sp.	0	2.5	4	3.5	1.1	0.7	0.3	0.2
p:Bacteroidetes; s:Salegentibacter_sp.	0	0	0.1	0.1	0.9	2.8	5.1	3.3
p:Bacteroidetes; s:Prevotella_oris	5.9	0.1	0	0	0	0.3	0	0
p:Firmicutes; s:Romboutsia_ilealis	1.1	0.2	0.1	0.9	1	1.2	1.3	0.5
	Week 0	Week 06	Week 11	Week 20	Week 25	Week 32	Week 37	Week 41

Brachybacterium phenoliresistens presented an increasing pattern in its relative abundance values as from phase PIII, i.e. after sulfate addition. This specie can degrade hydrocarbons under high salinity conditions and have been isolated from oil-contaminated sites (Chou et al., 2007; Wang et al., 2014). The ability to survive in saline environments explain the enrichment of this bacterium after exposure to sulfate. Moreover, the proportion of *B. phenoliresistens* further increased to 12.4% when higher DB22 concentrations were loaded into the system, which can be attributed to the ability of this species to tolerate high levels of phenol and degrade hydrocarbons. DB22 was converted to aromatic compounds in the preceding unit, which could not be further mineralized, but were transformed in R2 (Oliveira et al., 2022). This means that *B. phenoliresistens* could be involved in the transformation of hydrocarbons in R2.

4. Conclusion

Azo dye decolorization in the two-stage AD system occurs mainly as a result of hydrogen-producing reactions (in the form of H_2 and/or reduced cofactors) in a mechanism mediated by electron shuttles. Enzymes with high specificity (e.g. azoreductases from *L. lactis*) seems to play an important role as well. Acidogens from R1 were observed to be sensitive and undergo selection upon exposure to azo dyes, whereas microbial communities in R2 are exposed to lower levels of azo dye and therefore appear less sensitive. These results are relevant when considering organic matter and sulfate removals and biogas production in R2, as methanogens and SRB show less impact under these circumstances.

Acknowledgement

This work was supported by the Fundação do Amparo à Pesquisa do Estado de São Paulo (process numbers 2015/06246-7, 2018/24269-2 and 2020/11860-4) and the Coordenação de Aperfeiçoamento de Pessoal de Nível Superior (CAPES) – Brazil (Finance Code001). The authors also would like to thank Dr. Nadieh de Jonge for her technical and scientific support.

Chapter 6

New insights into the mechanism of azo dye biodegradation by *Lactococcus lactis*

Abstract. Azo dye reduction by syntrophic microbial communities is still unclear, with conflicting observations reported in the literature. In this study, the biodegradation mechanism of a model azo dye by *L. lactis* strain LLSP-01 isolated from an acidogenic reactor system was investigated. Proteomics and RT-PCR analyses results showed that LLSP-01 azoreductase (AzoL) was not involved. The mechanism involved biosorption by glycoconjugates, particularly exopolysaccharides (EPS) and rhamnolipids, as proteins from the LPS O-antigen metabolism were statistically more abundant in cells challenged with the target compound. Electrons were transferred through the biofilm matrix by hopping, in a mechanism that involved a SDR family oxidoreductase and riboflavin carriers. Reductive cleavage of the azo bonds resulted in aromatic products that were partially degraded by a ring-cleaving dioxygenase before the complete depletion of oxygen in the reaction mixture. These results show that azo dye reduction by *L. lactis* is mediated by enzymes with broad range specificity, and not the typical azoreductases. This information can assist in the design of new strategies for the bioremediation of textile azo dyes.

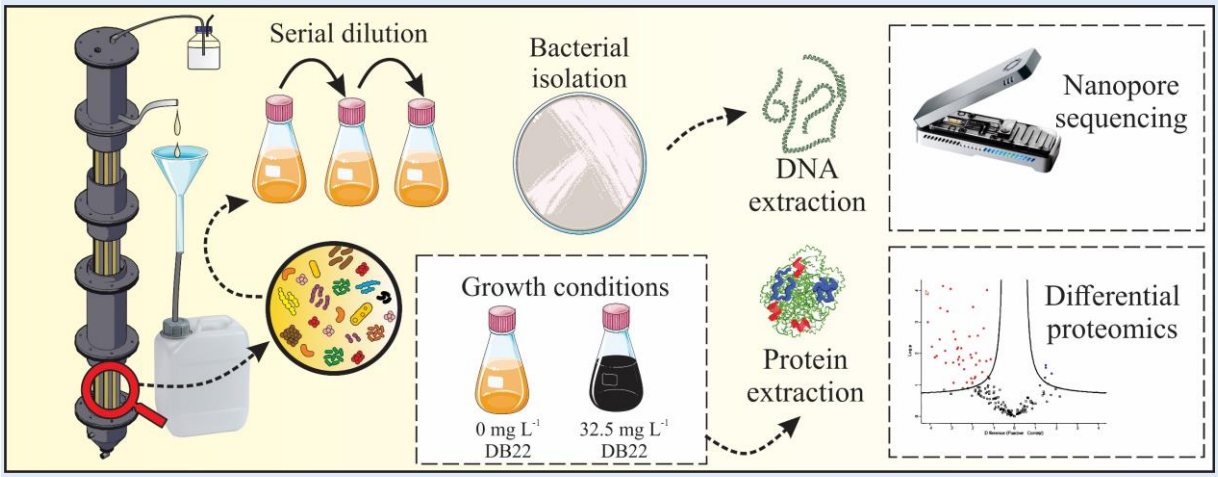

A modified version of this chapter will be submitted to a journal published by Elsevier. Elsevier does not count publication of an academic thesis as prior publication.

Oliveira, J.M.S., Poulsen, J.S., Foresti, E., Nielsen, J.L. 2022.

1. Introduction

Biological treatment of azo dyes has proven to be a safer and more cost effective alternative to solutions based on physical-chemical methods (Oliveira et al., 2020), and has shown to reduce the biotoxicity of azo dye wastewaters (Amaral et al., 2014; Carvalho et al., 2020). In reduced environments, azo dye is biodegraded cometabolically through a process termed *reductive decolorization*. This mechanism was speculated to involve a reaction in which reducing equivalents, as well as reduced cofactors, work as secondary electron donors to cleave the azo bonds (Santos et al., 2007).

In anaerobic reactors, reductive decolorization was found to be correlated with the conversion of carbohydrates into volatile organic acids and organic solvents, and particularly with hydrogen-producing pathways (Oliveira et al., 2022). This raises a question on whether enzymes involved in the carbohydrate metabolism catalyzes the reductive cleavage of the azo bonds instead of the typical azoreductases. In fact, some enzymes have broad range specificity and will act on many different substrates (Jackson et al., 2010). Moreover, azoreductases are more frequently found in aerobic bacteria, with few reports among strict anaerobes (Misal and Gawai, 2018; Morrison and John, 2015). It is therefore unclear if reductive decolorization by syntrophic microbial communities happens manly through the action of these specific enzymes in anoxic or anaerobic environments.

The advancement of high-throughput omics has brought new light into the study of aromatic hydrocarbons biodegradation, and the proteomics approach has been used to identify and quantify enzymes involved in the degradation pathway of such compounds (Kim et al., 2009). Xenobiotics-degrading cells grown in the presence of the target compound overexpress enzymes related to the catabolism of these compounds, and therefore these proteins are differentially more abundant (Almeida et al., 2013; Kim et al., 2004).

In this study, the degradation pathway of the azo dye Direct Black 22 (DB22) by *Lactococcus lactis* was investigated using label-free proteomics analysis. The bacterium was isolated from an acidogenic reactor system fed with synthetic textile wastewater and was significantly enriched throughout its operation (Oliveira et al., 2022). The findings provide novel information on the biodegradation of textile azo dyes, which can help in the design of new strategies and technologies for the bioremediation of such compounds.

2. Materials and Methods

2.1. Azo dye and synthetic textile wastewater

Direct Black 22 (DB22, CAS 6473-13-8) was acquired from a local dye supplier (Aupicor Quimica©, Pomerode, Brazil). Dye molecular weight and purity were 1083.97 g mol^{-1} and 42%, respectively. The dye was previously hydrolyzed by increasing pH to 11 and heating at 80 ºC for 1 h to simulate the actual state of the dye in textile effluents (Santos et al., 2004). The basal medium used in the study was based on the composition of a real textile wastewater (Amorim et al., 2013) and contained: DB22 (32.5 mg L^{-1}), glucose (1.70 gCOD L^{-1}), KH_2PO_4 (0.25 g L^{-1}), Na_2SO_4 (0.50 g L^{-1}), NaCl (0.50 g L^{-1}), yeast extract (0.40 g L^{-1}), $NaHCO_3$ (0.15 g g^{-1} COD) and 1 mL L^{-1} trace elements solution (Appendix D).

2.2. Anaerobic bacterium isolation

A bacterium capable of decolorizing DB22 was isolated anaerobically from a continuous acidogenic reactor operated with synthetic textile wastewater (Oliveira et al., 2022). A serial dilution series (10^{-1} to 10^{-20}) of the DB22 degrading consortium was applied in antibiotic flasks (50 mL) containing 25 mL of filter-sterilized medium (composition shown in 2.1). The flasks were flushed with N_2 for 1 min and incubated at 30 ºC under static conditions for a period of 48 h. The highest dilution which gave satisfactory color removal were plated in sterilized solid medium (synthetic textile wastewater added by 1.5% bacteriological agar) using pour plate technique. Petri dishes were incubated at 30ºC in a Gas-Pack jar with anaerobic sachets Oxoid™ AnaeroGen™ (Thermo Fisher Scientific™, Massachusetts, USA) for at least 24 h.

2.3. Whole-genome sequencing

2.3.1. High molecular weight DNA extraction

High molecular weight DNA was obtained using the DNeasy® Blood & Tissue Kit (Qiagen, Hilden, Germany) and following the manufacturer's protocol. DNA quantity was verified using a Qubit 2.0 fluorometer (Thermo Fisher Scientific, USA) with Qubit dsDNA BR Assay kit (Thermo Fischer Scientific, USA). DNA integrity was evaluated using the TapeStation 2200 with genomic DNA ScreenTapes (Agilent, USA).

2.3.2. Genome sequencing

DNA repair, end preparation and ligation of sequencing adaptors were performed using the Native barcoding genomic DNA protocol in conjunction with the Ligation Sequencing Kit (MinION; Oxford Nanopore Technologies). The DNA library was loaded onto a MinION R9.4.1 flow cell and sequenced for 72 h using MinKNOW on a computer.

2.3.3. Bioinformatics

Base calling was performed with Guppy v3.2.10, which is integrated into MinKNOW. Porechop v0.2.3 was used to remove sequencing adapters and for the demultiplexing of Nanopore reads (https://github.com/rrwick/Porechop). The quality of the sequences was assessed using NanoPlot v1.24.0 (De Coster et al., 2018). Reads were filtered for length (>600 bp) and quality (>Q8) using NanoFilt v.2.6.0 (https://github.com/wdecoster/nanofilt) and long-read assembly was conducted with Canu v2.0 (Koren et al., 2017). The consensus genome was constructed after two rounds of polishing with Racon v1.3.3 (Vaser et al., 2017) and Medaka v1.0.1 (https://github.com/nanoporetech/medaka). Genome assembly and completeness were assessed using BUSCO (benchmarking universal single-copy orthologs) v5.0.0 (Manni et al., 2021).

2.4. Decolorization assays

Decolorization assays were conducted in quadruplicates in serum bottles (250 mL) containing 100 mL of the basal medium (composition shown in 2.1). The flasks were inoculated with overnight grown cultures of *L. lactis* (10%, v v^{-1}) and incubated at 30 ºC and 150 rpm. Samples (1 mL) were collected periodically for color and optical density (OD_{600}) measurements. Decolorization efficiency was calculated as shown in the Eq. (1). Color interference on OD_{600} measurements was eliminated by subtracting the absorbance values of centrifuged samples.

$$Decolorization = \frac{\int_{400\ nm}^{700\ nm} A_0.\,\mathrm{d}\lambda - \int_{400\ nm}^{700\ nm} A_t.\,\mathrm{d}\lambda}{\int_{400\ nm}^{700\ nm} A_0.\,\mathrm{d}\lambda}\ .100 \qquad (Eq.1)$$

in which A_0 is the initial absorbance of the sample; A_t is the absorbance of the sample at a time *t*; and dλ is an infinitesimal wavelength interval.

2.5. Proteomics analysis

2.5.1. Protein extraction

Bacterial cultures grown until mid-logarithmic growth phase (OD600 = 0.24) were harvested by centrifugation at 4000 x g for 8 min and rinsed with ultrapure water. Growth conditions were similar to those described earlier (Section 2.4). Cell pellets were treated with a protease inhibitor cocktail and resuspended in a mixture containing 385 µL TEAB buffer (50 mM triethylammonium bicarbonate, 1% (w/w) sodium deoxycholate, pH 8.0) and 385 µL B-PER lysis buffer (Thermo Fisher Scientific, Waltham, Massachusetts, United States). Samples were transferred to Covaris® AFA milliTUBEs and cells were disrupted using a Covaris® focused-ultrasonicator system (Woburn, Massachusetts, United States). Extracted proteins were quantified using the Qubit Protein BR Assay Kit.

2.5.2. Peptide analysis

A total of 100 µg of proteins were transferred to Protein LoBind® tubes, after which acetone precipitation was performed in the samples. Peptide digestion and purification were conducted using the PreOmics® iST kit (Planegg, Germany) and following the manufacturer's protocol. Tryptic peptides were analyzed using liquid chromatography – electrospray ionization tandem mass spectrometry (LC-ESI-MS/MS), as described elsewhere (García-Moreno et al., 2020).

2.5.3. Bioinformatic processing

Protein identification and quantification were performed with MaxQuant v2.0.3.1 (Cox and Mann, 2008), using the Andromeda search engine with default settings (Cox et al., 2011). The false discovery rate used was 1%. Carbamidomethylation was set as fixed modification, whereas acetylation of protein N-termini and oxidation of methionine were set as variable modifications. Samples spectra were searched against the predicted proteome from *L. lactis* isolate LLSP-01. The MaxLFQ algorithm was used to quantify proteins with at least one unique or razor peptide. The protein groups and evidence files were inputted into MSstats for further statistical analysis (Choi et al., 2014). Contaminants and peptide and charge with only one or two measurements across runs were removed. Data was optimized for statistical modelling using log-transformation with base 2 and quantile normalization to remove systematic bias between MS runs. Protein summarization was performed using the Tukey's median polish and linear mixed effects model with Empirical Bayes moderation was used to compare the two conditions

(control and DB22-exposed groups) for differentially abundant proteins (Föll and Fahrner, 2022).

2.6. RNA isolation and RT-PCR analysis

L. lactis LLSP-01 was grown under the same conditions as described earlier for the proteomics analysis. Exponentially growing cells incubated without or with DB22 (1 and 32.5 mg L^{-1}) were harvested by centrifugation at 4000 x g for 8 min. RNA extraction was conducted using the RNeasy® kit (Qiagen, Hilden, Germany) according to the manufacturer's protocol. RNA quality was assessed using TapeStation 2200 with genomic RNA ScreenTape (Agilent, USA) and concentration was measured using Qubit 2.0 (Thermo Fisher Scientific, USA) with Qubit RNA BR Assay kit (Thermo Fischer Scientific, USA).

Complimentary DNA (cDNA) was synthetized by reverse transcription of total RNA (1 µg) using the SuperScript™ III First-Strand Synthesis System (Thermo Fisher Scientific, USA). cDNA was amplified by PCR using *L. lactis* LLSP-01 azoreductase (AzoL) primers designed using the RealTime PCR Design Tool (Integrated DNA technologies, Coralville, USA). Primers used were AzoL-fw (5'-GGT CCT GTT GGT TTA GCA AAT G-3') and AzoL-rev (5'-GTC CTT CAA CGG CAA TTT GTC-3'). PCR settings were as following: initial denaturation at 95 ºC for 2 min; amplification for 25 cycles at 95 ºC for 15 s, 58.6 ºC for 15 s, and 72 ºC for 20 s; and a final extension of 5 min at 72 ºC.

3. Results and Discussion

3.1. DB22 decolorization by *L. lactis*

L. lactis reached decolorization efficiencies of up to 84.1% after incubation for 37 h at 30 ºC (Figure 6. 1). Cells exposed to DB22 presented lower growth rates, suggesting that the azo dye was toxic to *L. lactis*. However, cells grown under DB22-induced stress presented higher optical densities after 37 h (OD_{600} = 0.417), while non-exposed cells (control) reached the stationary phase earlier, after 17 hours (OD_{600} = 0.338). It was hypothesized that the higher biomass yields achieved in the presence of DB22 resulted from the higher concentration of substrate in these experiments, as DB22 can serve as additional substrate to support *L. lactis* growth. However, this phenomenon could be also provoked by metabolic changes induced by the azo dye. The physiological and metabolic responses of *L. lactis* challenged with DB22 were further investigated using label-free proteomics analysis.

Figure 6. 1. Effects of the azo dye Direct Black 22 (DB22, 32 mg L^{-1}) on the growth of *L. lactis* **(A)** and DB22 decolorization efficiency **(B)** over 38 h. Dashed lines represent the times in which samples were harvested for protein extraction. Assays were conducted in quadruplicates.

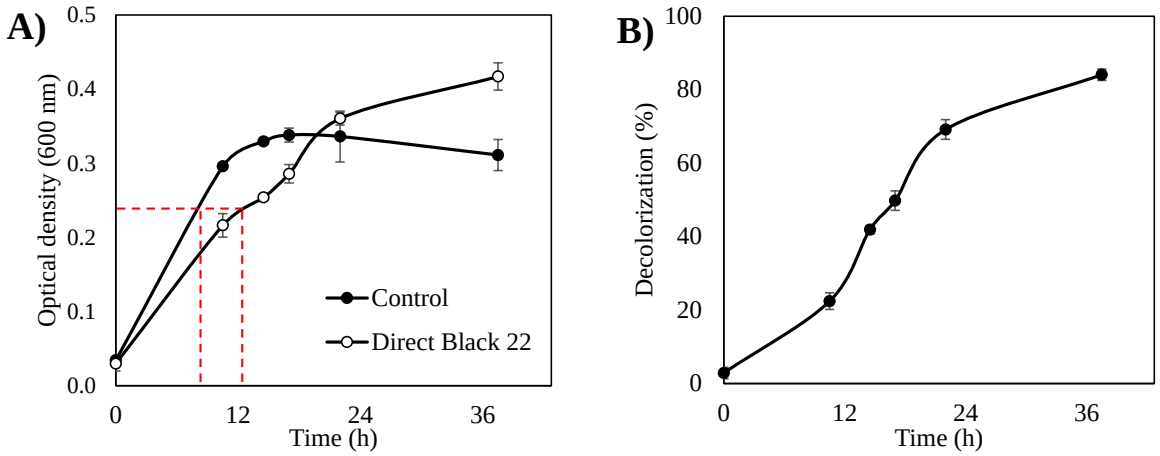

3.2. Strain verification and genome quality

The whole genome of *L. lactis* was sequenced in a MinION R9.4.1 flow cell (Flow cell ID FAQ35713), generating a total of 1.1 M reads and a length of 2.3 Gb. After filtering on quality and trimming, 265,205 reads remained. The estimated completeness of the genome was 96.0% and the contamination was 1.6% based on BUSCO analysis. A nucleotide BLAST search against NCBI showed that the strain had a 97.8% similarity with *Lactococcus lactis* IO-1 (AP012281).

3.3. Proteomics analysis of *L. lactis* challenged with the azo dye

A total of 9080 proteins were detected in the differential proteomics analysis, of which 68 significantly changed in abundance when *L. lactis* was exposed to 32.5 mg L^{-1} DB22 ($p \leq 0.05$; $\log_2FC < -1$ or $\log_2FC > 1$). While 61 proteins were relatively less abundant, only 7 proteins increased in abundance upon growth in the presence of the azo dye and two were detected only in the positive group (Figure 6. 2 and Table 6. 1; see Appendix D for the full list).

The experiment conducted with biological quadruplicates revealed a change in the metabolic pathways favoring L-ribulose production from L-arabinose, as L-arabinose isomerase had the highest increment in abundance in the presence of DB22 ($\log_2FC = 2.78$). L-Ribulose is a precursor of D-Ribulose 5-phosphate, which is related to the biosynthesis of riboflavin through the pentose phosphate pathway (Kanehisa, 2000; Kanehisa et al., 2008). Riboflavin is as well-known redox mediator involved in the co-metabolic degradation of azo dyes (Imran et al., 2016).

A SDR family oxidoreductase also had an increase in its abundance ($log_2FC = 1.57$) compared to the control group. Short-chain dehydrogenases/reductases is a family of NADPH-dependent oxidoreductases (Kavanagh et al., 2008), which play a major role in decolorization of azo dyes (Singh et al., 2015).

Proteins involved in the LPS O-antigen metabolism were also more abundant in the proteomes of *L. lactis* exposed to the azo dye. dTDP-glucose 4,6-dehydratase ($log_2FC = 1.31$) converts dTDP-α-D-glucose into dTDP-4-dehydro-6-deoxy-α-D-glucose, while this later is converted into dTDP-4-dehydro-β-L-rhamnose in a reaction catalyzed by dTDP-4-dehydro-rhamnose 3,5-epimerase (identified only in samples exposed to DB22) (Marolda and Valvano, 1995). These proteins are involved in the production of both cell wall polysaccharides and rhamnose-containing EPS in *L. lactis* (Boels et al., 2004), which might be related to the higher OD yields observed in cells exposed to the azo dye.

Figure 6. 2. Volcano plot generated to compare proteins differentially abundant in *L. lactis* LLSP-01 cells grown in the absence or in the presence of the azo dye Direct Black 22 (32 mg L^{-1}). Vertical and horizontal dashed lines represent, respectively, the log fold change (log_2FC) and p-value thresholds used to pronounce statistical significance.

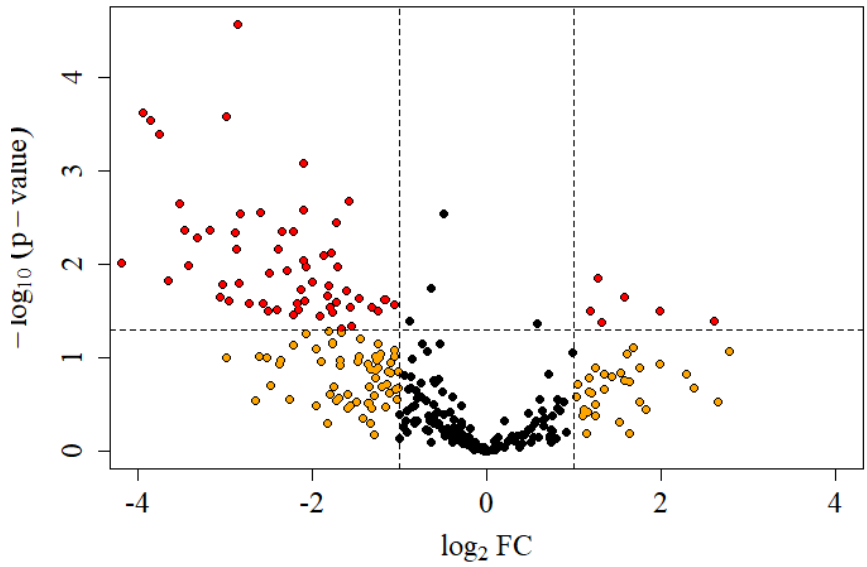

Table 6. 1. The top proteins differientally abundant in *L. lactis* LLSP-01 cells grown in the presence of 32.5 mg L^{-1} Direct Black 22.

p-value	log_2FC	Accession	Protein name or description
I - Upregulated			
8.5E-02	2.78	WP_058211938.1	L-arabinose isomerase
4.0E-02	2.60	WP_046781838.1	WxL domain-containing protein
3.1E-02	1.99	WP_058217091.1	BMP family ABC transporter substrate-binding protein
2.2E-02	1.57	WP_058219886.1	SDR family oxidoreductase
4.2E-02	1.31	WP_033899140.1	dTDP-glucose 4,6-dehydratase
1.4E-02	1.27	WP_064973379.1	ring-cleaving dioxygenase
3.1E-02	1.19	WP_003129660.1	vitamin B12 independent methionine synthase
--	--	WP_010905193.1	dTDP-4-dehydrorhamnose 3,5-epimerase
--	--	WP_058210984.1	phosphopyruvate hydratase
II - Downregulated			
9.7E-03	-4.20	WP_004254538.1	DNA starvation/stationary phase protection
2.4E-04	-3.94	WP_058223384.1	aldo/keto reductase
2.9E-04	-3.86	WP_003129551.1	DNA-directed RNA polymerase subunit delta
4.3E-03	-3.47	WP_003129453.1	cell division regulator GpsB
1.0E-02	-3.42	WP_057720276.1	ammonia-dependent NAD(+) synthetase
5.2E-03	-3.32	WP_058220094.1	30S ribosomal protein S7
4.3E-03	-3.18	WP_003130887.1	phosphate signaling complex protein PhoU
2.2E-02	-3.06	WP_081041499.1	5-bromo-4-chloroindolyl phosphate hydrolase
1.6E-02	-3.04	WP_038599155.1	FMN-dependent NADH-azoreductase
2.6E-04	-2.98	WP_003131560.1	superoxide dismutase [Mn]
2.5E-02	-2.96	WP_003132352.1	50S ribosomal protein L20
4.7E-03	-2.89	WP_058219555.1	elongation factor Ts
6.9E-03	-2.87	WP_015426160.1	transcription regulator
2.7E-05	-2.87	WP_029344674.1	universal stress protein
1.6E-02	-2.84	WP_003130829.1	RNA polymerase sigma factor RpoD
2.8E-03	-2.83	WP_003131820.1	IreB family regulatory phosphoprotein
2.6E-02	-2.74	WP_003130364.1	response regulator transcription factor
2.6E-02	-2.57	WP_003130880.1	phosphate ABC transporter substrate-binding protein

In a recent study, it was proved that the decolorization of an azo dye by *Aliiglaciecola lipolytica* initiated with dye adsorption onto cells by EPS. EPS overproduction contributed to biosorption and self-flocculation, and the adsorbed dye was degraded through the action of oxidoreductases such as azoreductase and laccase (Wang et al., 2020). Other studies have reported the relevant contribution of biofilm mediated degradation in the bioremediation of xenobiotics by EPS-producing microorganisms (Premnath et al., 2021).

dTDP-glucose 4,6-dehydratase and dTDP-4-dehydro-β-L-rhamnose are also key enzymes involved in the biosynthesis of rhamnolipids, which are extracellular glycoconjugates that act as emulsifiers (Chong and Li, 2017). These biosurfactants have an important role in the bioremediation of organic pollutants, as they can reduce surface tension and therefore increase the bioavailability of these compounds (Bhatt et al., 2021). Rhamnolipids were found to promote the dissolution, biosorption, adsorption and enhanced degradation of organic contaminants (Bhatt et al., 2021; Mnif and Ghribi, 2016; Zhang et al., 2011).

Moreover, *L. lactis* presented increased abundance of a WxL domain-containing protein ($log_2FC = 2.60$). WxL region is a cell wall biding domain, and therefore proteins fused to this domain are displayed on the bacterial surface (Brinster et al., 2007). Protein-displaying bacteria can act as bioadsorbents (Plavec et al., 2019), further evidencing that *L. lactis* initiate DB22 decolorization with biosorption followed by reduction of the azo bonds mediated by a SDR family oxidoreductase and using riboflavin as redox mediator.

Surprisingly, a ring-cleavage dioxygenase was also upregulated in the presence of DB22 ($log_2FC = 1.27$). This enzyme catalyzes the ring fission of aromatic compounds such as benzene, naphthalene and aromatic amines (Vaillancourt et al., 2004). Moreover, ring-cleaving dioxygenases were found to be involved in the detoxification of direct azo dyes by a facultative anaerobe (Chen et al., 2021). *L. lactis* decolorization assays were conducted under anoxic conditions, as nitrogen was not flushed in the serum bottles to simulate the growth conditions of the inoculum source. It is hypothesized that this enzyme had a substantial contribution in the biodegradation of DB22 in the initial stage of the experiment, i.e. before oxygen was totally depleted.

Several transcription regulators and proteins involved in the regulation of cell growth were statistically less abundant in the cells challenged with the azo dye. These proteins include cell division regulator GpsB ($log_2FC = -3.47$), phosphate signaling complex protein PhoU ($log_2FC = -3.18$), DNA-directed RNA polymerase subunit delta ($log_2FC = -3.86$), transcription

regulator (log_2FC = -2.87) and RNA polymerase sigma factor RpoD (log_2FC = -2.84). Ribosomal proteins and other proteins involved in the cellular process of translation (e.g., elongation factor Ts) were downregulated as well. These results explain the decreased growth rates in *L. lactis* cells grown in the presence of DB22, showing that the azo dye and its biodegradation products induce several stress responses in *L. lactis*.

3.4. FMN-dependent NADH azoreductase not involved in the decolorization of DB22 by strain LLSP-01

Interestingly, an FMN-dependent NADH azoreductase, which catalyzes reductive cleavage of azo bonds (Santos et al., 2007), was identified with higher abundances in the control group (log_2FC = -3.04) . Morrison and John (2015) observed azoreductase activity in extracts from the periplasmic fraction of *Clostridium perfringens* cells in both the dye- and the non-dye exposed group. The authors further showed that the charged groups on sulfonated dyes caused the release of azoreductase into the extracellular matrix, and that protein release was not caused by cell lysis or leakage. This resulted in increased azoreductase activity in extracts from the periplasmic fractions of cells not previously exposed to sulfonated azo dyes. It was hypothesized, therefore, that azoreductase was released upon exposure to DB22, therefore explaining the lower abundance of the enzyme within cells challenged with the dye.

To test this hypothesis, we checked for signal peptides in the *L. lactis* LLSP-01 AzoL protein, which was found not to contain any of these short amino acid sequences (Teufel et al., 2022). This means that the AzoL could not be translocated across the bacterial membrane. Further analysis using RT-PCR gave no AzoL amplicons for the control group nor for cells exposed to lower (1 mg L^{-1}) or higher (32.5 mg L^{-1}) concentrations of DB22, while the band corresponding to AzoL was clearly observed in the genomic DNA of *L. lactis* (Figure 6. 3). These results agree with the findings from the proteomics analysis. It was hypothesized that AzoL is not continuously expressed during the growth of *L. lactis* and this enzyme was not involved in the decolorization of DB22.

3.5. Direct Black 22 biodegradation mechanism

DB22 biodegradation by *L. lactis* initiates with adsorption to the biofilm matrix, as glycoconjugates are produced in excess in the presence of the azo compound (

Figure **6. 4**). EPS and rhamnolipids overproduction were revealed by the enrichment of two enzymes involved in the LPS O-antigen metabolism, i.e. dTDP-glucose 4,6-dehydratase

(RmlB) and dTDP-4-dehydro-β-L-rhamnose (RmlC). The adsorbed dye is indirectly reduced by a SDR family oxidoreductase. Electrons produced in the interior of the cells are carried through the biofilm matrix by hopping, in a mechanism mediated by riboflavin carriers. Hopping was found to be the prevailing pathway for extracellular electron transfer across EPS matrices (Xiao et al., 2017).

Figure 6. 3. *L. Lactis* LLSP-01 azoreductase (AzoL) RT-PCR amplicons. Lane A1 – cDNA of *L. lactis* cells not exposed to Direct Black 22 (DB22); Lane B1 – cDNA of *L. lactis* cells exposed to 1 mg L^{-1} DB22; Lane C1 – cDNA of *L. lactis* cells exposed to 32.5 mg L^{-1} DB22; Lane D1: genomic DNA of *L. lactis*.

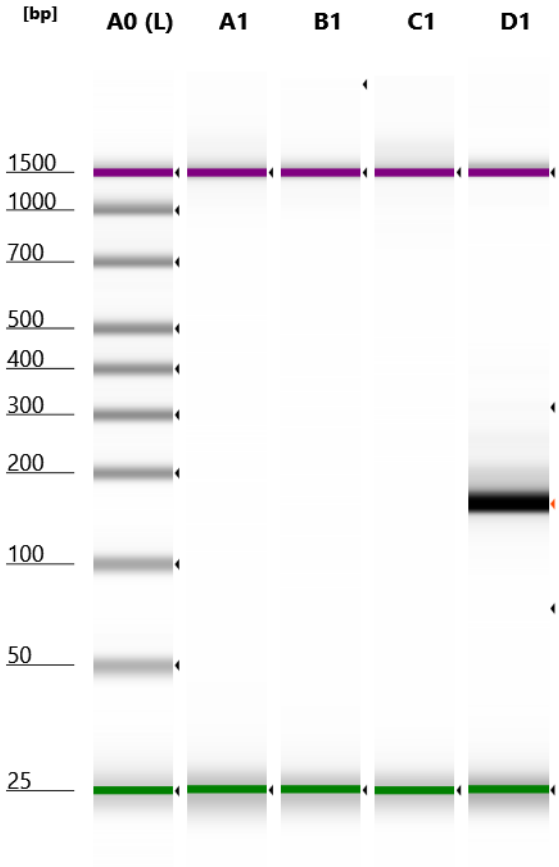

Reductive cleavage of the azo bonds yields monocyclic aromatic amines such as 1,2,4-triaminobenzene, oxalic acid p-phenylenediamine and 2-aminobenzenesulfonate. These molecules can be converted to catechol derivatives and to 3-sulfocatechol (Figure 6. 5), in reactions catalyzed by aniline dioxygenase (Arora, 2015; Perei et al., 2001). Further degradation by ring-cleaving dioxygenases (Vaillancourt et al., 2004) results in the formation of compounds with the skeleton of the 2-aminomuconic acid and 3-sulfomuconate.

Figure 6. 4. Proposed biodegradation mechanism of the azo dye Direct Black 22 (DB22) by strain LLSP-01. RmlB (dTDP-glucose 4,6-dehydratase) and RmlC (dTDP-4-dehydro-β-L-rhamnose) were differentially more abundant in the presence of the azo dye. These enzymes are involved in the production of glycoconjugates in *L. lactis*, including rhamnose-containing exopolysaccharides and rhamnolipds. It is hypothesized that DB22 is adsorbed into the biofilm matrix and indirectly reduced by a SDR family oxidoreductase. Reducing equivalents are transfferred through the extracellular matrix by hopping, in a mechanism mediated by riboflavin carriers.

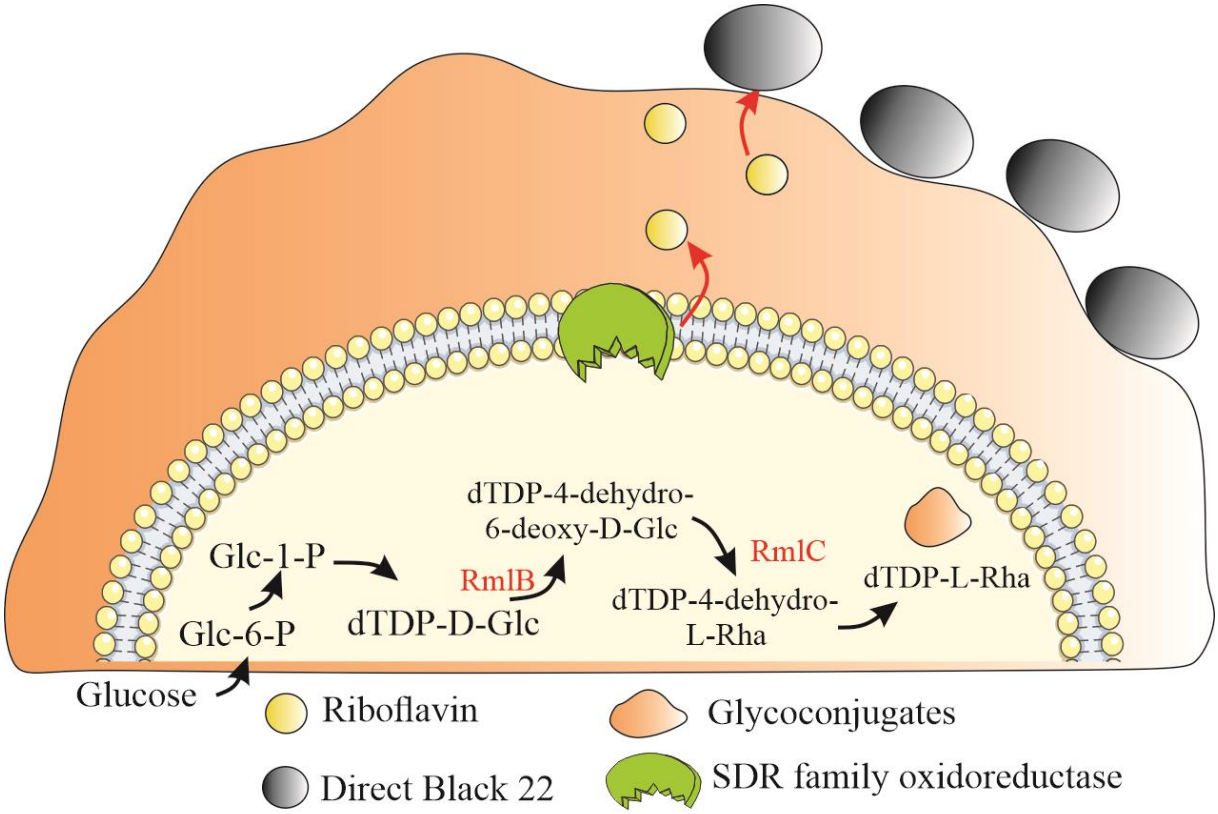

Ring-cleaving dioxygenases act by incorporating two atoms of oxygen to the molecule (Vaillancourt et al., 2004). *L. lactis* is a facultative anaerobe isolated from a continuous acidogenic reactor system. In the bioreactor system, the textile effluent was pumped at a flow rate of 17.1 L d^{-1} and the feed tank was not flushed with nitrogen to strip the oxygen. It was hypothesized that that the wastewater contained dissolved oxygen that could serve as substrate for the ring-cleaving dioxygenase enzyme immediately upon entrance in the reactor. To simulate the same conditions, nitrogen was not flushed in the flasks during the proteomics experiment with *L. lactis*, and DB22 products were partially degraded before the complete depletion of oxygen in the flasks.

Figure 6. 5. Partial degradation of Direct Black 22 (DB22) reduction products by *L. lactis* LLSP-01. Aromatic products such as 2,4-triaminobenzene, oxalic acid p-phenylenediamine and 2-aminobenzenesulfonate are converted to catecholic compounds, which have their aromatic rings cleaved by a ring-cleaving dioxygenase.

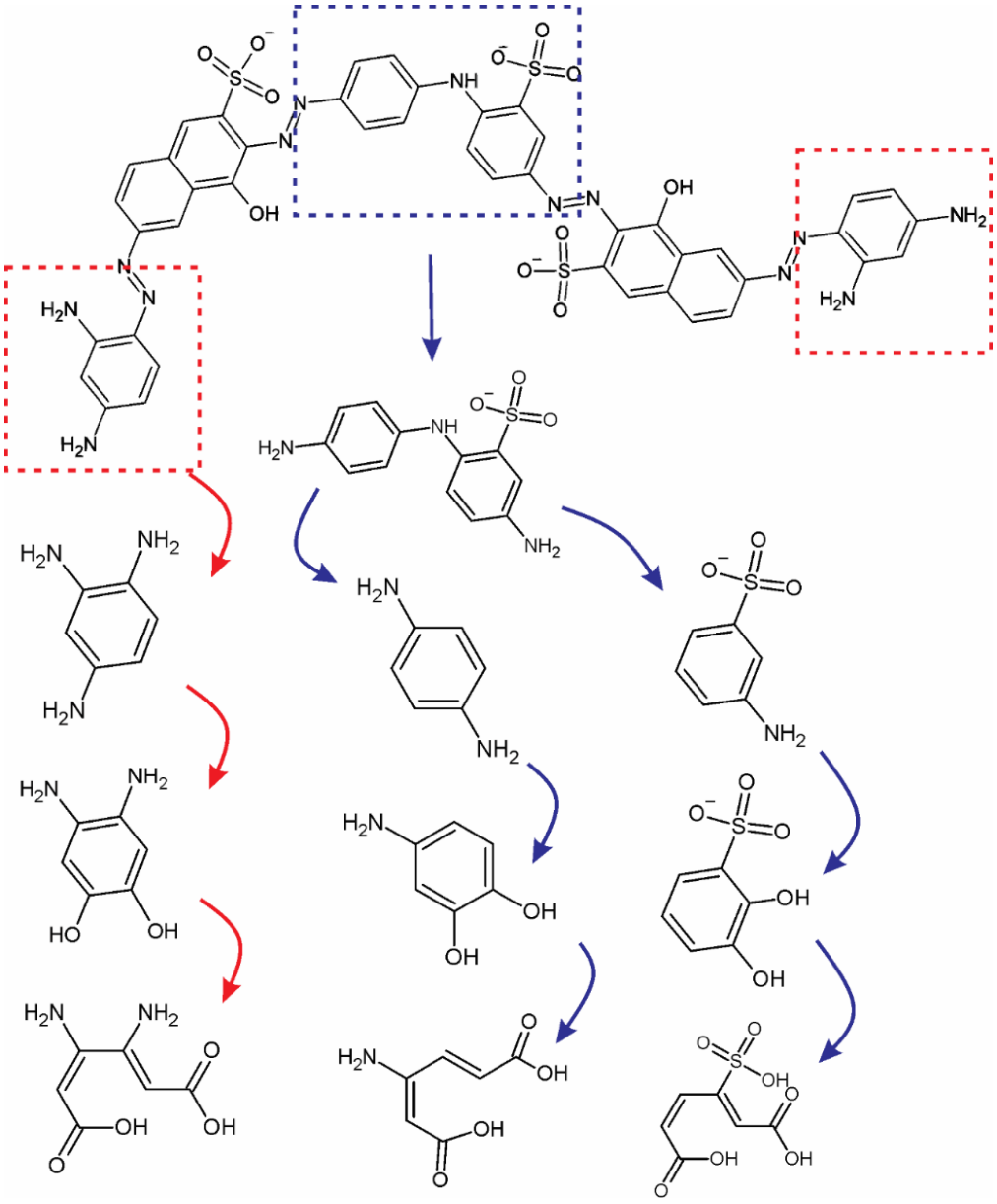

4. Conclusion

Biosorption plays an important role in the biodegradation of azo dyes by *L. lactis*, as the reduction mechanism initiates with adsorption to the biofilm matrix. The adsorbed dye is reduced by a SDR family oxidoreductase, showing that enzymes with broad range specificity are involved. Reducing equivalents are transferred through the biofilm matrix until the azo

compound by hopping, in a mechanism mediated by riboflavin. Resulting aromatic amines are partially degraded while oxygen is still present in reactions catalyzed by a ring-cleaving dioxygenase. These novel insights into the mechanism of azo dye biodegradation by *L. lactis* can assist in the development of new strategies and technologies for bioremediation of textile azo dyes and respective aromatic products.

Acknowledgement

This work was supported by the Fundação do Amparo à Pesquisa do Estado de São Paulo (process numbers 2015/06246-7, 2018/24269-2 and 2020/11860-4) and the Coordenação de Aperfeiçoamento de Pessoal de Nível Superior (CAPES) – Brazil (Finance Code001).

Chapter 7
Conclusion

In this study, we showed that multiple stage anaerobic treatment is an effective strategy for the treatment of azo dye wastewaters containing sulfate. This system's configuration showed feasibility for industrial applications due to its stable performance and higher azo dye load capacity when compared to single-stage systems. We have made further progress showing that reductive decolorization by syntrophic microbial communities is a co-metabolic process in which different microorganisms and metabolic routes are involved. Promiscuous enzymes were found to play an important role, but we do not know the relative importance of them compared to specific enzymes (e.g., azoreductases) which are supposedly involved as well. The main messages to take away from the experimental sections of this dissertation (Chapters 3-6) are summarized below:

i. The SPE-LC-ESI-MS/MS analysis developed for determining DB22 in biological reactor effluents revealed a structural change of the azo dye in aqueous solution, while the dying capacity was preserved. This technique has the potential of being tailored to consider the detection of the hydrolyzed fragments of azo dyes in wastewater for appropriate quantification, but was not the scope of the current step of this research;

ii. Multiple stage anaerobic treatment provided enhanced removals of color, organic matter and sulfate from a synthetic azo dye wastewater by eliminating issues related to the competition for reducing equivalents in the 1st-stage reactor;

iii. Reductive decolorization of azo dyes is a co-metabolic process in which several microbial communities and H_2-producing reactions are involved;

iv. The mechanism of azo dye reduction by a bacterium isolated from the two-stage anaerobic digestion system initiated with biosorption by glycoconjugates, particularly exopolysaccharides (EPS) and rhamnolipids. Electrons were transferred through the biofilm matrix until the dye by hopping, in a mechanism that involved an enzyme with broad substrate specificity and riboflavin carriers.

LIMITATIONS AND FUTURE RESEARCH

In spite of the optimistic conclusions of this dissertation, our work has important limitations. Microorganisms have distinct behavior when growing in pure or mixed cultures, and we cannot ensure that the DB22 decolorization mechanism by *L. lactis* observed was the same that occurred during the operation of two-stage AD system. A way around this would be combining protein-stable isotope probing and metagenomics to identify the putative degraders and pathways involved in reductive decolorization of azo dyes by mixed microbial communities. By doing so, it is possible to assess whether *L. lactis* contributed to DB22 decolorization when in syntrophic association with other species, and which are the other microorganisms involved.

Moreover, it is unknown whether some SRB can participate in reductive decolorization instead of only competing with azo degraders. Decolorization of an azo dye coupled to sulfate reduction was speculated before (Albuquerque et al., 2005), but no mechanism was proposed. Moreover, the competition between azo dyes and sulfate depends on the dye's reduction potential, and azo reduction can outcompete sulfate reduction in the case of certain azo dyes. We understand that azo dyes with distinct reduction potentials should be assessed under sulfidogenic conditions. The assays can be also carried using pure cultures of SRB which showed ability to decolorize azo dyes. However, the contribution of biogenic sulfide should be discounted using appropriate methods.

References

Acevedo Monroy, S.E., Kizilova, A., 2006. The Prokaryotes. Springer New York, New York, NY. https://doi.org/10.1007/0-387-30743-5

Adorno, M.A.T., Hirasawa, J.S., Varesche, M.B.A., 2014. Development and Validation of Two Methods to Quantify Volatile Acids (C2-C6) by GC/FID: Headspace (Automatic and Manual) and Liquid-Liquid Extraction (LLE). Am. J. Anal. Chem. 05, 406–414. https://doi.org/10.4236/ajac.2014.57049

Agneessens, L.M., Ottosen, L.D.M., Voigt, N.V., Nielsen, J.L., de Jonge, N., Fischer, C.H., Kofoed, M.V.W., 2017. In-situ biogas upgrading with pulse H2 additions: The relevance of methanogen adaption and inorganic carbon level. Bioresour. Technol. 233, 256–263. https://doi.org/10.1016/j.biortech.2017.02.016

Albertsen, M., Karst, S.M., Ziegler, A.S., Kirkegaard, R.H., Nielsen, P.H., 2015. Back to basics - The influence of DNA extraction and primer choice on phylogenetic analysis of activated sludge communities. PLoS One 10, 1–15. https://doi.org/10.1371/journal.pone.0132783

Albuquerque, M.G.E., Lopes, A.T., Serralheiro, M.L., Novais, J.M., Pinheiro, H.M., 2005. Biological sulphate reduction and redox mediator effects on azo dye decolourisation in anaerobic-aerobic sequencing batch reactors. Enzyme Microb. Technol. 36, 790–799. https://doi.org/10.1016/j.enzmictec.2005.01.005

Ali, S.S., Al-Tohamy, R., Xie, R., El-Sheekh, M.M., Sun, J., 2020. Construction of a new lipase- and xylanase-producing oleaginous yeast consortium capable of reactive azo dye degradation and detoxification. Bioresour. Technol. 313, 123631. https://doi.org/10.1016/j.biortech.2020.123631

Almeida, B., Kjeldal, H., Lolas, I., Knudsen, A.D., Carvalho, G., Nielsen, K.L., Barreto Crespo, M.T., Stensballe, A., Nielsen, J.L., 2013. Quantitative proteomic analysis of ibuprofen-degrading Patulibacter sp. strain I11. Biodegradation 24, 615–630. https://doi.org/10.1007/s10532-012-9610-5

Amaral, F.M., Florêncio, L., Kato, M.T., Santa-Cruz, P.A., Gavazza, S., 2017. Hydraulic retention time influence on azo dye and sulfate removal during the sequential anaerobic-aerobic treatment of real textile wastewater. Water Sci. Technol. 76, 3319–3327.

https://doi.org/10.2166/wst.2017.378

Amaral, F.M., Kato, M.T., Florêncio, L., Gavazza, S., 2014. Color, organic matter and sulfate removal from textile effluents by anaerobic and aerobic processes. Bioresour. Technol. 163, 364–369. https://doi.org/10.1016/j.biortech.2014.04.026

Amorim, S.M., Kato, M.T., Florencio, L., Gavazza, S., 2013. Influence of redox mediators and electron donors on the anaerobic removal of color and chemical oxygen demand from textile effluent. Clean - Soil, Air, Water 41, 928–933. https://doi.org/10.1002/clen.201200070

APHA, 2005. Standard Methods for the Examination of Water and Wastewater, 20th ed, American Public Health Association, American Water Works Association, Water Environment Federation. American Public Health Association, American Water Works Association, Water Environment Federation, Washington.

Arora, P.K., 2015. Bacterial degradation of monocyclic aromatic amine. Front. Microbiol. 6, 1–14. https://doi.org/10.3389/fmicb.2015.00820

Azbar, N., Yonar, T., Kestioglu, K., 2004. Comparison of various advanced oxidation processes and chemical treatment methods for COD and color removal from a polyester and acetate fiber dyeing effluent. Chemosphere 55, 35–43. https://doi.org/10.1016/j.chemosphere.2003.10.046

Baldi, F., Pecorini, I., Iannelli, R., 2019. Comparison of single-stage and two-stage anaerobic co-digestion of food waste and activated sludge for hydrogen and methane production. Renew. Energy 143, 1755–1765. https://doi.org/10.1016/j.renene.2019.05.122

Barber, R.D., Zhang, L., Harnack, M., Olson, M. V., Kaul, R., Ingram-Smith, C., Smith, K.S., 2011. Complete genome sequence of Methanosaeta concilii, a specialist in aceticlastic methanogenesis. J. Bacteriol. 193, 3668–3669. https://doi.org/10.1128/JB.05031-11

Bhatia, D., Sharma, N.R., Singh, J., Kanwar, R.S., 2017. Biological methods for textile dye removal from wastewater: A review. Crit. Rev. Environ. Sci. Technol. 47, 1836–1876. https://doi.org/10.1080/10643389.2017.1393263

Bhatt, P., Verma, A., Gangola, S., Bhandari, G., Chen, S., 2021. Microbial glycoconjugates in organic pollutant bioremediation: recent advances and applications. Microb. Cell Fact. 20, 1–18. https://doi.org/10.1186/s12934-021-01556-9

Bijmans, M.F.M., Buisman, C.J.N., Meulepas, R.J.W., Lens, P.N.L., 2011. Sulfate Reduction for Inorganic Waste and Process Water Treatment, Second Edi. ed, Comprehensive Biotechnology, Second Edition. Elsevier B.V. https://doi.org/10.1016/B978-0-08-088504-9.00471-2

Boels, I.C., Beerthuyzen, M.M., Kosters, M.H.W., Van Kaauwen, M.P.W., Kleerebezem, M., De Vos, W.M., 2004. Identification and Functional Characterization of the Lactococcus lactis rfb Operon, Required for dTDP-Rhamnose Biosynthesis. J. Bacteriol. 186, 1239–1248. https://doi.org/10.1128/JB.186.5.1239-1248.2004

Box, G.E.P., Wetz, J., 1973. Criteria for judging adequacy of estimation by an approximating response function. Technical Report No.9 95.

Braga, A.F.M., Ferraz Júnior, A.D.N., Zaiat, M., 2016. Thermophilic biohydrogen production using a UASB reactor: Performance during long-term operation. J. Chem. Technol. Biotechnol. 91, 967–976. https://doi.org/10.1002/jctb.4665

Brasil, 1981. Lei Federal Nº. 6.938 De 31 De Agosto De 1981.

Braúna, C.H.D.C., Mota, S., Santos, A.B. Dos, 2009. Descoloração redutiva do corante azo RR2 na ausência e presença de mediador redox e aceptor de elétrons nitrato. Eng. Sanit. e Ambient. 14, 275–284. https://doi.org/10.1590/S1413-41522009000200015

Brinster, S., Furlan, S., Serror, P., 2007. C-terminal WxL domain mediates cell wall binding in Enterococcus faecalis and other gram-positive bacteria. J. Bacteriol. 189, 1244–1253. https://doi.org/10.1128/JB.00773-06

Bruylants, A., Feytmants-de Medicis, E., 2010. Cleavage of the carbon-nitrogen double bond. Carbon-Nitrogen Double Bond. 465–504. https://doi.org/10.1002/9780470771204.ch10

Burton, J.P., Devillard, E., Cadieux, P.A., Hammond, J.A., Reid, G., 2004. Detection of Atopobium vaginae in Postmenopausal Women by Cultivation-Independent Methods Warrants Further Investigation. J. Clin. Microbiol. 42, 1829–1831. https://doi.org/10.1128/JCM.42.4.1829-1831.2004

Buss, J.L., Ponka, P., 2003. Hydrolysis of pyridoxal isonicotinoyl hydrazone and its analogs. Biochim. Biophys. Acta - Gen. Subj. 1619, 177–186. https://doi.org/10.1016/S0304-4165(02)00478-6

Byberg, R., Cobb, J., Martin, L.D., Thompson, R.W., Camesano, T.A., Zahraa, O., Pons, M.N.,

2013. Comparison of photocatalytic degradation of dyes in relation to their structure. Environ. Sci. Pollut. Res. 20, 3570–3581. https://doi.org/10.1007/s11356-013-1551-y

Caporaso, J.G., Kuczynski, J., Stombaugh, J., Bittinger, K., Bushman, F.D., Costello, E.K., Fierer, N., Peña, A.G., Goodrich, J.K., Gordon, J.I., Huttley, G.A., Kelley, S.T., Knights, D., Koenig, J.E., Ley, R.E., Lozupone, C.A., Mcdonald, D., Muegge, B.D., Pirrung, M., Reeder, J., Sevinsky, J.R., Turnbaugh, P.J., Walters, W.A., Widmann, J., Yatsunenko, T., Zaneveld, J., Knight, R., 2010. QIIME allows analysis of high- throughput community sequencing data. Nat. Methods 7, 335–336. https://doi.org/10.1038/nmeth0510-335

Caporaso, J.G., Lauber, C.L., Walters, W.A., Berg-Lyons, D., Lozupone, C.A., Turnbaugh, P.J., Fierer, N., Knight, R., 2011. Global patterns of 16S rRNA diversity at a depth of millions of sequences per sample. Proc. Natl. Acad. Sci. 108, 4516–4522. https://doi.org/10.1073/pnas.1000080107

Carrillo-Reyes, J., Celis, L.B., Alatriste-Mondragón, F., Razo-Flores, E., 2014. Decreasing methane production in hydrogenogenic UASB reactors fed with cheese whey. Biomass and Bioenergy 63, 101–108. https://doi.org/10.1016/j.biombioe.2014.01.050

Carvalho, J.R.S., Amaral, F.M., Florencio, L., Kato, M.T., Delforno, T.P., Gavazza, S., 2020. Microaerated UASB reactor treating textile wastewater: The core microbiome and removal of azo dye Direct Black 22. Chemosphere 242, 125157. https://doi.org/10.1016/j.chemosphere.2019.125157

Castelló, E., Nunes Ferraz-Junior, A.D., Andreani, C., Anzola-Rojas, M. del P., Borzacconi, L., Buitrón, G., Carrillo-Reyes, J., Gomes, S.D., Maintinguer, S.I., Moreno-Andrade, I., Palomo-Briones, R., Razo-Flores, E., Schiappacasse-Dasati, M., Tapia-Venegas, E., Valdez-Vázquez, I., Vesga-Baron, A., Zaiat, M., Etchebehere, C., 2019. Stability problems in the hydrogen production by dark fermentation: Possible causes and solutions. Renew. Sustain. Energy Rev. 119. https://doi.org/10.1016/j.rser.2019.109602

Catanho, M., Malpass, G.R.P., Motheo, A. de J., 2006. Avaliação dos tratamentos eletroquímico e fotoeletroquímico na degradação de corantes têxteis. Quim. Nova 29, 983–989. https://doi.org/10.1590/s0100-40422006000500018

Cavalcante, W. de A., Leitão, R.C., Gehring, T.A., Angenent, L.T., Santaella, S.T., 2017. Anaerobic fermentation for n-caproic acid production: A review. Process Biochem. 54, 106–119. https://doi.org/10.1016/j.procbio.2016.12.024

Cervantes, F.J., dos Santos, A.B., de Madrid, M.P., Stams, A.J.M., van Lier, J.B., 2005. Reductive decolourisation of azo dyes by mesophilic and thermophilic methanogenic consortia. Water Sci. Technol. 52, 351–356. https://doi.org/10.2166/wst.2005.0538

Chen, G., An, X., Li, H., Lai, F., Yuan, E., Xia, X., Zhang, Q., 2021. Detoxification of azo dye Direct Black G by thermophilic Anoxybacillus sp. PDR2 and its application potential in bioremediation. Ecotoxicol. Environ. Saf. 214, 112084. https://doi.org/10.1016/j.ecoenv.2021.112084

Chiaradia, M.C., Collins, C.H., Jardim, I.C.S.F., 2008. O estado da arte da cromatografia associada à espectrometria de massas acoplada à espectrometria de massas na análise de compostos tóxicos em alimentos. Quim. Nova 31, 623–636. https://doi.org/10.1590/s0100-40422008000300030

Choi, M., Chang, C.-Y., Clough, T., Broudy, D., Killeen, T., MacLean, B., Vitek, O., 2014. MSstats: an R package for statistical analysis of quantitative mass spectrometry-based proteomic experiments. Bioinformatics 30, 2524–2526. https://doi.org/10.1093/bioinformatics/btu305

Chong, H., Li, Q., 2017. Microbial production of rhamnolipids: Opportunities, challenges and strategies. Microb. Cell Fact. 16, 1–12. https://doi.org/10.1186/s12934-017-0753-2

Chou, J.H., Lin, K.Y., Lin, M.C., Sheu, S.Y., Wei, Y.H., Arun, A.B., Young, C.C., Chen, W.M., 2007. Brachybacterium phenoliresistens sp. nov., isolated from oil-contaminated coastal sand. Int. J. Syst. Evol. Microbiol. 57, 2674–2679. https://doi.org/10.1099/ijs.0.65019-0

Christie, R.M., 2015. Colour Chemistry, 2nd ed, Color Research and Application. The Royal Society of Chemistry, Cambridge, UK.

Cohen, A., Breure, A.M., Andel, J.G.V.A.N., Deursen, A.V.A.N., 1980. Influence of phase separation on the anaerobic digestion of glucose - maximum COD-turnover rate during continuous operation. Water Res. 14, 1439–1448.

Copaciu, F., Coman, V., Simedru, D., Beldean-Galea, S., Opriş, O., Ristoiu, D., 2013. Determination of two textile dyes in wastewater by solid phase extraction and liquid chromatography/electrospray ionization tandem mass spectrometry analysis. J. Liq. Chromatogr. Relat. Technol. 36, 1646–1660. https://doi.org/10.1080/10826076.2012.695312

Cox, J., Mann, M., 2008. MaxQuant enables high peptide identification rates, individualized p.p.b.-range mass accuracies and proteome-wide protein quantification. Nat. Biotechnol. 26, 1367–1372. https://doi.org/10.1038/nbt.1511

Cox, J., Neuhauser, N., Michalski, A., Scheltema, R.A., Olsen, J. V., Mann, M., 2011. Andromeda: A Peptide Search Engine Integrated into the MaxQuant Environment. J. Proteome Res. 10, 1794–1805. https://doi.org/10.1021/pr101065j

Dai, R., Chen, X., Luo, Y., Ma, P., Ni, S., Xiang, X., Li, G., 2016. Inhibitory effect and mechanism of azo dyes on anaerobic methanogenic wastewater treatment: Can redox mediator remediate the inhibition? Water Res. 104, 408–417. https://doi.org/10.1016/j.watres.2016.08.046

Dai, R., Chen, X., Xiang, X., Wang, Y., Wang, F., 2018. Understanding azo dye anaerobic bio-decolorization with artificial redox mediator supplement: Considering the methane production. Bioresour. Technol. 249, 799–808. https://doi.org/10.1016/j.biortech.2017.10.072

de Aquino, S., Fuess, L.T., Pires, E.C., 2017. Media arrangement impacts cell growth in anaerobic fixed-bed reactors treating sugarcane vinasse: Structured vs. randomic biomass immobilization. Bioresour. Technol. 235, 219–228. https://doi.org/10.1016/j.biortech.2017.03.120

De Coster, W., D'Hert, S., Schultz, D.T., Cruts, M., Van Broeckhoven, C., 2018. NanoPack: visualizing and processing long-read sequencing data. Bioinformatics 34, 2666–2669. https://doi.org/10.1093/bioinformatics/bty149

de Souza, S.M. de A.G.U., Bonilla, K.A.S., de Souza, A.A.U., 2010. Removal of COD and color from hydrolyzed textile azo dye by combined ozonation and biological treatment. J. Hazard. Mater. 179, 35–42. https://doi.org/10.1016/j.jhazmat.2010.02.053

Del Pilar Anzola-Rojas, M., Da Fonseca, S.G., Da Silva, C.C., De Oliveira, V.M., Zaiat, M., 2015. The use of the carbon/nitrogen ratio and specific organic loading rate as tools for improving biohydrogen production in fixed-bed reactors. Biotechnol. Reports 5, 46–54. https://doi.org/10.1016/j.btre.2014.10.010

Demirel, B., Yenigün, O., 2002. Two-phase anaerobic digestion processes: a review. J. Chem. Technol. Biotechnol. 77, 743–755. https://doi.org/10.1002/jctb.630

Deng, D., Weidhaas, J.L., Lin, L.S., 2016. Kinetics and microbial ecology of batch sulfidogenic bioreactors for co-treatment of municipal wastewater and acid mine drainage. J. Hazard. Mater. 305, 200–208. https://doi.org/10.1016/j.jhazmat.2015.11.041

Ding, Y., Sun, C., Xu, X., 2009. Simultaneous identification of nine carcinogenic dyes from textiles by liquid chromatography/electrospray ionization mass spectrometry via negative/positive ion switching mode. Eur. J. Mass Spectrom. 15, 705–713. https://doi.org/10.1255/ejms.1032

Donlon, B., Razo-Flores, E., Luijten, M., Swarts, H., Lettinga, G., Field, J., 1997. Detoxification and partial mineralization of the azo dye mordant orange 1 in a continuous upflow anaerobic sludge-blanket reactor. Appl. Microbiol. Biotechnol. 47, 83–90. https://doi.org/10.1007/s002530050893

Dos Santos, A.B., Cervantes, F.J., Yaya-Beas, R.E., Van Lier, J.B., 2003. Effect of redox mediator, AQDS, on the decolourisation of a reactive azo dye containing triazine group in a thermophilic anaerobic EGSB reactor. Enzyme Microb. Technol. 33, 942–951. https://doi.org/10.1016/j.enzmictec.2003.07.007

Dos Santos, A.B., Traverse, J., Cervantes, F.J., Van Lier, J.B., 2005. Enhancing the electron transfer capacity and subsequent color removal in bioreactors by applying thermophilic anaerobic treatment and redox mediators. Biotechnol. Bioeng. 89, 42–52. https://doi.org/10.1002/bit.20308

Dubin, P., Wright, K.L., 1975. Reduction of azo food dyes in cultures of proteus vulgaris. Xenobiotica 5, 563–571. https://doi.org/10.3109/00498257509056126

DuBois, M., Gilles, K.A., Hamilton, J.K., Rebers, P.A., Smith, F., 1956. Colorimetric Method for Determination of Sugars and Related Substances. Anal. Chem. 28, 350–356. https://doi.org/10.1021/ac60111a017

Dueholm, M.S., Nierychlo, M., Andersen, K.S., Rudkjøbing, V., Knutsson, S., Consortium, the M.G., Albertsen, M., Nielsen, P.H., 2021. MiDAS 4: A global catalogue of full-length 16S rRNA gene sequences and taxonomy for studies of bacterial communities in wastewater treatment plants. https://doi.org/https://doi.org/10.1101/2021.07.06.451231

Edgar, R.C., 2013. UPARSE: Highly accurate OTU sequences from microbial amplicon reads. Nat. Methods 10, 996–998. https://doi.org/10.1038/nmeth.2604

Edlund, P.O., Lee, E.D., Henion, J.D., Budde, W.L., 1989. The determination of sulfonated azo dyes in municipal wastewater by ion spray liquid chromatography tandem mass spectrometry. Biomed. Environ. Mass Spectrom. 18, 233–240. https://doi.org/10.1002/bms.1200180405

EPA, 1997. Profile of the Textile Industry. Environmental Protection Agency, Washington, USA.

Fernandes, B.S., Peixoto, G., Albrecht, F.R., Saavedra del Aguila, N.K., Zaiat, M., 2010. Potential to produce biohydrogen from various wastewaters. Energy Sustain. Dev. 14, 143–148. https://doi.org/10.1016/j.esd.2010.03.004

Ferraz, A.D.N., Kato, M.T., Florencio, L., Gavazza, S., 2011. Textile effluent treatment in a UASB reactor followed by submerged aerated biofiltration. Water Sci. Technol. 64, 1581–1589. https://doi.org/10.2166/wst.2011.674

Firmino, P.I.M., da Silva, M.E.R., Cervantes, F.J., dos Santos, A.B., 2010. Colour removal of dyes from synthetic and real textile wastewaters in one- and two-stage anaerobic systems. Bioresour. Technol. 101, 7773–7779. https://doi.org/10.1016/j.biortech.2010.05.050

Florêncio, T. de M., Godoi, L.A.G., Rocha, V.C., Oliveira, J.M.S., Motteran, F., Gavazza, S., Vicentine, K.F.D., Damianovic, M.H.R.Z., 2021. Anaerobic structured-bed reactor for azo dye decolorization in the presence of sulfate ions. J. Chem. Technol. Biotechnol. https://doi.org/10.1002/jctb.6695

Föll, M., Fahrner, M., 2022. MaxQuant and MSstats for the analysis of label-free data (Galaxy Training Materials) [WWW Document]. URL https://training.galaxyproject.org/training-material/topics/proteomics/tutorials/maxquant-msstats-dda-lfq/tutorial.html (accessed 5.8.22).

Forgacs, E., Cserháti, T., Oros, G., 2004. Removal of synthetic dyes from wastewaters: A review. Environ. Int. 30, 953–971. https://doi.org/10.1016/j.envint.2004.02.001

Franca, R.D.G., Oliveira, M.C., Pinheiro, H.M., Lourenço, N.D., 2019. Biodegradation Products of a Sulfonated Azo Dye in Aerobic Granular Sludge Sequencing Batch Reactors Treating Simulated Textile Wastewater. ACS Sustain. Chem. Eng. 7, 14697–14706. https://doi.org/10.1021/acssuschemeng.9b02635

Fuess, Lucas Tadeu, 2017, 2017. BIODIGESTÃO ANAERÓBIA TERMOFÍLICA DE

VINHAÇA EM SISTEMAS COMBINADOS DO TIPO ACIDOGÊNICO-METANOGÊNICO PARA POTENCIALIZAÇÃO DA RECUPERAÇÃO DE BIOENERGIA EM BIORREFINARIAS DE CANA-DE-AÇÚCAR DE PRIMEIRA GERAÇÃO Tese apresentada à Escola de Engenharia de São C 344.

Fuess, L.T., Fuentes, L., Bovio-Winkler, P., Eng, F., Etchebehere, C., Zaiat, M., Oller do Nascimento, C.A., 2021. Biohydrogen-producing from bottom to top? Quali-quantitative characterization of thermophilic fermentative consortia reveals microbial roles in an upflow fixed-film reactor. Chem. Eng. J. Adv. 7, 100125. https://doi.org/10.1016/j.ceja.2021.100125

Fuess, L.T., Kiyuna, L.S.M., Ferraz, A.D.N., Persinoti, G.F., Squina, F.M., Garcia, M.L., Zaiat, M., 2017. Thermophilic two-phase anaerobic digestion using an innovative fixed-bed reactor for enhanced organic matter removal and bioenergy recovery from sugarcane vinasse. Appl. Energy 189, 480–491. https://doi.org/10.1016/j.apenergy.2016.12.071

Fuess, L.T., Mazine Kiyuna, L.S., Garcia, M.L., Zaiat, M., 2016. Operational strategies for long-term biohydrogen production from sugarcane stillage in a continuous acidogenic packed-bed reactor. Int. J. Hydrogen Energy 41, 8132–8145. https://doi.org/10.1016/j.ijhydene.2015.10.143

Fuh, M.R., Chia, K.J., 2002. Determination of sulphonated azo dyes in food by ion-pair liquid chromatography with photodiode array and electrospray mass spectrometry detection. Talanta 56, 663–671. https://doi.org/10.1016/S0039-9140(01)00625-7

García-Depraect, O., Martínez-Mendoza, L.J., Diaz, I., Muñoz, R., 2022. Two-stage anaerobic digestion of food waste: Enhanced bioenergy production rate by steering lactate-type fermentation during hydrolysis-acidogenesis. Bioresour. Technol. 358, 127358. https://doi.org/10.1016/j.biortech.2022.127358

García-Moreno, P.J., Gregersen, S., Nedamani, E.R., Olsen, T.H., Marcatili, P., Overgaard, M.T., Andersen, M.L., Hansen, E.B., Jacobsen, C., 2020. Identification of emulsifier potato peptides by bioinformatics: application to omega-3 delivery emulsions and release from potato industry side streams. Sci. Rep. 10, 690. https://doi.org/10.1038/s41598-019-57229-6

Gavazza, S., Guzman, J.J.L., Angenent, L.T., 2015. Electrolysis within anaerobic bioreactors stimulates breakdown of toxic products from azo dye treatment. Biodegradation 26, 151–

160. https://doi.org/10.1007/s10532-015-9723-8

Godoi, L.A.G., Damianovic, M.H.R.Z., Foresti, E., 2015. Sulfidogenesis interference on methane production from carbohydrate-rich wastewater. Water Sci. Technol. 72, 1644–1652. https://doi.org/10.2166/wst.2015.383

Gottlieb, A., Shaw, C., Smith, A., Wheatley, A., Forsythe, S., 2003. The toxicity of textile reactive azo dyes after hydrolysis and decolourisation. J. Biotechnol. 101, 49–56. https://doi.org/10.1016/S0168-1656(02)00302-4

Gyalai-Korpos, M., Fehér, A., Barta, Z., Réczey, K., 2014. Evaluation of an online fermentation monitoring system. Acta Aliment. 43, 76–87. https://doi.org/10.1556/AAlim.43.2014.1.8

Hammer, Ø., Harper, D.A.T., Ryan, P.D., 2001. PAST : Paleontological Statistics Software Package for Education and Data Analysis. Palaeontol. Electron. 4, 1–9.

Holčapek, M., Jandera, P., Přikryl, J., 1999. Analysis of sulphonated dyes and intermediates by electrospray mass spectrometry. Dye. Pigment. 43, 127–137. https://doi.org/10.1016/S0143-7208(99)00051-0

Holčapek, M., Jandera, P., Zderadička, P., 2001. High performance liquid chromatography-mass spectrometric analysis of sulphonated dyes and intermediates. J. Chromatogr. A 926, 175–186. https://doi.org/10.1016/S0021-9673(01)00933-5

Imran, M., Arshad, M., Negm, F., Khalid, A., Shaharoona, B., Hussain, S., Mahmood Nadeem, S., Crowley, D.E., 2016. Yeast extract promotes decolorization of azo dyes by stimulating azoreductase activity in Shewanella sp. strain IFN4. Ecotoxicol. Environ. Saf. 124, 42–49. https://doi.org/10.1016/j.ecoenv.2015.09.041

Itoh, H., Suzuta, T., Hoshino, T., Takaya, N., 2008. Novel dehydrogenase catalyzes oxidative hydrolysis of carbon-nitrogen double bonds for hydrazone degradation. J. Biol. Chem. 283, 5790–5800. https://doi.org/10.1074/jbc.M709027200

Jackson, C.J., Gillam, E.M.J., Ollis, D.L., 2010. Directed Evolution of Enzymes, in: Comprehensive Natural Products III. Elsevier, pp. 654–673. https://doi.org/10.1016/B978-0-08-102690-8.00675-8

Jadhav, J.P., Phugare, S.S., Dhanve, R.S., Jadhav, S.B., 2010. Rapid biodegradation and decolorization of Direct Orange 39 (Orange TGLL) by an isolated bacterium Pseudomonas aeruginosa strain BCH. Biodegradation 21, 453–463. https://doi.org/10.1007/s10532-009-

9315-6

Jayapal, M., Jagadeesan, H., Shanmugam, M., Danisha J, P., Murugesan, S., 2018. Sequential anaerobic-aerobic treatment using plant microbe integrated system for degradation of azo dyes and their aromatic amines by-products. J. Hazard. Mater. 354, 231–243. https://doi.org/10.1016/j.jhazmat.2018.04.050

Júnior, A.D.N.F., 2010. Tratamento de Efluente Têxtil em Reator UASB seguido de Biofiltro Aerado Submerso.

Kalia, J., Raines, R.T., 2008. Hydrolytic Stability of Hydrazones and Oximes. Angew. Chemie Int. Ed. 47, 7523–7526. https://doi.org/10.1002/anie.200802651

Kanehisa, M., 2000. KEGG: Kyoto Encyclopedia of Genes and Genomes. Nucleic Acids Res. 28, 27–30. https://doi.org/10.1093/nar/28.1.27

Kanehisa, M., Araki, M., Goto, S., Hattori, M., Hirakawa, M., Itoh, M., Katayama, T., Kawashima, S., Okuda, S., Tokimatsu, T., Yamanishi, Y., 2008. KEGG for linking genomes to life and the environment. Nucleic Acids Res. 36, 480–484. https://doi.org/10.1093/nar/gkm882

Kapdan, I.K., Alparslan, S., 2005. Application of anaerobic-aerobic sequential treatment system to real textile wastewater for color and COD removal. Enzyme Microb. Technol. 36, 273–279. https://doi.org/10.1016/j.enzmictec.2004.08.040

Kavanagh, K.L., Jörnvall, H., Persson, B., Oppermann, U., 2008. Medium- and short-chain dehydrogenase/reductase gene and protein families: The SDR superfamily: Functional and structural diversity within a family of metabolic and regulatory enzymes. Cell. Mol. Life Sci. 65, 3895–3906. https://doi.org/10.1007/s00018-008-8588-y

Khandare, R. V., Govindwar, S.P., 2015. Phytoremediation of textile dyes and effluents: Current scenario and future prospects. Biotechnol. Adv. 33, 1697–1714. https://doi.org/10.1016/j.biotechadv.2015.09.003

Kim, S.-J., Jones, R.C., Cha, C.-J., Kweon, O., Edmondson, R.D., Cerniglia, C.E., 2004. Identification of proteins induced by polycyclic aromatic hydrocarbon in Mycobacterium vanbaalenii PYR-1 using two-dimensional polyacrylamide gel electrophoresis andde novo sequencing methods. Proteomics 4, 3899–3908. https://doi.org/10.1002/pmic.200400872

Kim, S.J., Kweon, O., Cerniglia, C.E., 2009. Proteomic applications to elucidate bacterial

aromatic hydrocarbon metabolic pathways. Curr. Opin. Microbiol. 12, 301–309. https://doi.org/10.1016/j.mib.2009.03.006

Koren, S., Walenz, B.P., Berlin, K., Miller, J.R., Bergman, N.H., Phillippy, A.M., 2017. Canu: scalable and accurate long-read assembly via adaptive k -mer weighting and repeat separation. Genome Res. 27, 722–736. https://doi.org/10.1101/gr.215087.116

Kunz, A., Peralta-Zamora, P., De Moraes, S.G., Durán, N., 2002. Novas tendências no tratamento de efluentes têxteis. Quim. Nova 25, 78–82. https://doi.org/10.1590/S0100-40422002000100014

Kurade, M.B., Waghmode, T.R., Patil, S.M., Jeon, B.H., Govindwar, S.P., 2017. Monitoring the gradual biodegradation of dyes in a simulated textile effluent and development of a novel triple layered fixed bed reactor using a bacterium-yeast consortium. Chem. Eng. J. 307, 1026–1036. https://doi.org/10.1016/j.cej.2016.09.028

Lebrero, R., Toledo-Cervantes, A., Muñoz, R., del Nery, V., Foresti, E., 2016. Biogas upgrading from vinasse digesters: a comparison between an anoxic biotrickling filter and an algal-bacterial photobioreactor. J. Chem. Technol. Biotechnol. 91, 2488–2495. https://doi.org/10.1002/jctb.4843

Li, J., Ding, X.M., Liu, D.D., Guo, F., Chen, Y., Zhang, Y.B., Liu, H.M., 2013. Simultaneous determination of eight illegal dyes in chili products by liquid chromatography-tandem mass spectrometry. J. Chromatogr. B Anal. Technol. Biomed. Life Sci. 942–943, 46–52. https://doi.org/10.1016/j.jchromb.2013.10.010

Li, Y., Zhang, Y., Quan, X., Zhang, J., Chen, S., Afzal, S., 2014. Enhanced anaerobic fermentation with azo dye as electron acceptor: simultaneous acceleration of organics decomposition and azo decolorization. J. Environ. Sci. (China) 26, 1970–1976. https://doi.org/10.1016/j.jes.2014.07.009

Lima, U. de A., Aquarone, E., Borzani, W., Schmidell, W., 2001. Biotecnologia Industrial. Biotecnol. Ind. Vol. III.

Luton, P.E., Wayne, J.M., Sharp, R.J., Riley, P.W., 2002. The mcrA gene as an alternative to 16S rRNA in the phylogenetic analysis of methanogen populations in landfill. Microbiology 148, 3521–3530. https://doi.org/10.1099/00221287-148-11-3521

Madigan, M.T., Martinko, J.M., Bender, K.S., Buckley, D.H., Stahl, D.A., 2014. Brock Biology

of Microorganisms, Igarss 2014. Pearson.

Malik, P.K., Saha, S.K., 2003. Oxidation of direct dyes with hydrogen peroxide using ferrous ion as catalyst. Sep. Purif. Technol. 31, 241–250. https://doi.org/10.1016/S1383-5866(02)00200-9

Manni, M., Berkeley, M.R., Seppey, M., Simão, F.A., Zdobnov, E.M., 2021. BUSCO Update: Novel and Streamlined Workflows along with Broader and Deeper Phylogenetic Coverage for Scoring of Eukaryotic, Prokaryotic, and Viral Genomes. Mol. Biol. Evol. 1–8. https://doi.org/10.1093/molbev/msab199

Mariano, A.P., Keshtkar, M.J., Atala, D.I.P., Filho, F.M., MacIel, M.R.W., Filho, R.M.I., Stuart, P., 2011. Energy requirements for butanol recovery using the flash fermentation technology. Energy and Fuels 25, 2347–2355. https://doi.org/10.1021/ef200279v

Marolda, C.L., Valvano, M.A., 1995. Genetic analysis of the dTDP-rhamnose biosynthesis region of the Escherichia coli VW187 (O7:K1) rfb gene cluster: Identification of functional homologs of rfbB and rfbA in the rff cluster and correct location of the rffE gene. J. Bacteriol. 177, 5539–5546. https://doi.org/10.1128/jb.177.19.5539-5546.1995

Matuszewski, B.K., Constanzer, M.L., Chavez-Eng, C.M., 2003. Strategies for the Assessment of Matrix Effect in Quantitative Bioanalytical Methods Based on HPLC-MS/MS. Anal. Chem. 75, 3019–3030.

Mendes, S., Farinha, A., Ramos, C.G., Leitão, J.H., Viegas, C.A., Martins, L.O., 2011. Synergistic action of azoreductase and laccase leads to maximal decolourization and detoxification of model dye-containing wastewaters. Bioresour. Technol. 102, 9852–9859. https://doi.org/10.1016/j.biortech.2011.07.108

Menezes, O., Brito, R., Hallwass, F., Florêncio, L., Kato, M.T., Gavazza, S., 2019. Coupling intermittent micro-aeration to anaerobic digestion improves tetra-azo dye Direct Black 22 treatment in sequencing batch reactors. Chem. Eng. Res. Des. 146, 369–378. https://doi.org/10.1016/j.cherd.2019.04.020

Mirbolooki, H., Amirnezhad, R., Pendashteh, A.R., 2017. Treatment of high saline textile wastewater by activated sludge microorganisms. J. Appl. Res. Technol. 15, 167–172. https://doi.org/10.1016/j.jart.2017.01.012

Misal, S.A., Gawai, K.R., 2018. Azoreductase: a key player of xenobiotic metabolism.

Bioresour. Bioprocess. 5. https://doi.org/10.1186/s40643-018-0206-8

Mnif, I., Ghribi, D., 2016. Glycolipid biosurfactants: main properties and potential applications in agriculture and food industry. J. Sci. Food Agric. 96, 4310–4320. https://doi.org/10.1002/jsfa.7759

Mockaitis, G., Pantoja, J.L.R., Rodrigues, J.A.D., Foresti, E., Zaiat, M., 2014. Continuous anaerobic bioreactor with a fixed-structure bed (ABFSB) for wastewater treatment with low solids and low applied organic loading content. Bioprocess Biosyst. Eng. 37, 1361–1368. https://doi.org/10.1007/s00449-013-1108-y

Morrison, J.M., John, G.H., 2015. Non-classical azoreductase secretion in Clostridium perfringens in response to sulfonated azo dye exposure. Anaerobe 34, 34–43. https://doi.org/10.1016/j.anaerobe.2015.04.007

Morrison, J.M., Wright, C.M., John, G.H., 2012. Identification, Isolation and characterization of a novel azoreductase from Clostridium perfringens. Anaerobe 18, 229–234. https://doi.org/10.1016/j.anaerobe.2011.12.006

Müller, A.L., Kjeldsen, K.U., Rattei, T., Pester, M., Loy, A., 2015. Phylogenetic and environmental diversity of DsrAB-type dissimilatory (bi)sulfite reductases. ISME J. 9, 1152–1165. https://doi.org/10.1038/ismej.2014.208

Müller, B., Sun, L., Schnürer, A., 2013. First insights into the syntrophic acetate-oxidizing bacteria - a genetic study. Microbiologyopen 2, 35–53. https://doi.org/10.1002/mbo3.50

Muyzer, G., Stams, A.J.M., 2008. The ecology and biotechnology of sulphate-reducing bacteria. Nat. Rev. Microbiol. 6, 441–454. https://doi.org/10.1038/nrmicro1892

Ogg, C.D., Patel, B.K.C., 2009. Sporolituus thermophilus gen. nov., sp. nov., a citrate-fermenting thermophilic anaerobic bacterium from geothermal waters of the Great Artesian Basin of Australia. Int. J. Syst. Evol. Microbiol. 59, 2848–2853. https://doi.org/10.1099/ijs.0.010306-0

Oktem, Y.A., Ince, O., Donnelly, T., Sallis, P., Ince, B.K., 2006. Determination of optimum operating conditions of an acidification reactor treating a chemical synthesis-based pharmaceutical wastewater. Process Biochem. 41, 2258–2263. https://doi.org/10.1016/j.procbio.2006.05.016

Oliveira, J.M.S., 2022. [dataset] Two-stage anaerobic digestion system for biodegradation of

azo dye in the presence of sulfate. Mendeley Data. V3. https://doi.org/10.17632/h5hhpm86hp.3

Oliveira, J.M.S., Damianovic, M.H.R.Z., Foresti, E., 2022. Two-stage anaerobic digestion system for biotransformation of an azo dye in the presence of sulfate: Minimizing competition for reducing equivalents. J. Water Process Eng. 47, 102819. https://doi.org/10.1016/j.jwpe.2022.102819

Oliveira, J.M.S., de Lima e Silva, M.R., Issa, C.G., Corbi, J.J., Damianovic, M.H.R.Z., Foresti, E., 2020. Intermittent aeration strategy for azo dye biodegradation: A suitable alternative to conventional biological treatments? J. Hazard. Mater. 385, 9. https://doi.org/10.1016/j.jhazmat.2019.121558

Özcan, E., Selvi, S.S., Nikerel, E., Teusink, B., Toksoy Öner, E., Çakır, T., 2019. A genome-scale metabolic network of the aroma bacterium Leuconostoc mesenteroides subsp. cremoris. Appl. Microbiol. Biotechnol. 103, 3153–3165. https://doi.org/10.1007/s00253-019-09630-4

Özen, A.S., Doruker, P., Aviyente, V., 2007. Effect of cooperative hydrogen bonding in azo-hydrazone tautomerism of azo dyes. J. Phys. Chem. A 111, 13506–13514. https://doi.org/10.1021/jp0755645

Paliy, O., Shankar, V., 2016. Application of multivariate statistical techniques in microbial ecology. Mol. Ecol. 25, 1032–1057. https://doi.org/10.1111/mec.13536

Pandey, A., Singh, P., Iyengar, L., 2007. Bacterial decolorization and degradation of azo dyes. Int. Biodeterior. Biodegrad. 59, 73–84. https://doi.org/10.1016/j.ibiod.2006.08.006

Perei, K., Rákhely, G., Kiss, I., Polyák, B., Kovács, K.L., 2001. Biodegradation of sulfanilic acid by Pseudomonas paucimobilis. Appl. Microbiol. Biotechnol. 55, 101–107. https://doi.org/10.1007/s002530000474

Pérez-Díaz, I.M., McFeeters, R.F., 2009. Modification of azo dyes by lactic acid bacteria. J. Appl. Microbiol. 107, 584–589. https://doi.org/10.1111/j.1365-2672.2009.04227.x

Perna, V., Castelló, E., Wenzel, J., Zampol, C., Fontes Lima, D.M., Borzacconi, L., Varesche, M.B., Zaiat, M., Etchebehere, C., 2013. Hydrogen production in an upflow anaerobic packed bed reactor used to treat cheese whey. Int. J. Hydrogen Energy 38, 54–62. https://doi.org/10.1016/j.ijhydene.2012.10.022

Phugare, S.S., Kalyani, D.C., Surwase, S.N., Jadhav, J.P., 2011. Ecofriendly degradation, decolorization and detoxification of textile effluent by a developed bacterial consortium. Ecotoxicol. Environ. Saf. 74, 1288–1296. https://doi.org/10.1016/j.ecoenv.2011.03.003

Pinheiro, H.M., Touraud, E., Thomas, O., 2004. Aromatic amines from azo dye reduction: Status review with emphasis on direct UV spectrophotometric detection in textile industry wastewaters. Dye. Pigment. 61, 121–139. https://doi.org/10.1016/j.dyepig.2003.10.009

Plavec, T.V., Štrukelj, B., Berlec, A., 2019. Screening for new surface anchoring domains for lactococcus lactis. Front. Microbiol. 10, 1–13. https://doi.org/10.3389/fmicb.2019.01879

Plumb, J.J., Bell, J., Stuckey, D.C., 2001. Microbial Populations Associated with Treatment of an Industrial Dye Effluent in an Anaerobic Baffled Reactor. Appl. Environ. Microbiol. 67, 3226–3235. https://doi.org/10.1128/AEM.67.7.3226

Pomeroy, R., 1954. Auxiliary Pretreatment by Zinc Acetate in Sulfide Analyses. Anal. Chem. 26, 571–572. https://doi.org/10.1021/ac60087a047

Prato-Garcia, D., Cervantes, F.J., Buitrón, G., 2013. Azo dye decolorization assisted by chemical and biogenic sulfide. J. Hazard. Mater. 250–251, 462–468. https://doi.org/10.1016/j.jhazmat.2013.02.025

Premnath, N., Mohanrasu, K., Guru Raj Rao, R., Dinesh, G.H., Prakash, G.S., Ananthi, V., Ponnuchamy, K., Muthusamy, G., Arun, A., 2021. A crucial review on polycyclic aromatic Hydrocarbons - Environmental occurrence and strategies for microbial degradation. Chemosphere 280, 130608. https://doi.org/10.1016/j.chemosphere.2021.130608

Rau, J., Stolz, A., 2003. Oxygen-insensitive nitroreductases NfsA and NfsB of Escherichia coli function under anaerobic conditions as Lawsone-dependent azo reductases. Appl. Environ. Microbiol. 69, 3448–3455. https://doi.org/10.1128/AEM.69.6.3448-3455.2003

Reemtsma, T., 2003. Liquid chromatography-mass spectrometry and strategies for trace-level analysis of polar organic pollutants. J. Chromatogr. A 1000, 477–501. https://doi.org/10.1016/S0021-9673(03)00507-7

Rehorek, A., Plum, A., 2007. Characterization of sulfonated azo dyes and aromatic amines by pyrolysis gas chromatography/mass spectrometry. Anal. Bioanal. Chem. 388, 1653–1662. https://doi.org/10.1007/s00216-007-1390-0

Rehorek, A., Tauber, M., Gübitz, G., 2004. Application of power ultrasound for azo dye degradation. Ultrason. Sonochem. 11, 177–182. https://doi.org/10.1016/j.ultsonch.2004.01.030

Ribeiro, J.C., Mota, V.T., de Oliveira, V.M., Zaiat, M., 2022. Hydrogen and organic acid production from dark fermentation of cheese whey without buffers under mesophilic condition. J. Environ. Manage. 304, 114253. https://doi.org/10.1016/j.jenvman.2021.114253

Richardson, D., Vitolo, L.W., I, E.B., Webb, J., 1989. Pyridoxal isonicotinoyl hydrazone and analogues Study. Biol. Met. 69–76.

Richardson, S.D., McGuire, J.M., Thruston, A.D., Baughman, G.L., 1992. Structural characterization of sulfonated azo dyes using liquid secondary ion mass spectrometry/tandem mass spectrometry. Org. Mass Spectrom. 27, 289–299. https://doi.org/10.1002/oms.1210270322

Ripley, L.E., Boyle, W.C., Converse, J.C., 1986. Improved Alkalimetric Monitoring for Anaerobic Digestion of High-Strength Wastes. Water 58, 406–411.

Saady, N.M.C., 2013. Homoacetogenesis during hydrogen production by mixed cultures dark fermentation: Unresolved challenge. Int. J. Hydrogen Energy 38, 13172–13191. https://doi.org/10.1016/j.ijhydene.2013.07.122

Saddoud, A., Hassaïri, I., Sayadi, S., 2007. Anaerobic membrane reactor with phase separation for the treatment of cheese whey. Bioresour. Technol. 98, 2102–2108. https://doi.org/10.1016/j.biortech.2006.08.013

Santos, A.B., Cervantes, F.J., van Lier, J.B., 2007. Review paper on current technologies for decolourisation of textile wastewaters: Perspectives for anaerobic biotechnology. Bioresour. Technol. 98, 2369–2385. https://doi.org/10.1016/j.biortech.2006.11.013

Santos, A.B., Cervantes, F.J., Van Lier, J.B., 2004. Azo dye reduction by thermophilic anaerobic granular sludge, and the impact of the redox mediator anthraquinone-2,6-disulfonate (AQDS) on the reductive biochemical transformation. Appl. Microbiol. Biotechnol. 64, 62–69. https://doi.org/10.1007/s00253-003-1428-y

Santos, A.B., de Madrid, M.P., de Bok, F.A.M., Stams, A.J.M., van Lier, J.B., Cervantes, F.J., 2006. The contribution of fermentative bacteria and methanogenic archaea to azo dye

reduction by a thermophilic anaerobic consortium. Enzyme Microb. Technol. 39, 38–46. https://doi.org/10.1016/j.enzmictec.2005.09.003

Santos, A.B. dos, 2001. Aplicação conjunta de tratamento anaeróbio termofílico por lodo granular e de mediadores redox na remoção de cor de águas residuárias têxteis. Eng. Sanit. e Ambient. 10, 253–259. https://doi.org/10.1590/S1413-41522005000300010

Saratale, R.G., Gandhi, S.S., Purankar, M. V., Kurade, M.B., Govindwar, S.P., Oh, S.E., Saratale, G.D., 2013. Decolorization and detoxification of sulfonated azo dye C.I. Remazol Red and textile effluent by isolated Lysinibacillus sp. RGS. J. Biosci. Bioeng. 115, 658–667. https://doi.org/10.1016/j.jbiosc.2012.12.009

Şen, S., Demirer, G.N., 2003. Anaerobic treatment of real textile wastewater with a fluidized bed reactor. Water Res. 37, 1868–1878. https://doi.org/10.1016/S0043-1354(02)00577-8

Sen, S.K., Raut, Smita, Bandyopadhyay, P., Raut, Sangeeta, 2016. Fungal decolouration and degradation of azo dyes: A review. Fungal Biol. Rev. 30, 112–133. https://doi.org/10.1016/j.fbr.2016.06.003

Shah, H.N., Gharbia, S.E., 1992. Biochemical and chemical studies on strains designated Prevotella intermedia and proposal of a new pigmented species, Prevotella nigrescens sp. nov. Int. J. Syst. Bacteriol. 42, 542–546. https://doi.org/10.1099/00207713-42-4-542

Sharma, K., Derlon, N., Hu, S., Yuan, Z., 2014. Modeling the pH effect on sulfidogenesis inanaerobic sewer biofilm. Water Res. 49, 175–185. https://doi.org/10.1016/j.watres.2013.11.019

Sharma, S.C.D., Sun, Q., Li, J., Wang, Y., Suanon, F., Yang, J., Yu, C.P., 2016. Decolorization of azo dye methyl red by suspended and co-immobilized bacterial cells with mediators anthraquinone-2,6-disulfonate and Fe3O4 nanoparticles. Int. Biodeterior. Biodegrad. 112, 88–97. https://doi.org/10.1016/j.ibiod.2016.04.035

Shaul, G.M., Holdsworth, T.J., Dempsey, C.R., Dostal, K.A., 1991. Fate of water soluble azo dyes in the activated sludge process. Chemosphere 22, 107–119. https://doi.org/10.1016/0045-6535(91)90269-J

Shi, B., Li, G., Wang, D., Feng, C., Tang, H., 2007. Removal of direct dyes by coagulation: The performance of preformed polymeric aluminum species. J. Hazard. Mater. 143, 567–574. https://doi.org/10.1016/j.jhazmat.2006.09.076

Singh, A., Müller, B., Fuxelius, H.H., Schnürer, A., 2019. AcetoBase: a functional gene repository and database for formyltetrahydrofolate synthetase sequences. Database (Oxford). 2019, 1–14. https://doi.org/10.1093/database/baz142

Singh, A., Nylander, J.A.A., Schnürer, A., Bongcam-Rudloff, E., Müller, B., 2020. High-Throughput Sequencing and Unsupervised Analysis of Formyltetrahydrofolate Synthetase (FTHFS) Gene Amplicons to Estimate Acetogenic Community Structure. Front. Microbiol. 11, 1–13. https://doi.org/10.3389/fmicb.2020.02066

Singh, R.L., Singh, P.K., Singh, R.P., 2015. Enzymatic decolorization and degradation of azo dyes – A review. Int. Biodeterior. Biodegradation 104, 21–31. https://doi.org/10.1016/j.ibiod.2015.04.027

Solanki, K., Subramanian, S., Basu, S., 2013. Microbial fuel cells for azo dye treatment with electricity generation: A review. Bioresour. Technol. 131, 564–571. https://doi.org/10.1016/j.biortech.2012.12.063

Stams, A.J.M., Plugge, C.M., 2009. Electron transfer in syntrophic communities of anaerobic bacteria and archaea. Nat. Rev. Microbiol. 7, 568–577. https://doi.org/10.1038/nrmicro2166

Stolz, A., 2001. Basic and applied aspects in the microbial degradation of azo dyes. Appl. Microbiol. Biotechnol. 56, 69–80. https://doi.org/10.1007/s002530100686

Sullivan, A.G., Garner, R., Gaskell, S.J., 1998. Structural Analysis of Sulfonated Monoazo Dyestuff Intermediates by Electrospray Tandem Mass Spectrometry and Matrix-assisted Laser Desorption / Ionization Post-source Decay Mass Spectrometry 1215, 1207–1215.

Takahashi, N., Yamada, T., 2000. Glucose metabolism by Prevotella intermedia and Prevotella nigrescens. Oral Microbiol. Immunol. 15, 188–195. https://doi.org/10.1034/j.1399-302X.2000.150307.x

Talarposhti, A.M., Donnelly, T., Anderson, G.K., 2001. Colour removal from a simulated dye wastewater using a two-phase anaerobic packed bed reactor. Water Res. 35, 425–432. https://doi.org/10.1016/S0043-1354(00)00280-3

Tan, L., Ning, S., Zhang, X., Shi, S., 2013. Aerobic decolorization and degradation of azo dyes by growing cells of a newly isolated yeast Candida tropicalis TL-F1. Bioresour. Technol. 138, 307–313. https://doi.org/10.1016/j.biortech.2013.03.183

Taylor, K.A.C.C., 1996. A simple colorimetric assay for muramic acid and lactic acid. Appl. Biochem. Biotechnol. - Part A Enzym. Eng. Biotechnol. 56, 49–58. https://doi.org/10.1007/BF02787869

Telke, A.A., Joshi, S.M., Jadhav, S.U., Tamboli, D.P., Govindwar, S.P., 2010. Decolorization and detoxification of Congo red and textile industry effluent by an isolated bacterium Pseudomonas sp. SU-EBT. Biodegradation 21, 283–296. https://doi.org/10.1007/s10532-009-9300-0

Teufel, F., Almagro Armenteros, J.J., Johansen, A.R., Gíslason, M.H., Pihl, S.I., Tsirigos, K.D., Winther, O., Brunak, S., von Heijne, G., Nielsen, H., 2022. SignalP 6.0 predicts all five types of signal peptides using protein language models. Nat. Biotechnol. https://doi.org/10.1038/s41587-021-01156-3

Vaillancourt, F.H., Bolin, J.T., Eltis, L.D., 2004. Ring-Cleavage Dioxygenases, in: Pseudomonas. Springer US, Boston, MA, pp. 359–395. https://doi.org/10.1007/978-1-4419-9088-4_13

Van Der Zee, F.P., Bisschops, I.A.E., Blanchard, V.G., Bouwman, R.H.M., Lettinga, G., Field, J.A., 2003. The contribution of biotic and abiotic processes during azo dye reduction in anaerobic sludge. Water Res. 37, 3098–3109. https://doi.org/10.1016/S0043-1354(03)00166-0

Van Der Zee, F.P., Villaverde, S., 2005. Combined anaerobic-aerobic treatment of azo dyes - A short review of bioreactor studies. Water Res. 39, 1425–1440. https://doi.org/10.1016/j.watres.2005.03.007

Varesche, M.B., Zaiat, M., Vieira, L.G.T., Vazoller, R.F., Foresti, E., 1997. Microbial colonization of poplyurethane foam matrices in horizontal-flow anaerobic immobilized-sludge reactor. Appl. Microbiol. Biotechnol. 48, 534–538. https://doi.org/10.1007/s002530051092

Vaser, R., Sović, I., Nagarajan, N., Šikić, M., 2017. Fast and accurate de novo genome assembly from long uncorrected reads. Genome Res. 27, 737–746. https://doi.org/10.1101/gr.214270.116

Vismann, B., 1996. Sulfide species and total sulfide toxicity in the shrimp Crangon crangon. J. Exp. Mar. Bio. Ecol. 204, 141–154. https://doi.org/10.1016/0022-0981(96)02577-4

Voyksner, R.D., Straub, R., Keever, J.T., Freeman, H.S., Hsu, W.N., 1993. Determination of Aromatic Amines Originating from Azo Dyes by Chemical Reduction Combined with Liquid Chromatography/Mass Spectrometry. Environ. Sci. Technol. 27, 1665–1672. https://doi.org/10.1021/es00045a025

Waghmode, T.R., Kurade, M.B., Khandare, R. V., Govindwar, S.P., 2011. A sequential aerobic/microaerophilic decolorization of sulfonated mono azo dye Golden Yellow HER by microbial consortium GG-BL. Int. Biodeterior. Biodegrad. 65, 1024–1034. https://doi.org/10.1016/j.ibiod.2011.08.002

Waghmode, T.R., Kurade, M.B., Sapkal, R.T., Bhosale, C.H., Jeon, B.H., Govindwar, S.P., 2019. Sequential photocatalysis and biological treatment for the enhanced degradation of the persistent azo dye methyl red. J. Hazard. Mater. 115–122. https://doi.org/10.1016/j.jhazmat.2019.03.004

Wang, J., Yin, Y., 2017. Principle and application of different pretreatment methods for enriching hydrogen-producing bacteria from mixed cultures. Int. J. Hydrogen Energy 42, 4804–4823. https://doi.org/10.1016/j.ijhydene.2017.01.135

Wang, X., Zeng, G., Zhu, J., 2008. Treatment of jean-wash wastewater by combined coagulation, hydrolysis/acidification and Fenton oxidation. J. Hazard. Mater. 153, 810–816. https://doi.org/10.1016/j.jhazmat.2007.09.030

Wang, X., Zhang, Z., Jin, D., Zhou, L., Wu, L., Li, C., Zhao, L., An, W., Chen, Y., 2014. Draft genome sequence of Brachybacterium phenoliresistens strain W13A50, a halotolerant hydrocarbon-degrading bacterium. Genome Announc. 2, 13–14. https://doi.org/10.1128/genomeA.00899-14

Wang, Y., Jiang, L., Shang, H., Li, Q., Zhou, W., 2020. Treatment of azo dye wastewater by the self-flocculating marine bacterium Aliiglaciecola lipolytica. Environ. Technol. Innov. 19, 100810. https://doi.org/10.1016/j.eti.2020.100810

Weber, E.J., Stickney, V.C., 1993. Hydrolysis kinetics of Reactive Blue 19-Vinyl Sulfone. Water Res. 27, 63–67. https://doi.org/10.1016/0043-1354(93)90195-N

Widdel, F., Pfennig, N., 1982. Studies on dissimilatory sulfate-reducing bacteria that decompose fatty acids II. Incomplete oxidation of propionate by Desulfobulbus propionicus gen. nov., sp. nov. Arch. Microbiol. 131, 360–365. https://doi.org/10.1007/BF00411187

Wu, J., Eiteman, M.A., Law, S.E., 1998. Evaluation of Membrane Filtration and Ozonation. J. Environ. Eng. 124, 272–277.

Xiao, Y., Zhang, E., Zhang, J., Dai, Y., Yang, Z., Christensen, H.E.M., Ulstrup, J., Zhao, F., 2017. Extracellular polymeric substances are transient media for microbial extracellular electron transfer. Sci. Adv. 3, 1–9. https://doi.org/10.1126/sciadv.1700623

Xin, J.Y., Cui, J.R., Niu, J.Z., Hua, S.F., Xia, C.G., Li, S. Ben, Zhu, L.M., 2004. Production of methanol from methane by methanotrophic bacteria. Biocatal. Biotransformation 22, 225–229. https://doi.org/10.1080/10242420412331283305

Yang, Q., Li, C., Li, H., Li, Y., Yu, N., 2009. Degradation of synthetic reactive azo dyes and treatment of textile wastewater by a fungi consortium reactor. Biochem. Eng. J. 43, 225–230. https://doi.org/10.1016/j.bej.2008.10.002

You, S.J., Teng, J.Y., 2009. Anaerobic decolorization bacteria for the treatment of azo dye in a sequential anaerobic and aerobic membrane bioreactor. J. Taiwan Inst. Chem. Eng. 40, 500–504. https://doi.org/10.1016/j.jtice.2009.01.007

Zahran, S.A., Ali-Tammam, M., Ali, A.E., Aziz, R.K., 2021. Compositional variation of the human fecal microbiome in relation to azo-reducing activity: a pilot study. Gut Pathog. 13, 1–12. https://doi.org/10.1186/s13099-021-00454-0

Zaroual, Z., Azzi, M., Saib, N., Chainet, E., 2006. Contribution to the study of electrocoagulation mechanism in basic textile effluent. J. Hazard. Mater. 131, 73–78. https://doi.org/10.1016/j.jhazmat.2005.09.021

Zeng, Q., Wang, Y., Zan, F., Khanal, S.K., Hao, T., 2021. Biogenic sulfide for azo dye decolorization from textile dyeing wastewater. Chemosphere 283, 131158. https://doi.org/10.1016/j.chemosphere.2021.131158

Zhang, C., Wang, S., Yan, Y., 2011. Isomerization and biodegradation of beta-cypermethrin by Pseudomonas aeruginosa CH7 with biosurfactant production. Bioresour. Technol. 102, 7139–7146. https://doi.org/10.1016/j.biortech.2011.03.086

Zhang, F., Yediler, A., Liang, X., 2007. Decomposition pathways and reaction intermediate formation of the purified, hydrolyzed azo reactive dye C.I. Reactive Red 120 during ozonation. Chemosphere 67, 712–717. https://doi.org/10.1016/j.chemosphere.2006.10.076

Zimmermann, T., Kulla, H.G., Leisinger, T., 1982. Properties of Purified Orange I1 Azoreductase, the Enzyme Initiating Azo Dye Degradation by Pseudumunas KF46. Eur. J. Biochem. 129, 197–203.

Appendix A

CHAPTER 3:

Broken into pieces: the challenges of determining sulfonated azo dyes in biological reactor effluents using LC-ESI-MS/MS analysis

J. M. S. Oliveira[a]*, C. A. Sabatini[a], A. J. Santos-Neto[b] and E. Foresti[a]

[a] Department of Hydraulics and Sanitation, São Carlos School of Engineering, University of São Paulo, Av. Trabalhador São Carlense, 400, 13566-590, São Carlos, SP, Brazil

[b] São Carlos Institute of Chemistry (IQSC), Av. Trabalhador São Carlense, 400, 13566-590, São Carlos, SP, Brazil.

Table S. 1. Composition of the trace elements stock solution.

	Concentration (g L^{-1})
$FeSO_4.7H_2O$	0.75
$NiSO_4.7H_2O$	0.50
$MnCl_2.4H_2O$	0.50
$ZnSO_4.7H_2O$	0.50
H_3BO_3	0.10
$CoCl_2.6H_2O$	0.05
$CuSO_4.5H_2O$	0.005
$Na_2MoO_4.2H_2O$	0.004
EDTA disodium salt	1.00

Figure S. 1. ESI^{-}MS spectrum of hydrolized Direct Black 22 obtained in Full-Scan mode in the range 80 – 1000 Da.

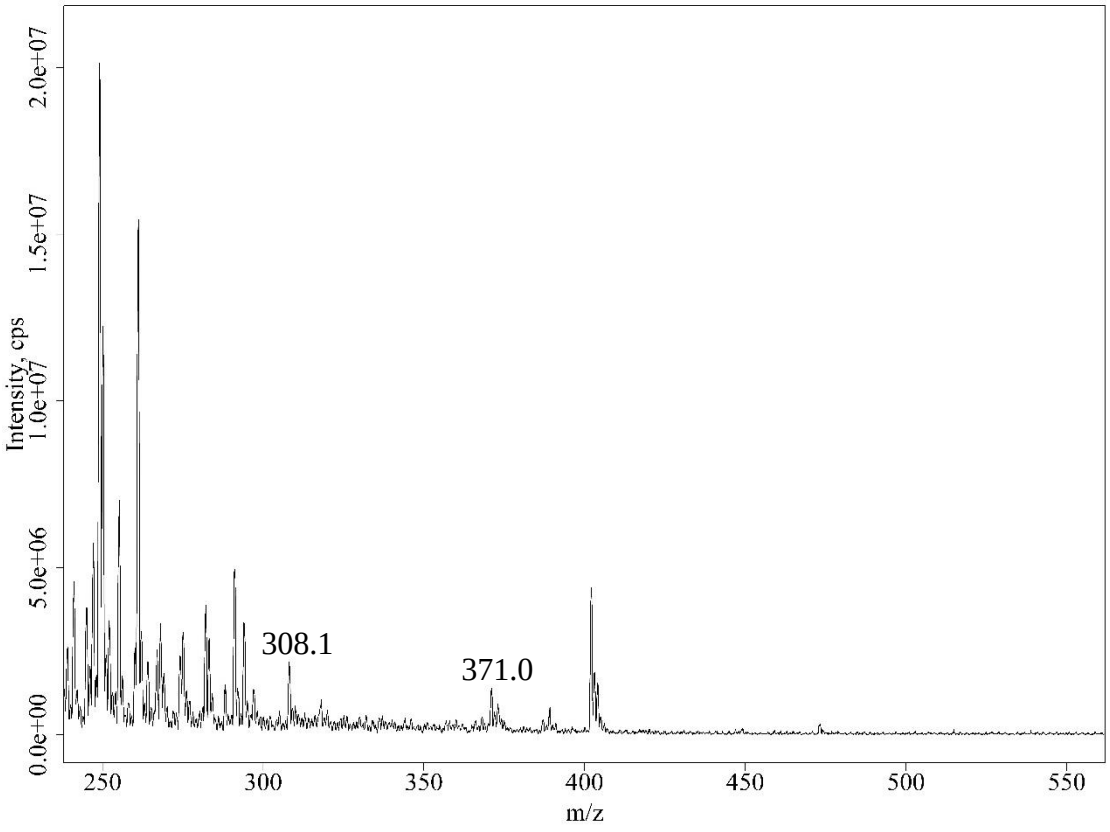

Appendix B

CHAPTER 4

Two-stage anaerobic digestion system for biodegradation of azo dye in the presence of sulfate: minimizing competition for reducing equivalents

Jean M. S. Oliveira [a], Márcia H. R. Z. Damianovic [a], Eugênio Foresti [a].

[a] Biological Processes Laboratory (LPB), University of São Paulo (USP), 1100 João Dagnone Avenue, 13563-120 São Carlos, SP, Brazil.

Figure S. 2. Anaerobic structured-bed reactor (1st-stage reactor, R1) used in the two-stage anaerobic digestion system. Profile (A), cross-sectional area showing polyurethane foam rods array (B), and 3D realistic visualization of the lower portion of the bioreactor (C). In the figure: 1 – feed inlet; 2 – bottom discharge; 3 – sections with 5 mm diameter constrictions; 4 – effluent; 5 – biogas sampling point; a-e – liquid sampling points.

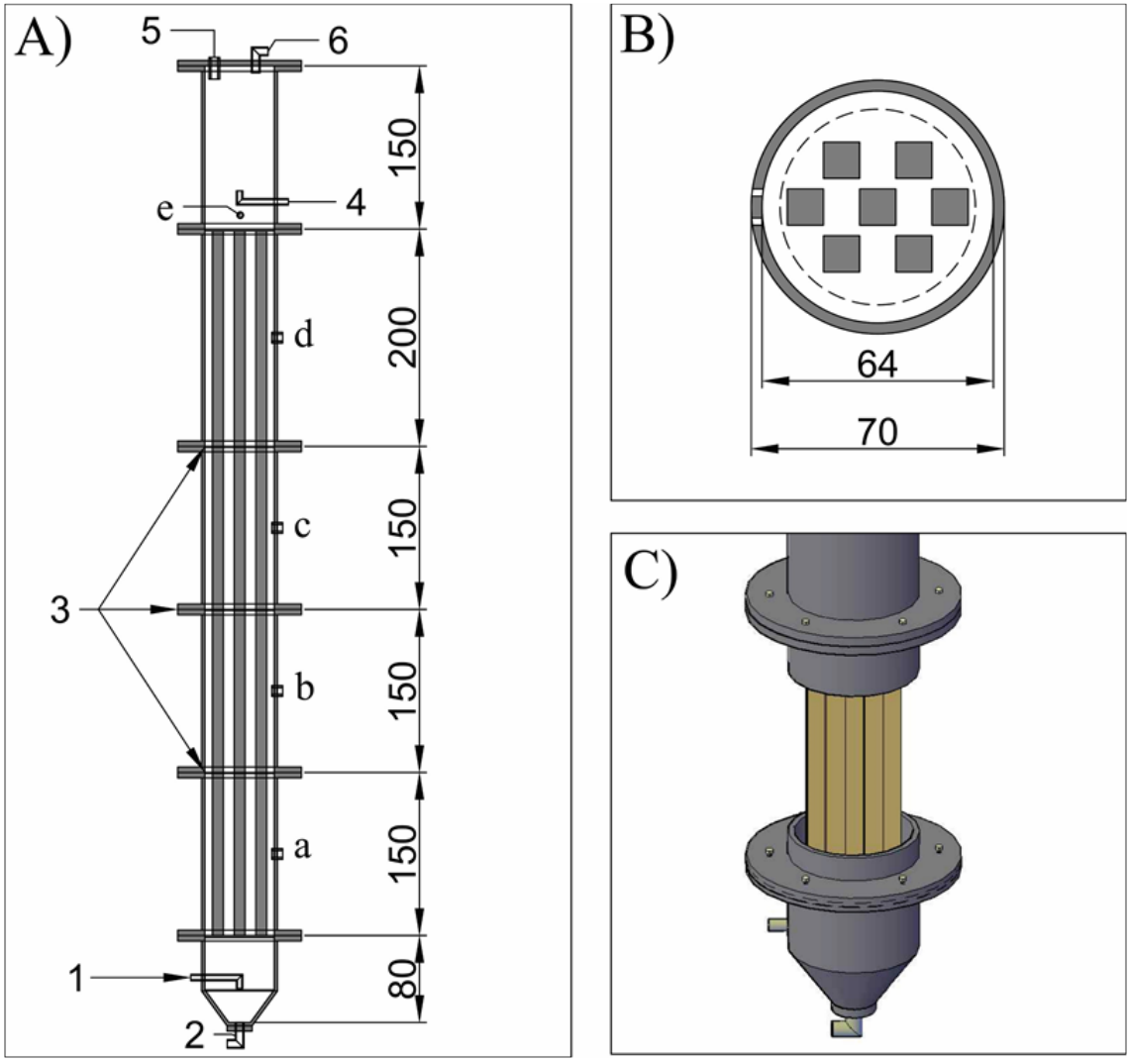

Figure S. 3. Upflow anaerobic sludge blanket (2nd-stage reactor, R2) used in the two-stage anaerobic digestion system. Internal diameter: 52 mm.

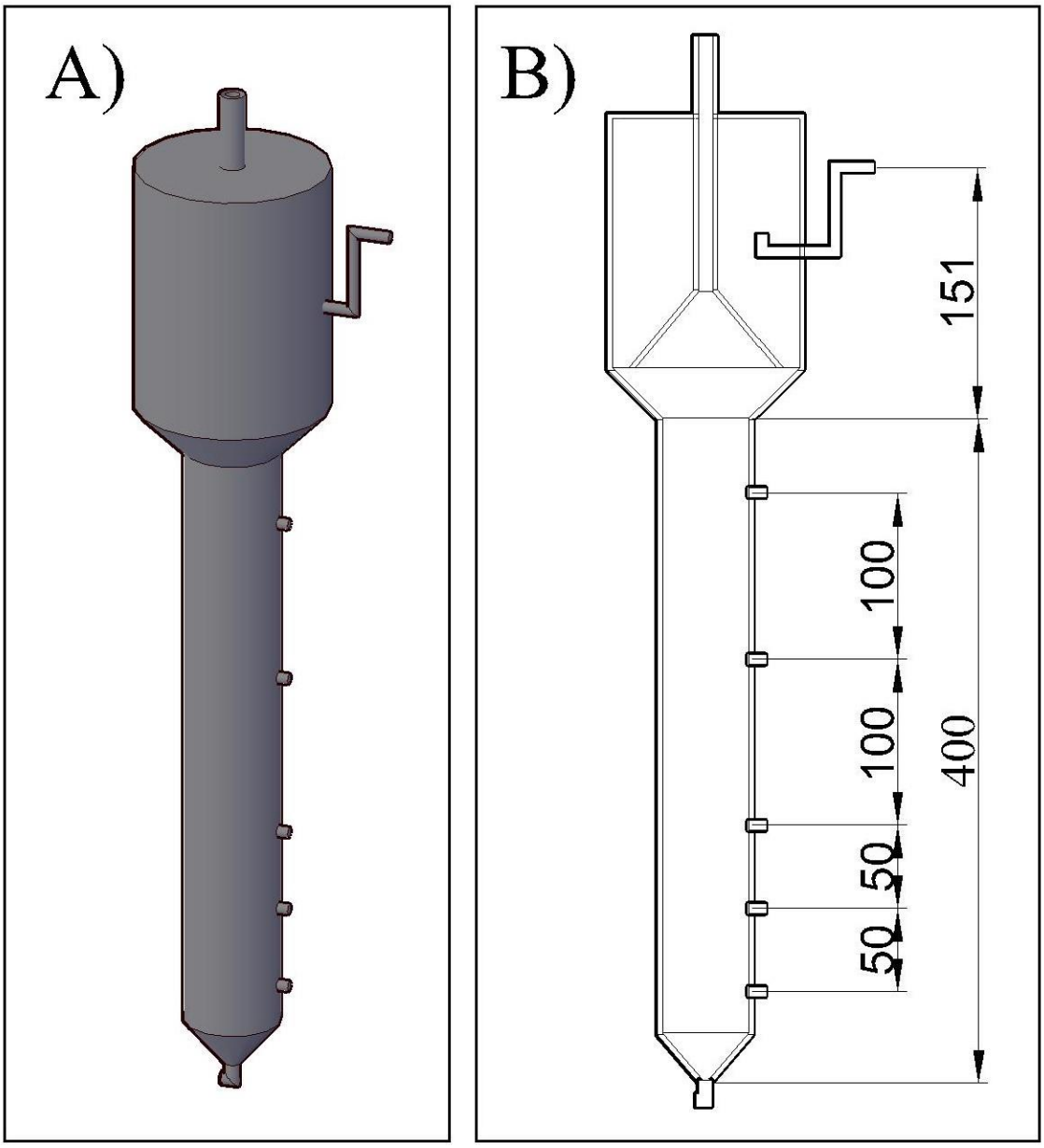

Figure S. 4. Anaerobic structured-bed reactor (1st-stage reactor, R1) used in the two-stage anaerobic digestion system. Details of the experimental setup: (a) wastewater inlet; (b) wastewater outlet; (c) outlet biogas tube; (d) hydric seal; (e) U-shape tube; (f) biogas flow meter; and (g) peristaltic pump.

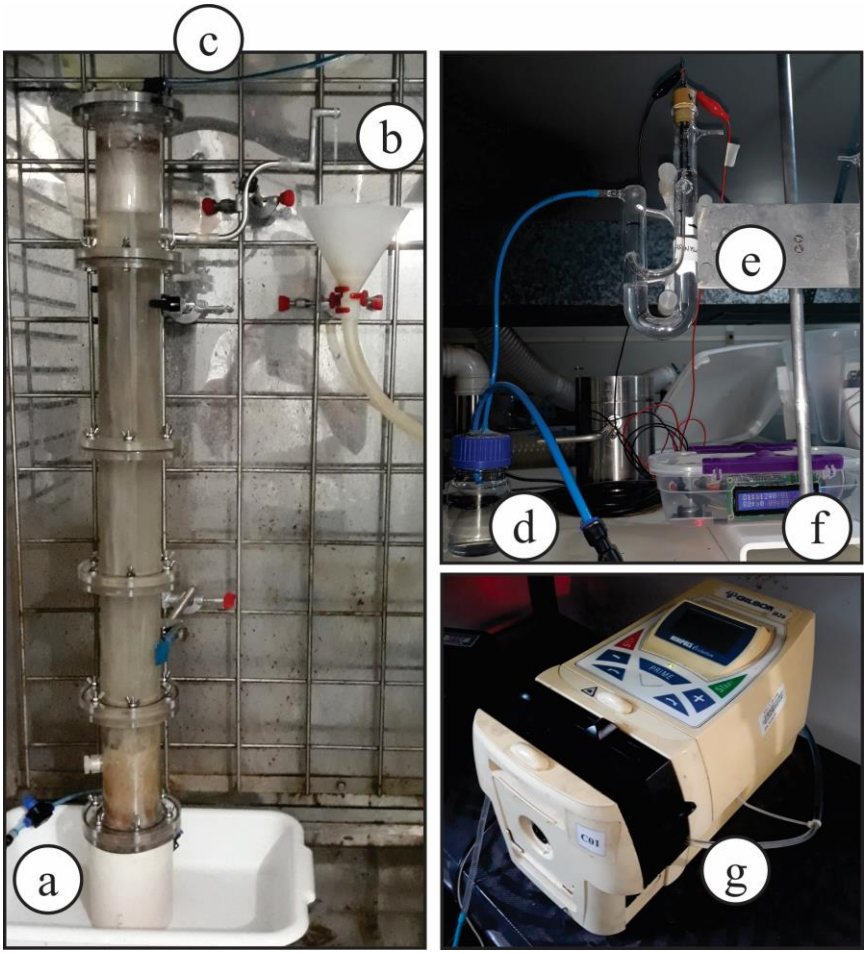

Figure S. 5. Experimental setup. 1st-stage reactor (left) and 2nd-stage reactor (right) operated in series.

Table S. 2. Physical-chemical properties of Direct Black 22 (CAS 6473-13-8)

Property	**Value**
Molar mass	1083.97 g mol^{-1}
Monoisotopic mass	1083.11994526 Da
Formula	$C_{44}H_{32}N_{13}Na_3O_{11}S_3$
Charge (pH 5-9)	-3
Isoelectric point	1.8
Maximum absorbance wavelength	481 nm

Source: chemicalize.com

Table S. 3. Composition of the trace elements stock solution.

	Concentration (g L^{-1})
$FeSO_4.7H_2O$	0.75
$NiSO_4.7H_2O$	0.50
$MnCl_2.4H_2O$	0.50
$ZnSO_4.7H_2O$	0.50
H_3BO_3	0.10
$CoCl_2.6H_2O$	0.05
$CuSO_4.5H_2O$	0.005
$Na_2MoO_4.2H_2O$	0.004
EDTA disodium salt	1.00

Figure S. 6 Influent and effluent pH in the A) 1st-sta ge reactor, R1; and B) 2nd-stage reactor, R2.

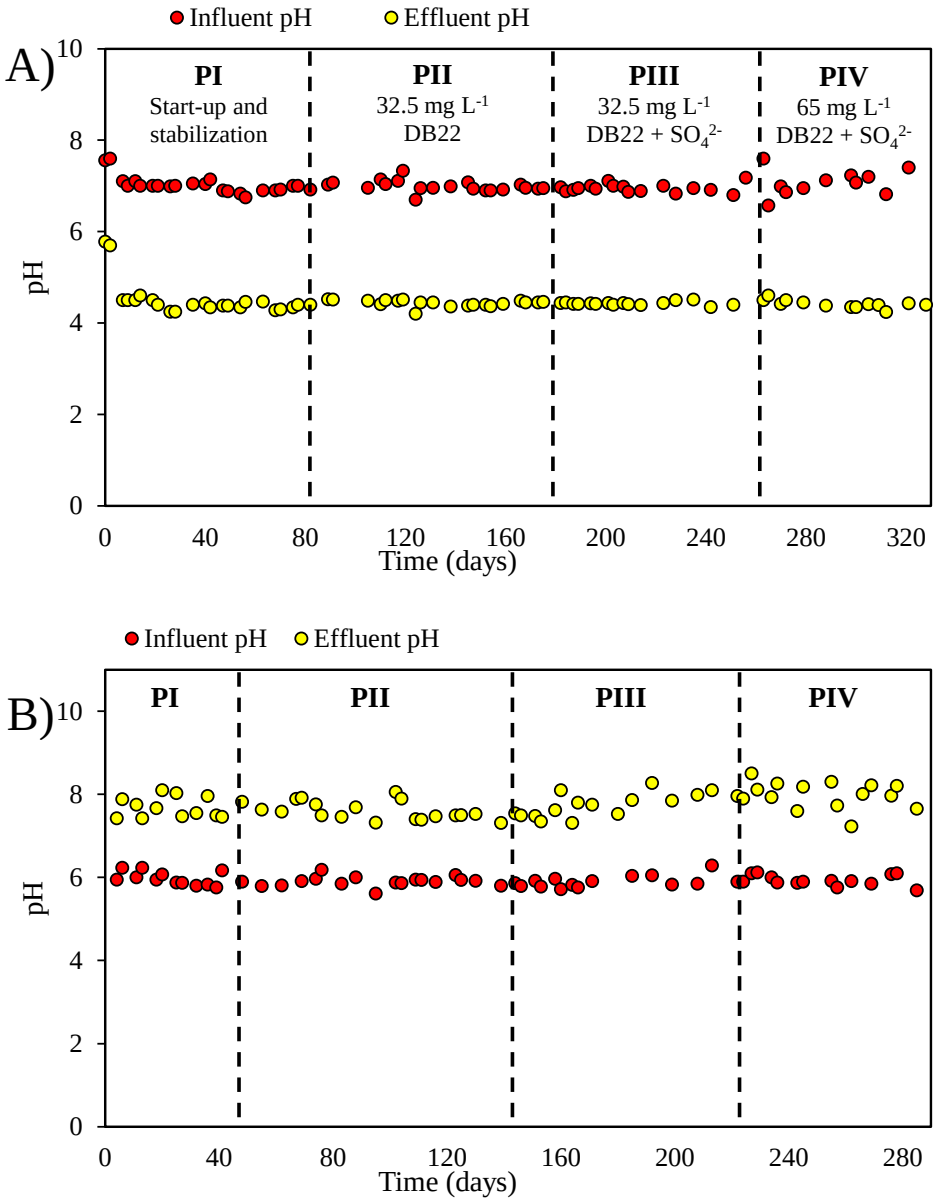

Figure S. 7. Measured sulfide (S^{2-}) concentrations and theoretical estimates in the effluent of the 2nd-stage reactor (R2). Theoretical estimates were calculated considering a stoichiometry coefficient of 0.33 mg of sulfide produced per mg of sulfate reduced, and further considering that sulfide remained in solution due to the high pH in R2.

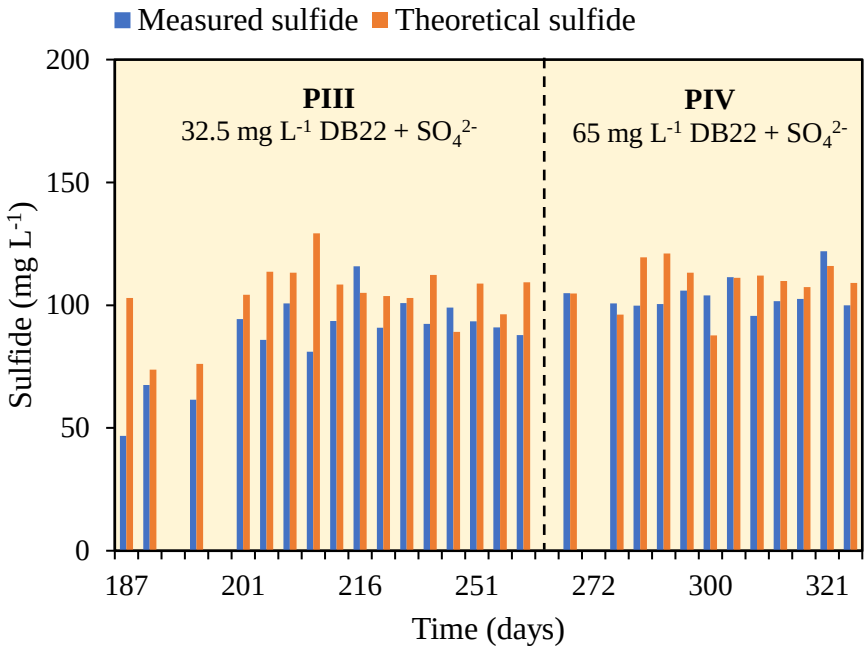

Figure S. 8. UV-VIS spectrum of samples from the two-phase anaerobic digestion system. A) PII: 32.5 mg L^{-1} DB22; B) PIII: 32.5 mg L^{-1} DB22 and 338 mg L^{-1} SO_4^{2-}; and C) PIV: 65 mg L^{-1} DB22 and 338 mg L^{-1} SO_4^{2-}.

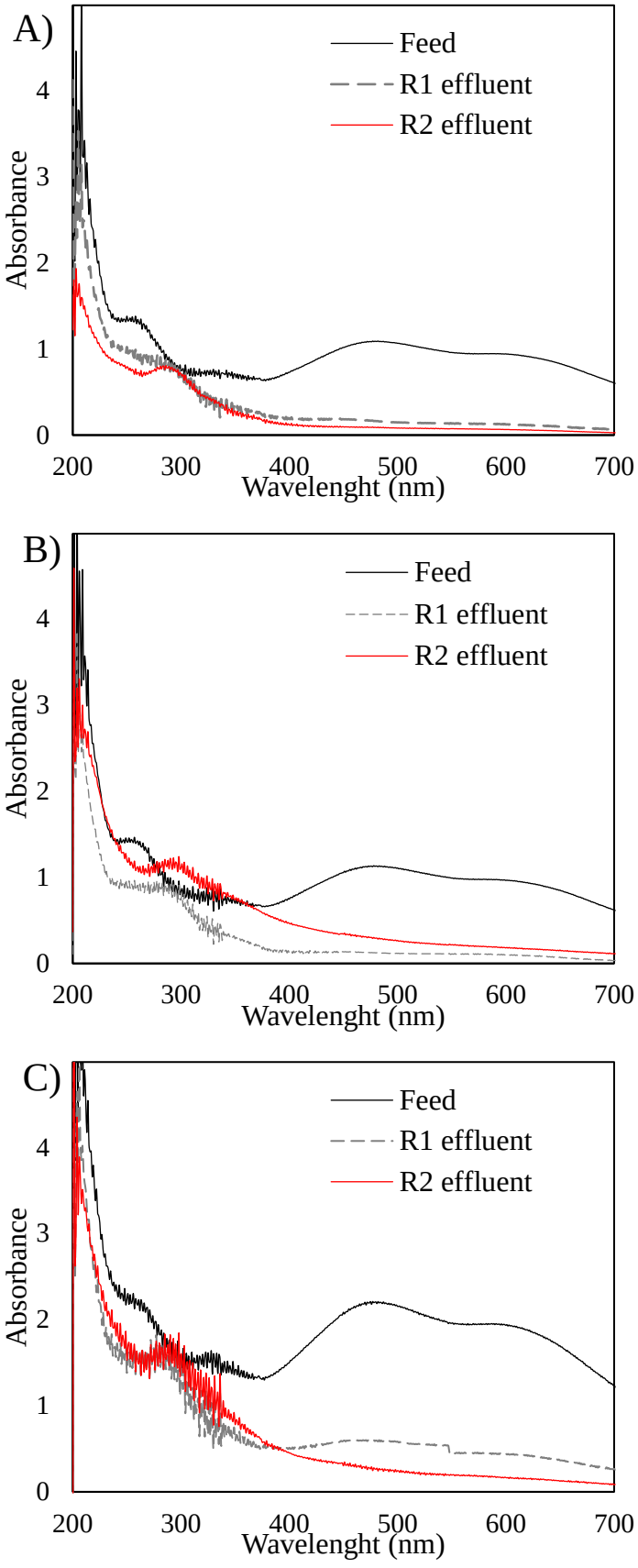

Appendix C

CHAPTER 5

Microbial communities and metabolic pathways involved in reductive decolorization of an azo dye in a two-stage AD system

J. M. S. Oliveira[1,2], J. S. Poulsen[2], E. Foresti[1], J. L. Nielsen[2]

[1]Biological Processes Laboratory (LPB), São Carlos School of Engineering (EESC), University of São Paulo (USP), 1100 João Dagnone Avenue, 13563-120 São Carlos, SP, Brazil.

[2]Center for Microbial Communities, Department of Chemistry and Bioscience, Aalborg University, Fredrik Bajers Vej 7H, DK-9220 Aalborg, Denmark

Table S. 4. Composition of the trace elements stock solution.

	Concentration (g L^{-1})
$FeSO_4.7H_2O$	0.75
$NiSO_4.7H_2O$	0.50
$MnCl_2.4H_2O$	0.50
$ZnSO_4.7H_2O$	0.50
H_3BO_3	0.10
$CoCl_2.6H_2O$	0.05
$CuSO_4.5H_2O$	0.005
$Na_2MoO_4.2H_2O$	0.004
EDTA disodium salt	1.00

Figure S. 9. Vertical profiling for carbohydrates concentration in the 1st-stage reactor (R1).

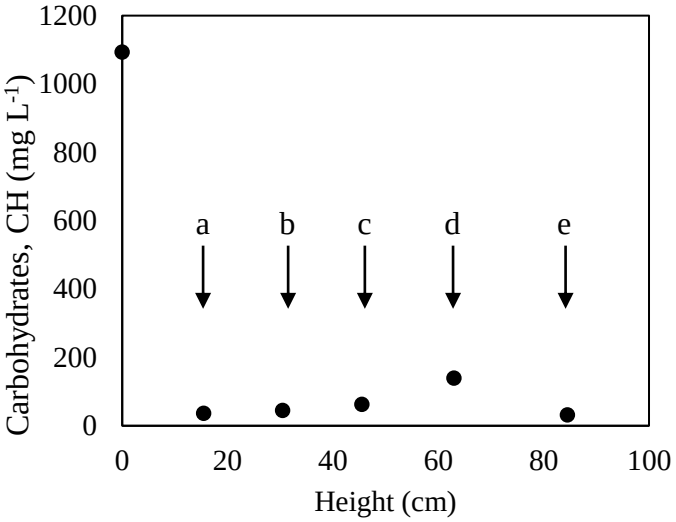

Figure S. 10. Phylum level distribution of microbial populations in the 1st-stage reactor (R1) identified after targeting the bacterial *16S rRNA* V4 region. Samples are faceted by the operational strategies used in the operation of the AD system.

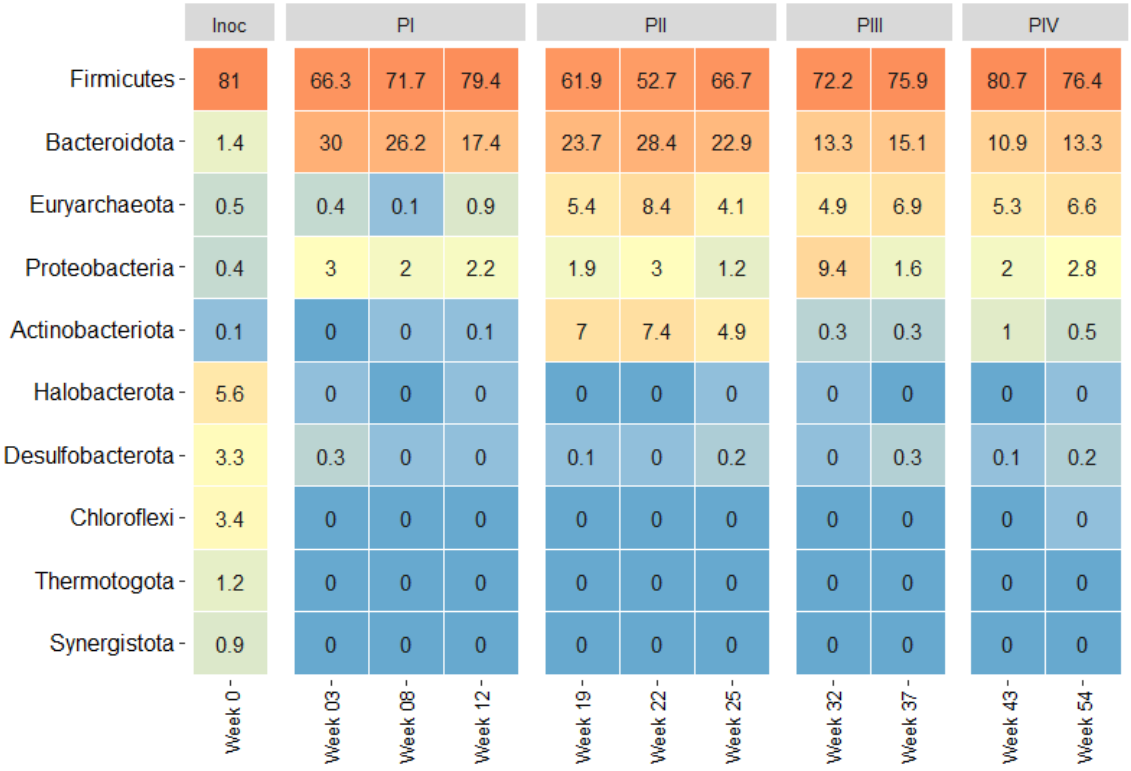

Appendix D

CHAPTER 6

New insights into the mechanism of azo dye biodegradation by Lactococcus lactis

J. M. S. Oliveira[1,2], J. S. Poulsen[2], E. Foresti[1], J. L. Nielsen[2]

[1]Biological Processes Laboratory (LPB), São Carlos School of Engineering (EESC), University of São Paulo (USP), 1100 João Dagnone Avenue, 13563-120 São Carlos, SP, Brazil.

[2]Center for Microbial Communities, Department of Chemistry and Bioscience, Aalborg University, Fredrik Bajers Vej 7H, DK-9220 Aalborg, Denmark

Table S. 5. Composition of the trace elements stock solution.

	Concentration (g L^{-1})
$FeSO_4.7H_2O$	0.75
$NiSO_4.7H_2O$	0.50
$MnCl_2.4H_2O$	0.50
$ZnSO_4.7H_2O$	0.50
H_3BO_3	0.10
$CoCl_2.6H_2O$	0.05
$CuSO_4.5H_2O$	0.005
$Na_2MoO_4.2H_2O$	0.004
EDTA disodium salt	1.00

Table S. 6. Proteins differientally abundant in *L. lactis* LLSP-01 cells grown in the presence of 32.5 mg L^{-1} Direct Black 22.

p-value	log_2FC	Accession	Protein name or description
I - Upregulated			
8.5E-02	2.78	WP_058211938.1	L-arabinose isomerase
4.0E-02	2.60	WP_046781838.1	WxL domain-containing protein
3.1E-02	1.99	WP_058217091.1	BMP family ABC transporter substrate-binding protein
2.2E-02	1.57	WP_058219886.1	SDR family oxidoreductase
4.2E-02	1.31	WP_033899140.1	dTDP-glucose 4,6-dehydratase
1.4E-02	1.27	WP_064973379.1	ring-cleaving dioxygenase
3.1E-02	1.19	WP_003129660.1	vitamin B12 independent methionine synthase
--	--	WP_010905193.1	dTDP-4-dehydrorhamnose 3,5-epimerase
--	--	WP_058210984.1	phosphopyruvate hydratase
II - Downregulated			
1.6E-02	-5.86	WP_010905107.1	50S ribosomal protein L32
9.7E-03	-4.20	WP_004254538.1	DNA starvation/stationary phase protection
2.4E-04	-3.94	WP_058223384.1	aldo/keto reductase
2.9E-04	-3.86	WP_003129551.1	DNA-directed RNA polymerase subunit delta
4.0E-04	-3.75	WP_003131954.1	30S ribosomal protein S6
1.5E-02	-3.65	WP_109245588.1	30S ribosomal protein S21
2.3E-03	-3.53	WP_003131952.1	30S ribosomal protein S18
4.3E-03	-3.47	WP_003129453.1	cell division regulator GpsB
1.0E-02	-3.42	WP_057720276.1	ammonia-dependent NAD(+) synthetase
5.2E-03	-3.32	WP_058220094.1	30S ribosomal protein S7
4.3E-03	-3.18	WP_003130887.1	phosphate signaling complex protein PhoU
2.2E-02	-3.06	WP_081041499.1	5-bromo-4-chloroindolyl phosphate hydrolase
1.6E-02	-3.04	WP_038599155.1	FMN-dependent NADH-azoreductase
2.6E-04	-2.98	WP_003131560.1	superoxide dismutase [Mn]
2.5E-02	-2.96	WP_003132352.1	50S ribosomal protein L20
4.7E-03	-2.89	WP_058219555.1	elongation factor Ts
6.9E-03	-2.87	WP_015426160.1	transcription regulator
2.7E-05	-2.87	WP_029344674.1	universal stress protein
1.6E-02	-2.84	WP_003130829.1	RNA polymerase sigma factor RpoD
2.8E-03	-2.83	WP_003131820.1	IreB family regulatory phosphoprotein
2.6E-02	-2.74	WP_003130364.1	response regulator transcription factor
2.8E-03	-2.60	WP_003130555.1	30S ribosomal protein S13
2.6E-02	-2.57	WP_003130880.1	phosphate ABC transporter substrate-binding protein
3.2E-02	-2.51	WP_003129874.1	30S ribosomal protein S12
1.2E-02	-2.49	WP_015426887.1	PTS mannose/fructose/sorbose transporter family subunit IID
3.1E-02	-2.40	WP_003130191.1	YneF family protein
6.9E-03	-2.40	WP_003129623.1	elongation factor P
4.4E-03	-2.36	WP_010906353.1	glucose-6-phosphate isomerase
1.2E-02	-2.30	WP_003130213.1	50S ribosomal protein L10
4.5E-03	-2.23	WP_058219675.1	endolytic transglycosylase MltG
3.4E-02	-2.22	WP_003129977.1	transcription termination/antitermination protein NusG
2.6E-02	-2.17	WP_004255340.1	DUF896 domain-containing protein

3.1E-02	-2.16	WP_003129948.1	MULTISPECIES: 50S ribosomal protein L5
1.9E-02	-2.13	WP_033900570.1	tryptophan--tRNA ligase
8.3E-04	-2.11	WP_014572780.1	nucleotide exchange factor GrpE
9.1E-03	-2.10	WP_058220241.1	hypothetical protein
2.6E-03	-2.10	WP_003130558.1	50S ribosomal protein L17
2.4E-02	-2.09	WP_029344478.1	50S ribosomal protein L11
1.1E-02	-2.08	WP_011915250.1	hypothetical protein
1.5E-02	-2.00	WP_003132639.1	DUF1912 family protein
3.6E-02	-1.91	WP_003131580.1	response regulator transcription factor
8.0E-03	-1.88	WP_058219348.1	DUF177 domain-containing protein
2.2E-02	-1.82	WP_003129394.1	ArsR family transcriptional regulator
1.7E-02	-1.81	WP_017864319.1	[acyl-carrier-protein] S-malonyltransferase
2.9E-02	-1.80	WP_011835873.1	uracil phosphoribosyltransferase
7.6E-03	-1.79	WP_058220184.1	DivIVA domain-containing protein
3.3E-02	-1.77	WP_058219795.1	hypothetical protein
3.6E-03	-1.73	WP_029343862.1	triose-phosphate isomerase
2.5E-02	-1.73	WP_003130319.1	manganese-dependent inorganic pyrophosphatase
1.1E-02	-1.71	WP_064974224.1	hypothetical protein
4.9E-02	-1.66	WP_058219505.1	N-acetyltransferase
1.9E-02	-1.61	WP_003129725.1	Asp-tRNA(Asn)/Glu-tRNA(Gln) amidotransferase subunit GatB
2.1E-03	-1.58	WP_003132177.1	ATP-dependent zinc metalloprotease FtsH
2.9E-02	-1.56	WP_003130321.1	peptidase T
4.6E-02	-1.55	WP_098408067.1	guanylate kinase
2.3E-02	-1.46	WP_003130214.1	50S ribosomal protein L7/L12
2.8E-02	-1.32	WP_003131585.1	chaperonin GroEL
3.2E-02	-1.24	WP_004254664.1	U32 family peptidase
2.4E-02	-1.17	WP_003131187.1	S-ribosylhomocysteine lyase
2.4E-02	-1.16	WP_012898339.1	F0F1 ATP synthase subunit delta
2.7E-02	-1.06	WP_017864684.1	tryptophan synthase subunit alpha